MODELING OF SPACE CHARGE LIMITED CURRENT IN SOLID

William Chandra

School of Electrical & Electronic Engineering

A thesis submitted to the Nanyang Technological University

in fulfillment of the requirement for the degree of

Doctor of Philosophy

2010

ACKNOWLEDGMENTS

Firstly, I would like to extend my deepest and greatest gratitude to my supervisor, A/P Ang Lay Kee, Ricky. He has given me continuous support and encouragement throughout my research and study. Many discussions, directions, guidance given by him have transformed and changed me to be a better person and student. I would also like to thank my co-supervisor: A/P Pey Kin Leong (former Head of Division of Microelectronics, EEE6) for his teaching and motivational support. I would also like to acknowledge the help from my fellow colleagues and mentors: Dr. Wu Lin, Zhang Peng, Lee Teck Seng, Dr. Koh Wee Shing, Dr. Patrick Lo Vui Lip, Dr. Rakesh Ranjan, Dr. Li Xiang, Dr. Ong Yi Ching, and Mr. Tung Chih Hang (senior research staff in IME). I could only benefit through the fruitful discussions and teachings from them regarding to my research. I would like to thank Dr. Lap Chan and Dr. Chee Mang from Global Foundries for their teaching and funding support for the first and half year of my PhD study. I would also like to acknowledge the funding support from ASTAR and MOE for my research. Lastly but not least, I would like to thank my family and God for the moral and spiritual support.

William Chandra

May 2010

TABLE OF CONTENTS

ACKNOWLEDGMENTS ii

TABLE OF CONTENTS iii

ABSTRACT vi

List of Figures viii

1 INTRODUCTION 1

1.1 Background 1

1.2 Objectives and Contributions 4

1.3 Organization of the Report 6

2 LITERATURE REVIEW 8

2.1 MG law for SCL Transport in a Trap-free Solid 11

2.2 SCL Transport with Shallow Traps 13

2.3 SCL Transport with Deep Traps 16

2.4 SCL Transport with Distributed Energy Levels of Traps 18

2.5 Applications of SCL Current in Solids 20

TABLE OF CONTENTS

3 TWO-DIMENSIONAL MODEL FOR SPACE CHARGE LIMITED (SCL) CURRENT IN SOLIDS 30

3.1 Introduction 30

3.2 Transition from CL to MG law 31

3.3 The Analytical 2D CL law and MG law 33

3.3.1 2D Trap-free MG law 34

3.3.2 2D Trap-filled MG law 36

3.3.3 Numerical Simulation Using Medici 36

3.4 Summary 41

4 CONTACT AND SIZE EFFECT OF 2D SPACE CHARGE LIMITED (SCL) CURRENT IN SOLIDS 42

4.1 Introduction 42

4.2 Theory 43

4.3 Results and Discussion 46

4.4 Summary 57

5 SPACE CHARGE LIMITED (SCL) CURRENT IN A GAP OF COMBINED VACUUM AND SOLID 58

5.1 Introduction 58

5.2 Model Formulation for Vacuum and Solid Gap 60

5.2.1 Results and Discussion for Vacuum and Solid Gap 61

5.3 Model Formulation for Solid and Vacuum Gap 63

5.3.1 Results and Discussion for Solid and Vacuum Gap 65

5.4 Summary 69

TABLE OF CONTENTS

6 SHOT NOISE REDUCTION IN SPACE CHARGE LIMITED (SCL) ELECTRON INJECTION THROUGH A SCHOTTKY CONTACT FOR A GaN DIODE **71**

6.1 Introduction 71

6.2 Model 74

6.3 Results and Discussion 77

6.4 Summary 83

7 CONCLUSION AND FUTURE RECOMMENDATIONS **86**

7.1 Conclusion 86

7.2 Recommendations for Further Research 89

AUTHOR'S PUBLICATIONS **91**

Bibliography **93**

A DERIVATION FOR 2D MG LAW FOR A PLANAR WIDTH 2D SHAPE **101**

B SOLVING EQUILIBRIUM 1D POISSON EQUATION IN MATRIX FORM **105**

C SOLVING 1D POISSON EQUATION COUPLED WITH CURRENT CONTINUITY EQUATION **108**

D LIST OF SYMBOLS **113**

ABSTRACT

Space charge limited (SCL) transport in solids involves high charge injections in which the amount of the charges injected into the solids is much larger than the thermal or intrinsic concentration of the solids. A two-dimensional (2D) analytical model of the space charge limited current (SCL) injection in a trap-free and a trap-limited solid will be developed. For a trap-limited solid, traps with exponentially distributed in energy is emphasized and studied. By considering the electrons are injected from an infinitely long emission strip of width W, the one-dimensional (1D) SCL current density is enhanced by a factor of $1+F\times(4/\pi)/(W/L)$, where $F=1/(l+2)$ measures the mean position of the injected electrons in a solid of length L, and l is the ratio of the distribution of the traps to the free carriers. The analytical formula is verified by using a 2D device simulator (Medici).

The thesis will also study a two-dimensional model of the space charge limited (SCL) current injection in a solid with a Schottky barrier at the injection interface. The injection of electrons is limited to the contact from thermionic emission and electron tunneling through the surface states. If thermionic emission through the barrier height dominates, SCL current is not reached and thus no enhancement in current is observed. But, if electron tunneling prevails over thermionic emission, SCL current is reached and the enhancement in current due to finite cathode size

ABSTRACT

is observed. The enhancement factor: $1+F \times G$, with $F = 1/3$ (for a trap-free SCL injection in a solid) and $G = (4/\pi)/(W/L)$ for an infinitely long emission strip of width W is again verified by using the device simulator including the effects of Schottky contact (positive barrier height for electrons).

In the thesis, a model of the SCL current injection inside a gap with a combination of both solid and vacuum between the cathode and anode will be developed. Both cases are presented whereby the electrons are passing through a vacuum gap and then solid, and vice versa. For a pure vacuum gap, the current density J will converge to Child-Langmuir (CL) law. For a solid diode, it will converge to Mott-Gurney (MG) law. In between, the scaling of n for current density J to the applied voltage V_G ($J \sim {V_G}^n$) is between $n = 3/2$ for CL law and $n = 2$ for MG law. Other parameters, such as electron mobility and gap spacing will also be studied.

Lastly, shot noise reduction in a solid associated with high charge current injection or SCL transport will be studied. A one-dimensional (1D) model of shot noise reduction of space charge limited (SCL) electron injection through a Schottky contact for a GaN diode is presented. The shot noise reduction due to both Coulomb repulsion and quantum partitioning is determined consistently where the former is due to the space charge electrostatic field created by the injected electrons, and the latter is due to the electron tunneling through the self-consistent potential profile near to the contact. The shot noise reduction is calculated in the form of Fano factor over a wide range of applied voltage for various values of Schottky barrier height, temperature, and length of the diode. At high voltage and high current regime, the shot noise suppression increases with large applied voltage, small diode length, low temperature, and small barrier height. The model also indicates that the distributed traps in a solid nearly have no effect to the shot noise reduction as compared to a trap-free solid.

LIST OF FIGURES

1.1 Band energy representation of metals, semiconductors, and insulators 2

2.1 Schematic simple set up of SCL transport in vacuum and solid 9

2.2 The injected electrons n_{inj} in the case of low injection and high injection level 12

2.3 Energy bands at thermal equilibrium with shallow traps 14

2.4 Energy bands at thermal equilibrium with deep traps 16

2.5 The plot of current-voltage relationship J vs V_G in a solid dielectric with deep traps in a log-log scale 17

2.6 Example of the SCL current measurement to extract traps information 21

2.7 Example of the current vs time ($I(t)$ vs t) plot in the normalized units 23

2.8 Examples of SCL current transport of the current-voltage characteristics in typical polymer Schottky diodes structure 25

2.9 Current-voltage characteristics for planar sandwich configuration of (a) $Au/pentacene/ITO$, (b) $Au/tetracene/Al$, and (c) $Au/pentacene/Al$ 27

2.10 Current I_D vs voltage V_D of CdS nanowire in log-log scale measured under different level of laser illuminations 28

List of Figures

2.11 The log-log plots of current vs voltage characteristic of two (square symbols with line) or ten (triangle symbols with line) embedded arrays of $\beta - FeSi_2$ nanocrystals 29

3.1 F as a function of β at various w_L 35

3.2 J vs V_G at $L = 100\ \mu m$ and $L = 200\ \mu m$ for trap-free solid 37

3.3 $\frac{J_{MG}[2D]}{J_{MG}[1D]}$ vs W/L at $L = 100\ \mu m$ and $L = 200\ \mu m$ for trap-free solid . 38

3.4 J vs V_G at $L = 10\ \mu m$ for a trap-filled solid of traps exponentially distributed in energy 39

3.5 $\frac{J_{TL}[2D]}{J_{TL}[1D]}$ vs W/L at $L = 10\ \mu m$ for a trap-filled solid of traps exponentially distributed in energy 40

4.1 J vs V_G for $L = 10\ \mu$m and $\mu_n = 10$ cm^2/V.s, $e\phi_b = 0$ to 1.08 eV with and without surface states 49

4.2 $\psi_n(x)$ vs x for $L = 10\ \mu$m, $\mu_n = 10$ cm^2/V.s, $V_G = 10$ kV, $e\phi_b = 0.13$ and 1.08 eV, with and without tunneling 51

4.3 J vs V_G for L=10 μm, $e\phi_b$=0.33 eV at varying n_i and μ_n 53

4.4 F vs V_G for $L = 10\ \mu$m and $\mu_n = 10$ cm^2/V.s, at varying $e\phi_b$ 55

4.5 $\frac{J_{MG}[2D]}{J_{MG}[1D]}$ vs W/L for $L = 10\ \mu$m and $\mu_n = 10$ cm^2/V.s at $V_G = 10$ kV and varying $e\phi_b$ 56

5.1 J vs V_G plotted in log-log scale for vacuum first and then solid 62

5.2 The exponential factor n of $J \sim {V_G}^n$ vs x_1 for vacuum first and then solid 64

5.3 J vs V_G plotted in log-log scale for solid first and then vacuum 66

5.4 The exponential factor n of $J \sim {V_G}^n$ vs x_1 for solid first and then vacuum 68

5.5 n vs $\epsilon_r \times \mu_n$ (in cm^2/V.s) plotted in linear-log scale 69

6.1 J-V_G in log-log scale for a GaN diode of L=10 μm and $\mu_n = 900$ cm^2/V.s 78

List of Figures

6.2 γ-V_G for GaN in linear-log scale at $L = 10$ μm and $\mu_n = 900$ cm^2/V.s 79

6.3 γ-$e\phi_b$ for GaN at $T = 300$ K 81

6.4 E_C vs x for GaN at $T = 300$ K and $\xi = 3$MV/cm 82

6.5 γ-$e\phi_b$ for GaN at $T = 300$K and fixed $L =$ (a) 10 μm for $V_G = 100$, 1kV, and 3 kV and (b) 100 nm for $V_G = 1$, 10V, and 30 V 84

A.1 The geometrical representation of the solid dielectric with length L and width W 102

CHAPTER 1
INTRODUCTION

1.1 Background

Charge transport in solid materials in general is characterized by the classification of its solid properties (insulators, semiconductors, and conductors) and by the source of charge injection such as: field injection (electric or magnetic field), light illumination, thermal excitation, etc. To begin with, the difference between insulators, semiconductors, and conductors was only known from their electrical conduction ability with conductors possessing the largest conduction and then followed by semiconductors, with insulators known of having very little or no ability to conduct electricity. Only after the emergence of the theory of quantum mechanics, Felix Blöch in 1928 provided a sound theoretical framework to understand the difference between these three classes of solids with his Blöch theorem. It provides the basis for the theory of the energy-band diagram in solids (see Fig. 1.1).

Every atom in a solid contains electrons that have their own atomic orbital which form discrete energy levels. The separation between each energy level is reduced as more atoms in a solid are brought together. With a large number of atoms that form

a solid, the separation becomes very small and forms a continuous band of energy. The lower energy band forms the valence band, which is occupied by the valence electrons and the upper band forms the conduction band which is unoccupied. When the valence electrons are excited to the conduction band, they will conduct current. The difference between conductors, semiconductors, and insulators lies within the "forbidden gap", or bandgap, between these two bands. In metals (conductors), the conduction band overlaps the valence band. The conduction band is partly filled and thus only a small excitation is required to trigger the electrical conduction. When a bandgap exists, more energy is needed to excite electrons to the conduction band. Since semiconductors have a much smaller bandgap than insulators, the former have a better conductivity.

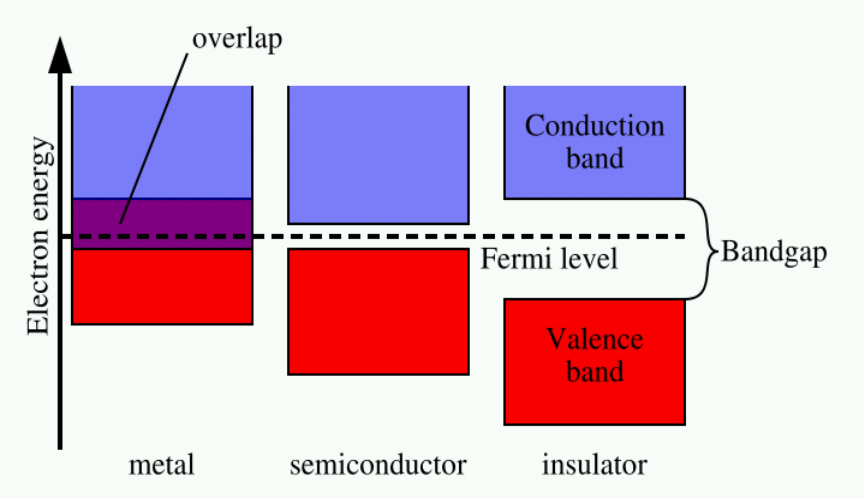

Figure 1.1: Band energy representation of metals, semiconductors, and insulators. In metals, there is an overlap between the conduction band and the valence band. In semiconductors, there is a small bandgap between the conduction and the valence bands. In insulators, there is a big bandgap separating the conduction and the valence bands.

In a quantum mechanical framework, the electrons in a metal can be described by a "nearly" free electron gas model of which the valence electrons of the constituent

atoms become conduction electrons and move freely through the volume of the metal. The weak perturbation of the electron movements comes from the periodic potential of ion cores. In contrary to metals, the Bragg reflection of electron waves in crystals creates the energy gap in semiconductors and insulators.

The development of the quantum theory in solids through the Blöch theorem opens up the possibilities of understanding the high charge current injection in solids which is not accessible before. Mott and Gurney in 1940 [1] made a pioneering work in high current injection in solids. In their work, they observed that it was possible to obtain injection of electrons from an Ohmic contact to an insulator, in a manner closely analogous to their injection from a thermionic cathode into vacuum which initially studied by Child and Langmuir [2, 3]. This high charge current injection is generally termed as *Space Charge Limited* (SCL) transport. The SCL current flow is limited to the maximum number of electrons injected from cathode to anode through the vacuum or solid gap until the electrons start to be reflected back to the cathode.

Although substantially similar in the underlying physics of the charge transport, the collisions and defects or imperfections in a solid create a somewhat different theoretical model than the regular SCL transport in vacuum or known as Child-Langmuir (CL) law. Immediately after the development of high charge current injection theory, also known as MG law in solids by Mott and Gurney, much research has been done by utilizing the MG law in various applications. The pioneering work of Mott and Gurney opens up the possibilities of many important applications in solid devices whereby SCL transport is the underlying mechanism in the principal of charge transport. The study of photoconductive materials was one of the first application that used the MG law extensively. Weimer and Cope studied amorphous selenium [4, 5, 6] and Forgue studied antimony trysulfide [7] to name just a few materials used for such purpose. By measuring the current-voltage relationship in the absence of illumination, the noise level is measured and observed for the corresponding

materials. The study of SCL photoconductive current has been done also under optical measurement by Rose and Lampert [8]. It was extended further by Goodman and Rose [9] to study the SCL photoconductive current in insulators with Schottky contact. The MG law was also used to study the traps in solid crystals by Smith and Rose using cadmium sulfide [10, 11, 12, 13], in semiconductors by Shockley and Prim [14] and Dacey [15], and in insulators by Lampert [16]. Measurement of SCL I-V characteristic of the materials is a relatively simple process and it has the ability of detecting traps at a very low concentration level. The occurrence of SCL current has also been observed in organic materials such as anthracene and p-terphenyl by Mark and Helfrich [17] with traps having exponentially distributed energy levels. Study of SCL current to investigate shot noise has also been done theoretically [18, 19, 20, 21] and experimentally [22, 23]. A more detailed description on the recent applications of SCL transport in solids will be reviewed in the next chapter.

1.2 Objectives and Contributions

The objectives and major contributions of this research are as follows:

Firstly, there are extensive and great amount of ongoing developments on using novel 2D structures in various applications such as: polymer Schottky diodes, organic semiconductors, OLED (organic light-emitting diodes), nanocrystals and nanowires. It has been reported that these materials are operating in SCL trap-free and SCL trap-filled regime [24, 25, 26, 27, 28, 29, 30, 31, 32, 33, 34, 35, 36, 37]. These novel devices typically have a very small contact size in which the width and length are comparable. The traditional 1D SCL current model in solids only accounts for 1D limit whereby the width is much longer than the length of the SCL transport direction. The understanding of the size effect especially when the width of the contact or cathode (electron injection) becomes comparable to the length of the dielectric in the

1.2 Objectives and Contributions

SCL transport in solids has been lacking. In this report, the study of size effect and how it will affect the current enhancement will be shown. The effect of various types of charge traps are also considered. The 2D model of MG law has been published in paper #1 in the author's publications list.

Secondly, in SCL transport, the current flow is determined by the bulk properties of the solid dielectric. However, this is only true if the contact effect is neglected, meaning that the solid dielectric and the cathode are able to form a good Ohmic contact which can provide unlimited supply of electrons. However, a good Ohmic contact is not always possible due to the difficulties in experimental preparations or the intrinsic properties of the solid. In this case, the injection of electrons from cathode to the solid dielectric depends on the property of the contact between the cathode and the dielectric. Whether, it is an Ohmic or a Schottky contact, it will affect the amount of electrons to be injected and thus affect the formation of SCL current. Detailed studies on the interplay between the effects of contact and size to the injection mechanism will be discussed. For simplicity, only unipolar or electron injection is considered. Therefore, there is no recombination in the bulk of the dielectric. The results of this topic have been published in paper #2 in the author publications list.

In a recent Scanning Tunneling Microscope (STM) experiment, it has been reported that the current-voltage characteristic of the sample is at the SCL regime [38] and the $I-V$ curve neither follows pure MG law nor pure CL law. A theoretical model will be developed for such a system with both vacuum and solid dielectric in the gap. With different parameters such as: mobility and length of device, the amount of SCL current in between the CL law (in vacuum) and MG law (in solid) will be shown. Our proposed new model has been published as paper #3 in the author's publications list.

Finally, the shot noise reduction for SCL transport in a solid will be investigated. While classical Coulomb correlation has been well-known to suppress the shot noise

in SCL transport in solids, it is important to know the comparable amount of the suppression due to quantum partitioning as a result of a finite contact barrier. With the presence of a Schottky contact that typically exists in real devices, it will be interesting to quantify the shot noise suppression. A detailed study over a wide range of Schottky barrier height, temperature, length of the device, applied voltage, and also in the presence of traps in a solid will be shown. This final topic of the thesis has been published as paper #4 in the author's publications list.

1.3 Organization of the Report

In Chap. 2, a short review of the theory of SCL transport in vacuum and in solids is given. The typical models of SCL transport in solids at different kinds of charge traps are presented. Some of the applications of using SCL current-voltage data to extract information of the traps will also be presented. In Chap. 3, the transition from SCL transport in vacuum (CL law) to SCL transport in solids (MG law) together with its enhancement due to 2D effect will be studied. In Chap. 4, the effect of non-injection contact and the interplay with the addition of surface states to the SCL current in solids will be explained. In Chap. 5, a new theoretical SCL current model will be developed by taking into the account of both free space and solid in the gap. The model will be able to predict the current-voltage relationship in the gap with a mixture of both CL law (in free space) and MG law (in solid). It is also able to explain an experimental finding [38]. In Chap. 6, the simulation study of SCL current with shot noise in solids will be shown. The effect of different degree of reduction of shot noise arises from various effects such as: traps, barrier height, temperature, and length of the semiconductor diode will be shown and explained. The conclusion of the thesis and the direction of future work and recommendations will be discussed in Chap. 7. In addition, we have added the details of the 2D boundary conditions we

1.3 Organization of the Report

used in Chap. 3 and Chap. 4 in Appendix A. Appendix B and C shows the details of the numerical codes we used in solving the equations in Chap. 4 and Chap. 4. For easy reference, we have put all the symbols and the definitions that we have used throughout this thesis in the list of symbols in Appendix D.

CHAPTER 2
LITERATURE REVIEW

In 1911, C. D. Child published a paper on the discharge mechanism in a vacuum tube from a hot cathode (CaO) [2]. In his experiment, he created a setup that consists of a vacuum tube with iron anode and hot platinum covered with CaO as cathode. He made the observations that once the potential difference between the electrodes is increased beyond a threshold point, the current becomes very much greater and the discharge becomes luminous seen as streams of cathode rays. The phenomena can be explained by assuming that as soon as the electric field is high enough to ionize the gas and create the positive ions, the positive ions bombard the surface of the cathode and produce impact ionization. Hot cathode enhances such ionization due to their high temperature, they are already in unstable equilibrium by sending out electrons even when not being bombarded. The higher the number of positive ions formed in the gas, the higher the number of positive ions that are bombarding the cathode. As a result, the corresponding number of electrons increase even further. Therefore, this positive feedback process creates the required amount of space charge resulting in a sudden increase of current.

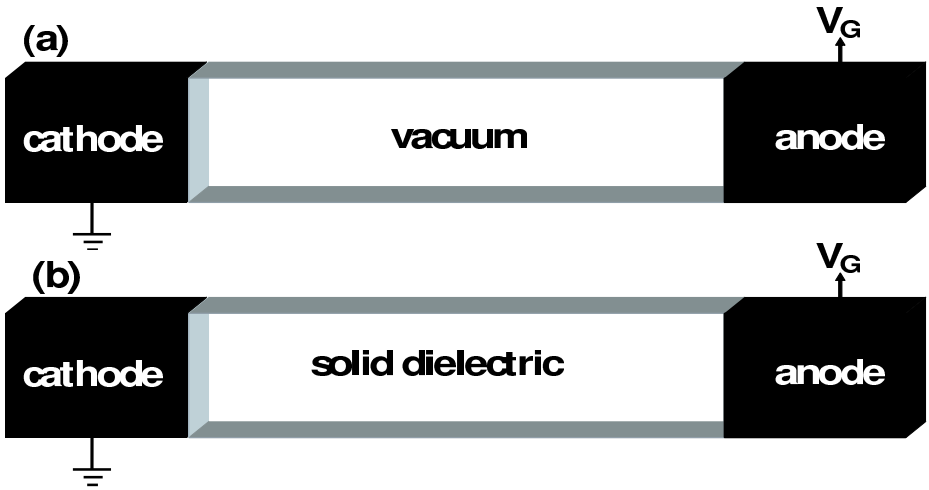

Figure 2.1: Schematic simple set up of SCL transport in (a) vacuum and (b) solid with length L between a cathode and an anode biased at a potential bias V_G

In 1913, Irving Langmuir, independently, also published a paper studied in details on the effect of space charge in vacuum by thermionic current [3]. Both Child and Langmuir basically studied the *very* same space charge effect in vacuum and obtained the same formula and thus the formula for SCL electron current density in vacuum is called the Child-Langmuir (CL) law, which is in the form of:

$$J_{CL} = \frac{4\epsilon_0}{9}\sqrt{\frac{2e}{m_e}}\frac{V_G^{3/2}}{L^2}. \tag{2.1}$$

Here, L is the vacuum gap spacing between cathode and anode, V_G is the applied bias or the gap voltage, ϵ_0 is the free space permittivity, e and m_e are the electronic charge and free electron mass, respectively (see Fig. 2.1a).

The study of SCL current injection in vacuum has inspired the study of SCL current in solids, which were pioneered by Mott and Gurney in 1940. For SCL transport in solids, the gap with length L between the cathode and anode consists of a solid dielectric material instead of vacuum or free space (see Fig. 2.1b). The voltage drop in the medium is contributed by the electrons that are injected from the cathode. If the number of electrons injected are significantly larger than the intrinsic

or thermal concentration of the medium, we will have the SCL conduction in solids. Mott and Gurney derived a formula also known as Mott-Gurney (MG) law for the SCL conduction in solids, given by [1, 39]:

$$J_{MG} = \frac{9}{8}\mu_n \epsilon_r \epsilon_0 \frac{{V_G}^2}{L^3}. \tag{2.2}$$

Here, ϵ_r is the relative or dielectric permittivity , and μ_n is the drift electron mobility. Both CL law and MG law in vacuum and in solid are derived from the Poisson equation and current continuity condition. The difference for the derivation comes from the physics governing the velocity of electrons inside the medium.

The CL law has V_G to the 3/2 power and L to the -2 power ($J_{CL} \sim {V_G}^{3/2}/L^2$) while the MG law has a power of two to V_G and a power of minus three to L ($J_{MG} \sim {V_G}^2/L^3$) . The difference arises from the frequent collisions of the electrons in the conduction band with thermal vibrations (phonons) and with the impurities or other structural imperfections in a solid. In vacuum, the velocity of electrons is derived from the Newton's law of motion with the force coming from electrical force. The velocity of electrons is a function of the electrical potential due to energy conservation, $\frac{1}{2}m_e v^2 = e\psi_n$, with ψ_n is the electron potential applied to the system. In solids, the velocity of electrons is limited to the mean free path or the average traveling distance between the abovementioned collisions, and is a function of electric field along the solid dielectric controlled by the electron mobility v = -$\mu_n \xi$.

Another important consequence of collisions in a solid dielectric is the unavoidable presence of traps. The traps exist in a solid, especially, in semiconductor and insulator, which will reduce the current flow since those traps will capture and thereby immobilize most of the injected carriers.

In the following sections, SCL transport mechanism in solid is described in the following cases: (a) a trap-free solid, (b) a solid with single energy level of shallow traps, (c) a solid with single energy level of deep traps, and (d) a solid with multiple

energy levels of traps distributed exponentially. Furthermore, the extraction of traps information from the measurement of steady state and transient SCL current in solid will also be shown.

2.1 MG law for SCL Transport in a Trap-free Solid

Mott-Gurney (MG) law is derived originally to account for SCL transport in a dielectric such as ionic crystals. It is necessary to understand why SCL transport is not possible in metals (conductors) by simply using the concept of *dielectric relaxation*. From basic electromagnetic theory, it is well known that a conducting material cannot support any free charge that is not compensated by an equal and opposite charge. Therefore, if some free charges are injected into the material, they must be neutralized by mobile carriers either from the material boundary or from a charge reservoir. This process known as the *dielectric relaxation* and it occurs within a finite amount of time τ_r, known as the dielectric relaxation time. From electromagnetic theory, it can be derived that the dielectric relaxation time is $\tau_r = \epsilon_r\epsilon_0/\sigma$ where σ is the electrical conductivity of a material. Since metals usually have high electrical conductivity, they have a small value of τ_r while the values are much larger in semiconductors and insulators.

Another important quantity besides the dielectric relaxation time is the transit time T_r, which is the amount of time needed by the injected charges to be transported across the dielectric of length L. The value is simply the distance for the charges to travel across a solid divided by the velocity of the charges, $T_r = L/v$. By neglecting the diffusion current contribution to the total current, v is the drift velocity, $v = \mu\xi$ where ξ is the average electric field, $\xi = V_G/L$. Hence, the value of transit time T_r inversely proportional to the applied voltage V_G.

2.1 MG law for SCL Transport in a Trap-free Solid

The ability of solid materials to achieve SCL transport depends on the relative values between τ_r and T_r. When V_G is small, the transit time T_r is large. If $\tau_r < T_r$, the dielectric has fast enough time to balance the amount of injected charges before they travel across the dielectric length L. Hence, there will be *no accumulation of space charge*. At this low level of injection, the injected electrons are much lower than the thermal or intrinsic electron concentration of a solid dielectric ($n_{inj} \ll n_i$), the current transport follows Ohm's law. However, as the amount of injected charges is increased (equivalent as increasing V_G), the value of T_r starts to decrease. At $\tau_r > T_r$, there will be *accumulation of space charge*. At such high injection level, the amount of injected electrons is much larger than the intrinsic concentration of the solid dielectric ($n_{inj} \gg n_i$), the transport mechanism follows the MG law. Hence, this is the reason to have SCL current flow at relatively high voltage bias. The typical example of low level injection and high level injection are shown in Fig. 2.2.

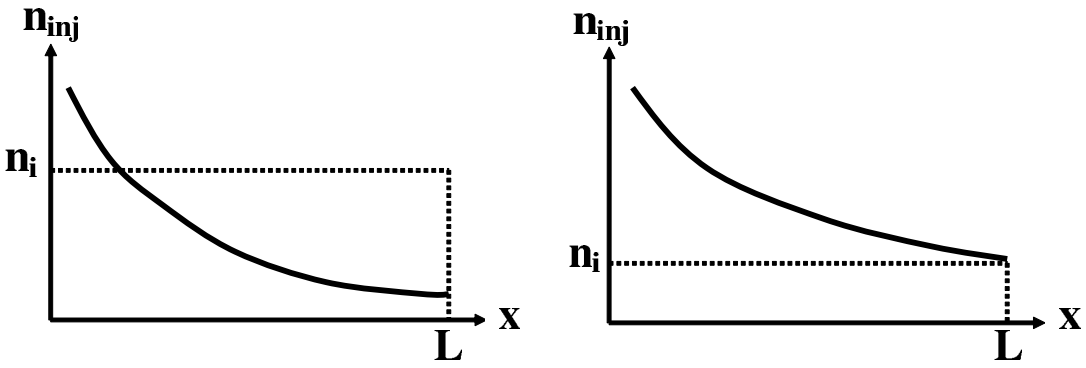

Figure 2.2: The injected electrons n_{inj} in the case of (a) low injection level with the injected electrons $n_{inj} \ll n_i$ and (b) high level of injection with the injected electrons $n_{inj} \gg n_i$

The transition voltage from Ohm's law to MG law can be calculated by considering the amount of charge injected is equal to the intrinsic or thermal concentration. With the total number of charge per unit area $Q = en_iL$ where n_i is thermal or intrinsic electron concentration, and also from Gauss law, $Q =$

$\epsilon_r\epsilon_0\xi \approx \epsilon_r\epsilon_0 V_{\Omega-MG}/L$ where E is the applied electric field. Hence, the transition voltage from Ohm's law to MG law is $V_{\Omega-MG} = en_iL^2/\epsilon_r\epsilon_0$. Below the transition voltage, with the amount of injected electrons is much smaller than the intrinsic concentration n_i, the current transport follows Ohm's law. Above the transition voltage, with the injected electrons are much higher than the intrinsic concentration n_i, the current transport follows MG law.

In summary, the derivation of MG law is based on the following assumptions: (a) diffusion current component is neglected (drift current dominates the total current), (b) the contact responsible for the charge injection is an Ohmic contact, (c) the amount of injected charge is much larger than the intrinsic concentration of the dielectric, and (d) there are no traps at the interface with the contact and in the bulk of dielectric. The first assumption is valid since the drift component dominates over the diffusion component when the applied bias $V_G \gg k_bT/e$ (thermal voltage) or $L \gg$ the diffusion length. The second assumption guarantees the contact can supply unlimited amount of charge into the dielectric and there is no voltage drop across the contact. The third assumption is explained by the illustration of transit time T_r and dielectric relaxation time τ_r. The fourth assumption will be studied in the next section for a review of the trap-limited MG law.

2.2 SCL Transport with Shallow Traps

The study of SCL transport in solids was extended by Rose in 1951 and 1955 [10, 11] by incorporating the effect of traps into dielectrics. Mott and Gurney provided the foundation for the theory of SCL current in solids but in actual materials, traps such as localized electronic states associated with impurities and structural imperfections are inevitably present. The amount of injected SCL current is lowered by the traps since the traps will capture and immobilize the injected carriers. In this section,

2.2 SCL Transport with Shallow Traps

SCL transport with shallow traps is elaborated. For the sake of argument and easy illustration, the transport carrier is assumed to be electrons.

Traps at energy E_t are shallow when the energy level of the traps E_t lies below bottom of the conduction band E_C and above the quasi Fermi level E_F, that is: $\frac{E_t - E_F}{k_b T} > 1$. Figure 2.3 shows an example of shallow traps at thermal equilibrium. At thermal equilibrium, the solid is in steady state and there is no external field applied to the material. Therefore, the Fermi level is called the equilibrium Fermi level, E_{F0}. At this condition, there is no current flowing to the solid and the Fermi level is flat. When some external bias is applied to the solid, the Fermi level is not flat and it is called as the quasi Fermi level, E_F. The quasi Fermi level is always above the equilibrium Fermi level, E_{F0}, since with more electrons flowing to the solid, the Fermi level will increase. In this example, the thermal equilibrium condition is used to give clearer and simpler picture to understand the concept.

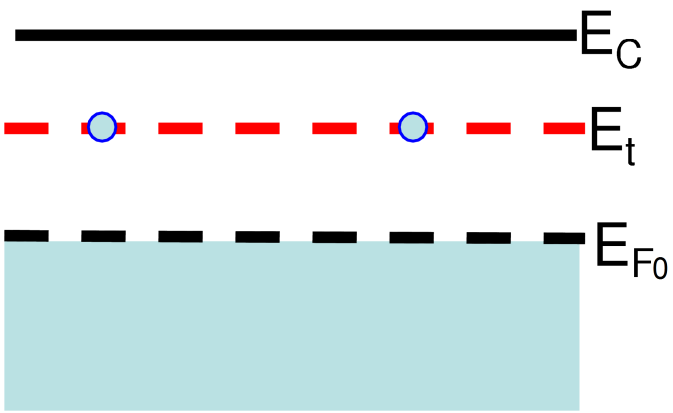

Figure 2.3: Energy bands at thermal equilibrium with shallow traps. The traps at energy level E_t are mostly empty of electrons

The derivation for the SCL transport follows the same procedure as the trap-free SCL model with one exception, the amount of free electrons that contributes to the total current is now reduced since some of them are trapped at shallow traps at

energy level, E_t. From the Fermi-Dirac distribution, the free electron concentration is expressed by:

$$n_f = N_C exp[(E_F - E_C)/k_b T], \tag{2.3}$$

where n_f is the free electron concentration and N_C is the effective density of states at conduction band E_C. While the filled electron trap concentration at energy E_t is expressed by:

$$n_t = N_{t0} exp[(E_F - E_t)/k_b T], \tag{2.4}$$

where n_t is the filled electron traps concentration at energy E_t and N_{t0} is total concentration of traps. The amount of SCL current density in solid in the presence of single energy level of traps E_t is given by:

$$J_{shallow} = \frac{9}{8}\left(\frac{\theta}{\theta+1}\right)\mu_n \epsilon_r \epsilon_0 \frac{{V_G}^2}{L^3}. \tag{2.5}$$

Here, $\theta = n_f/n_t$ measures the proportion of free electrons to the filled electron traps. Note that θ is a constant value, independent of injection level since the value depends only on the ratio of N_C/N_{t0} along with the difference between E_C and E_t. The value of the coefficient, $\frac{\theta}{\theta+1}$, in Eq. 2.5 can be simplified further depending on the relative amount of traps inside the solid materials. If there are large number of traps then the coefficient is approximately theta ($\frac{\theta}{\theta+1} \approx \theta$) since theta is much smaller than one ($\theta << 1$). However, if there are negligible amount of traps, then the coefficient is approximately one ($\frac{\theta}{\theta+1} \approx 1$) since theta is much bigger than one ($\theta >> 1$). The formula in Eq. 2.5 will recover to the trap-free MG law (see Eq. 2.2). The transition voltage from Ohm's law to SCL-MG with shallow traps is also scaled up with the same factor, namely, $V_{\Omega-shallow} = en_i L^2/\epsilon_r \epsilon_0 \left(\frac{\theta}{\theta+1}\right)$. Thus, the SCL current is significantly reduced when there are large number of traps ($\theta << 1$) and the transition voltage to reach SCL transport with shallow traps is increased. If there are several sets of shallow trap levels in the solid materials, the set with the smallest θ will dominate the current flow and this minimum value of θ will be the one to be used in Eq. 2.5.

In the next section, we will discuss on the effect of a single energy level with deep traps to the SCL current.

2.3 SCL Transport with Deep Traps

In the case of electron traps, traps are defined as deep traps when E_t lies below E_F and E_C, that is: $\frac{E_F - E_t}{k_b T} > 1$. Figure 2.4 shows an example of deep traps at thermal equilibrium.

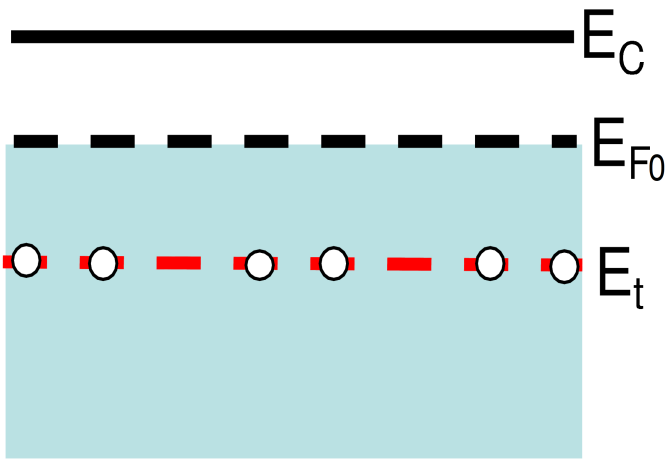

Figure 2.4: Energy bands at thermal equilibrium with deep traps. The traps at energy level E_t are mostly filled of holes.

Using the Fermi-Dirac expression, the concentration of traps unoccupied by electron or hole occupancy of traps in thermal equilibrium, can be expressed as follows:

$$p_{t0} = N_{t0} exp[(E_t - E_{F0})/k_b T]. \tag{2.6}$$

where $p_t 0$ is the occupied hole (unoccupied electron) trap concentration at energy E_t in thermal equilibrium. In the case of a solid with deep traps, electrons injected into a solid will fill these unoccupied electron traps. The transition voltage from Ohm's law to MG law with deep traps occurs at $V_{TFL} = V_{\Omega - deep} = e p_{t0} L^2 / \epsilon_r \epsilon_0$. The example

of current vs voltage relationship in the presence of deep traps at SCL injection in a solid is shown in Fig. 2.5.

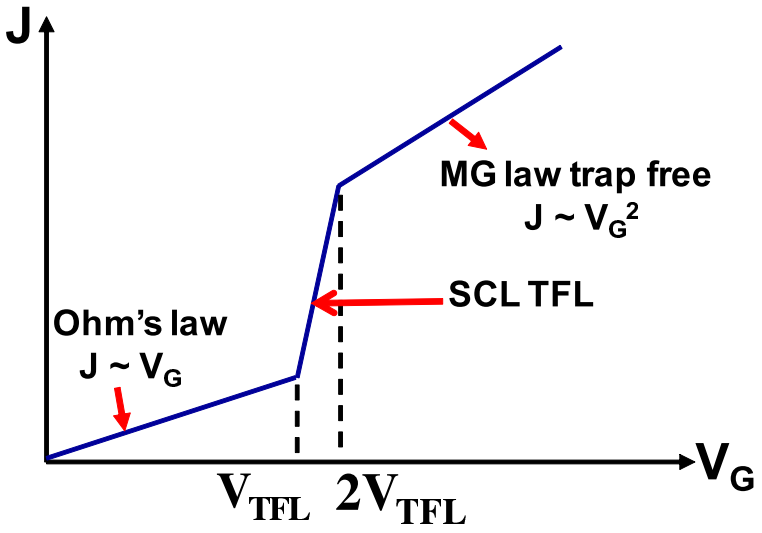

Figure 2.5: The plot of current-voltage relationship J vs V_G in a solid dielectric with deep traps in a log-log scale. The filling of deep traps happens at V_{TFL} to $2V_{TFL}$ indicated with a steep increase in current. Below V_{TFL}, current conduction follows Ohm's law. Above $2V_{TFL}$, current conduction follows MG law trap-free

At low level injection, with the amount of electrons injected is still much lower compared to the intrinsic concentration, the current-voltage relationship follows Ohm's law since there are inadequate free electrons to fill the deep traps at energy level E_t. When the injected electrons become comparable with thermal or intrinsic concentration n_i, the injected electrons are filling up the deep traps at the transition voltage $V_{\Omega-deep}$. That is why the transition voltage is also called the trap-filled limit voltage or V_{TFL}. At this point, there is no accumulation of space charge and there is a sudden steep increase in current until all the deep traps are filled at approximately two times the value of trap-filled limit voltage ($2V_{TFL}$). This phenomenon is important since it is normally misinterpreted experimentally as breakdown phenomenon due to a steep rise in the current at trap-filled limit voltage. Beyond $2V_{TFL}$, the current

follows the MG law trap-free again since all the deep traps have been filled and the free electrons go into the conduction band and contribute to current due to the regular accumulation of space charge.

2.4 SCL Transport with Distributed Energy Levels of Traps

For single-crystal materials with high chemical and structural purity, single energy level of traps E_t is a good approximation to analyze and study the SCL injection as in many cases of semiconductors, which have a crystalline or at least a polycrystalline structure. However, it is common in vitreous or amorphous materials such as insulators, to possess either no or short range order of periodicity. In these materials, because of the large degree of structural disorder, there will be a lot of trap sites with different energy levels. To represent these sets of traps, traps with an exponential energy distribution provide good insight. It is initially studied by Rose [10, 11] and then Mark and Helfrich in 1962 [17] who derived the SCL current formula analytically with traps exponentially distributed in energy.

For an exponential distribution in energy level of traps, the density of traps per unit energy range E can be expressed as follows;

$$N_t(E) = (N_{t0}/k_bT_t)exp[(E - E_C)/k_bT_t], \tag{2.7}$$

where $N_t(E)$ is the concentration of electron traps per unit energy range, N_{t0} is the total electron traps density, T_t is the characteristic temperature to characterize the trap distribution (the shape of the trap profile as a function of energy). The total number of filled electron traps n_t are calculated by integrating $N_t(E)$ with respect to dE from $E = -\infty$ to $E = E_F$. If the quasi Fermi level E_F is far enough from the equilibrium Fermi level E_{F_0}, the range of integration can be approximated from

2.4 SCL Transport with Distributed Energy Levels of Traps

$E = E_{F_0}$ to $E = E_F$ and thus the total number of electron traps n_t can be calculated to be:

$$n_t = \int_{-\infty}^{E_F} N_t(E)dE \approx \int_{E_{F_0}}^{E_F} N_t(E)dE,$$

$$n_t = N_{t0}\Big\{exp[(E_F - E_C)/k_bT_t] - \big(\frac{n_i}{N_c}\big)^{T/T_t}\Big\},$$

By assuming that $T_t > T$ and $n_t > n_f$ (equivalent to the case in which there are large number of traps to influence the behavior of SCL current), the second term in the n_t expression $\Big[\big(\frac{n_i}{N_c}\big)^{T/T_t}\Big]$ is negligible so the total number of traps can be simplified to be $n_t = N_{t0}exp[(E_F - E_C)/k_bT_t]$. Using $n_f = N_Cexp[(E_F - E_C)/k_bT]$, the relation between free and trapped electron concentration can be found, given by:

$$n_f = \frac{N_C}{{N_{t0}}^l}{n_t}^l, \tag{2.8}$$

where $l = T_t/T$. By following the same procedure to derive MG law in a trap-free solid by solving Poisson and drift current density equation, with the exception of putting in the expression for n_f as in Eq. 2.8, the analytical form of the SCL current can be shown to be:

$$J_{TL} = N_c\mu_n e^{1-l}\Big[\frac{\epsilon_r\epsilon_0 l}{N_{t0}(l+1)}\Big]^l\Big(\frac{2l+1}{l+1}\Big)^{(l+1)}\frac{{V_G}^{(l+1)}}{L^{(2l+1)}}. \tag{2.9}$$

The transition voltage from Ohm's law to trap-limited or $V_{\Omega-TL}$ and transition voltage from trap-limited to MG law or V_{TL-MG} can be calculated again based on the charge consideration setting n_t equal to n_i for $V_{\Omega-TL}$ and n_f equal to n_t for V_{TL-MG}. The expressions for the two transition voltages are given below:

$$V_{\Omega-TL} = \frac{en_iL^2}{\epsilon_0\epsilon_r}\Big(\frac{l+1}{2l+1}\Big)^{[(l+1)/l]}\frac{l+1}{l}\Gamma, \tag{2.10}$$

$$V_{TL-MG} = \frac{en_iL^2}{\epsilon_0\epsilon_r}\Gamma^l\Big[\frac{9}{8}\Big(\frac{l+1}{l}\Big)^l\Big(\frac{l+1}{2l+1}\Big)^{l+1}\Big]^{[1/(l-1)]}, \tag{2.11}$$

where $\Gamma = \frac{N_{t0}}{n_i}\Big(\frac{n_i}{N_c}\Big)^{1/l}$.

The characteristic or the shape of the traps distribution depends on the value of T_t. If $T_t < T$, the empty traps at the top of the distribution, near the conduction

band, always dominate those near the quasi Fermi level and the trap distribution varies rapidly with energy. Therefore, the analysis reduces to the shallow traps case. If T_t is large enough and $E_F - E_{F0} > k_b T_t$, the traps has a slow varying distribution. In this case, the trap distribution can be approximated with an uniform distribution, $N_t(E) = (N_{t0}/k_b T_t) exp[(E_{F0} - E_C)/k_b T_t] =$ constant. The total number of electron traps n_t can be calculated to be:

$$n_t = (N_{t0}/k_b T_t) exp[(E_{F0} - E_C)/k_b T_t](E_F - E_{F0}). \tag{2.12}$$

Using $n_f = n_i exp[(E_F - E_{F0})/k_b T]$, and by following the same procedure as in the traps exponentially distributed in energy, the SCL current formula can be found and is expressed as below:

$$J_{UN} = 2en_i\mu\frac{V_G}{L} exp\Big[\frac{2\epsilon_0\epsilon_r V_G}{(N_{t0}/k_b T_t) exp[(E_{F0} - E_C)/k_b T_t] k_b T e L^2}\Big]. \tag{2.13}$$

2.5 Applications of SCL Current in Solids

The study of SCL transport or high current injection in solids is useful to study traps in insulator. Many information about the nature of the traps such as the traps concentration, traps energy level inside the bandgap, etc can be deduced relatively simply and with great accuracy from the steady state and transient SCL current measurement. What we mean by great accuracy here is that the information of the traps can be extracted by using more than one independent methods that ensures the credibility and consistency of the result. One example of using experimental SCL measurement to find the information of traps is shown in Fig. 2.6.

The log-log plot of J vs V_G in Fig. 2.6 shows the current-voltage characteristic of a typical SCL measurement for an insulator (very low n_i) with a single set of shallow electron traps. At low injection level (low voltage bias V_G), the current conduction follows Ohm's law. With increasing applied bias V_G beyond the transition voltage,

$V_{\Omega-shallow}$, the current conduction goes into SCL-MG with shallow electron traps. As V_G is further increased, the electrons fill up all the shallow traps. The current jumps up and goes into SCL-MG trap-free regime. The value of trap-filled limit voltage V_{TFL} gives directly the concentrations of the shallow electron traps N_{t0}. The quantity of the displacement, D, in the current density vs voltage curve (see Fig. 2.6) between SCL-MG trap-free and SCL-MG with shallow traps regime gives the value of θ $(E_C - E_t)$. Assuming all the material-dependent parameters of an insulator are known, such as L, ϵ_r, N_C, the energetic location of the shallow traps (E_t - E_C) relative to the conduction band E_C can be found since $\theta = n_f/n_t = \frac{N_C}{N_{t0}} exp[-(E_C - E_t)]$. The value of θ can also be found from the transition voltage from Ohm's law to SCL-MG with shallow traps regime $V_{\Omega-shallow}$ although it is less practical than using the parameter D, as shown in Fig. 2.6.

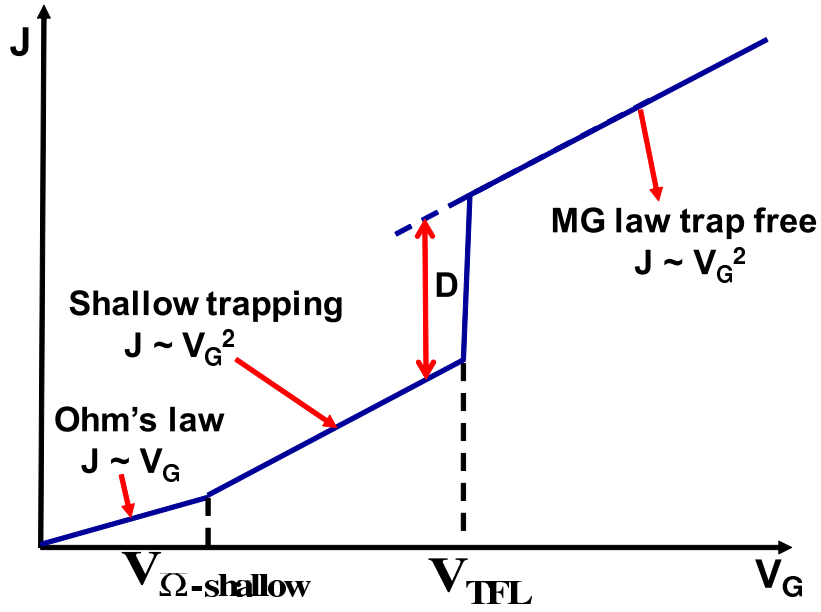

Figure 2.6: Example of the SCL current measurement to extract traps information for J vs V_G in log-log scale with a single set of shallow traps

Another example of determination of E_t in a case of shallow traps by conducting an experiment to measure the current-voltage characteristic of a solid can be done by

using a slightly different technique. In this method, the value of θ can be found first from the plotting of J vs V_G in log-log scale. In doing so, the plotting of ln θ vs $1/T$ will be a straight line with a slope of $(E_t$ - $E_C)/k_b$ and the intercept at $1/T = 0$ is ln (N_C/N_{t0}). Hence, the values of N_C and E_t can be found afterwards. This method has been frequently used than method in the first example due to its flexibility. The method is able to find the value of the effective density of states in the conduction band N_C (for electron transport) or the value of the effective density of states in the valence band N_V (for hole transport) if the values are not known beforehand. The value of the total traps concentration N_{t0} can still be found directly from the trap-filled limit voltage (V_{TFL}). Thus, this method has been widely used to extract the traps information from the experimental J vs VG curve for electron and hole SCL transport in many solid materials such as: CdS [40, 41], ZnTe [42], Se [43], I [44], etc.

In the case of traps with an exponential distribution in energy, the characteristic temperature T_t can be found from the plot of J vs V_G in log-log scale. If the mobility μ_n and N_C (for electron transport) or N_V (for hole transport) are known, the traps concentration N_{t0} can be found. This method has been used to determine the effective density of states of holes in the valence band N_V of anthracene which fits the description of traps exponentially distributed in energy [45, 46, 47].

The transient measurement of SCL current is also able to provide information of the free-carrier capture cross section for a trap and the thermal-release frequency for a trapped carrier [44, 13, 48, 17, 49, 50, 51, 52, 53, 54, 55, 56]. One example of the transient SCL current measurement to extract the traps information can be seen from Fig. 2.7 which has been studied by Many and Rakavi [44].

The figure shows different shape of transient current $I(t)$ over time in the normalized units after the application of a step function of voltage. The upper curve shows the typical transient current curve in the case of a trap-free insulator and the lower curve shows the transient current curve for an insulator with traps. At time

$t = 0$, there is an initial current since the electrons are injected into the insulator. The current increases until the leading front of the voltage step function reaching the anode. The peak of the current shows the maximum space charge injected into the insulators. From the peak current at time $t = t_1$ or t_2, the transit time, T_r of the insulators can be found which directly gives the mobility value of the insulator. Furthermore, the decaying part of the current near $t = t_3$ gives the trapping time information.

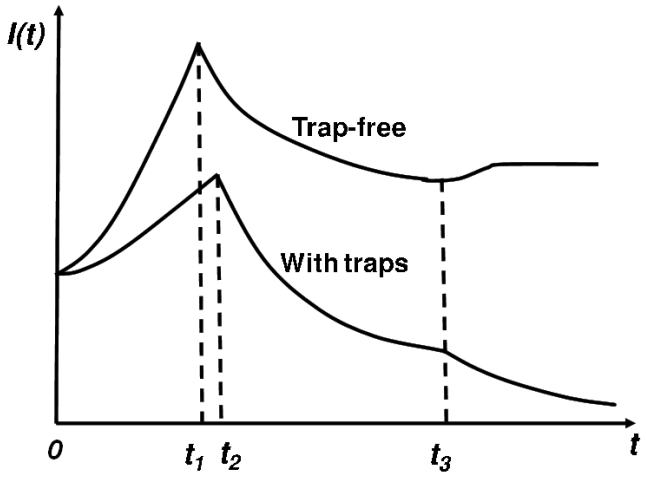

Figure 2.7: Example of the current vs time ($I(t)$ vs t) plot in the normalized units. The upper curve shows the example of typical transient current response over time in an insulator without traps and the lower curve shows the transient current for an insulator with traps. The peak of transient current response is at $t = t_1$ for trap-free case and it is at $t = t_2$ in insulator with traps

When the insulator is trap-free, there is no decaying part and the value of the transient current is constant over time since the electrons from the current do not interact with any traps (see upper curve). The initial current keeps increasing until it reaches its peak value at $t = t_1$. Between $t = 0$ to $t = t_1$, more space charges are flowing into the insulator due to the leading front of the step function voltage

bias being applied to the insulator. After $t = t_1$, the current starts to decay since more spaces charges flowing out than flowing into the insulator. Since the insulator is trap-free, there will be no trapping, thus the current reaches a constant steady state value.

If there are traps in the insulator, the decaying part over time can be measured and it gives the trapping time value for the insulator (see bottom curve). The peak current happens at slightly longer time than the time for the trap-free case ($t = t_2$) since in the trapping case, more charges are trapped near the injecting electrode, thus more time is needed to reach the peak value. After the current reaches its peak value, it starts to decay. The trapping time can be calculated from the decaying amount after the current reached its peak from the release rate of the traps.

Nowadays, in many novel devices, the current transport mechanism is governed by SCL transport. Due to the small intrinsic concentrations n_i and small size of the device, the current transport has been reported to be operating in the SCL transport regime. Some of the examples will be discussed to show the J vs V_G curves for SCL-MG transport in a solid with trap-free, shallow traps, and also traps exponentially distributed in energy. In a polymer Schottky diode structure, many studies have reported SCL conduction in the device [24, 25, 26, 27, 28, 29]. The typical structure consists of a conjugated polymer sandwiched in between two electrodes. One of the contacts is typically an Ohmic contact and the other contact is a Schottky or rectifying contact. Gold (Au) is usually used to form Ohmic contact with the conjugated polymer and aluminium (Al) as a rectifying contact with the polymer. Much of the studies have been focusing on the effect of adding dopants to the polymer such as oxygen and how it affects the rectifying properties of the structure [29, 57]. Other studies have been focusing on the electric field dependence mobility ($\ln \mu \propto \sqrt{\xi}$) and temperature dependence mobility of such structure ($\ln \mu \propto 1/T$) [28]. Some of the

examples of the current-voltage characteristics of polymer Schottky diodes showing SCL transport are shown in Fig. 2.8.

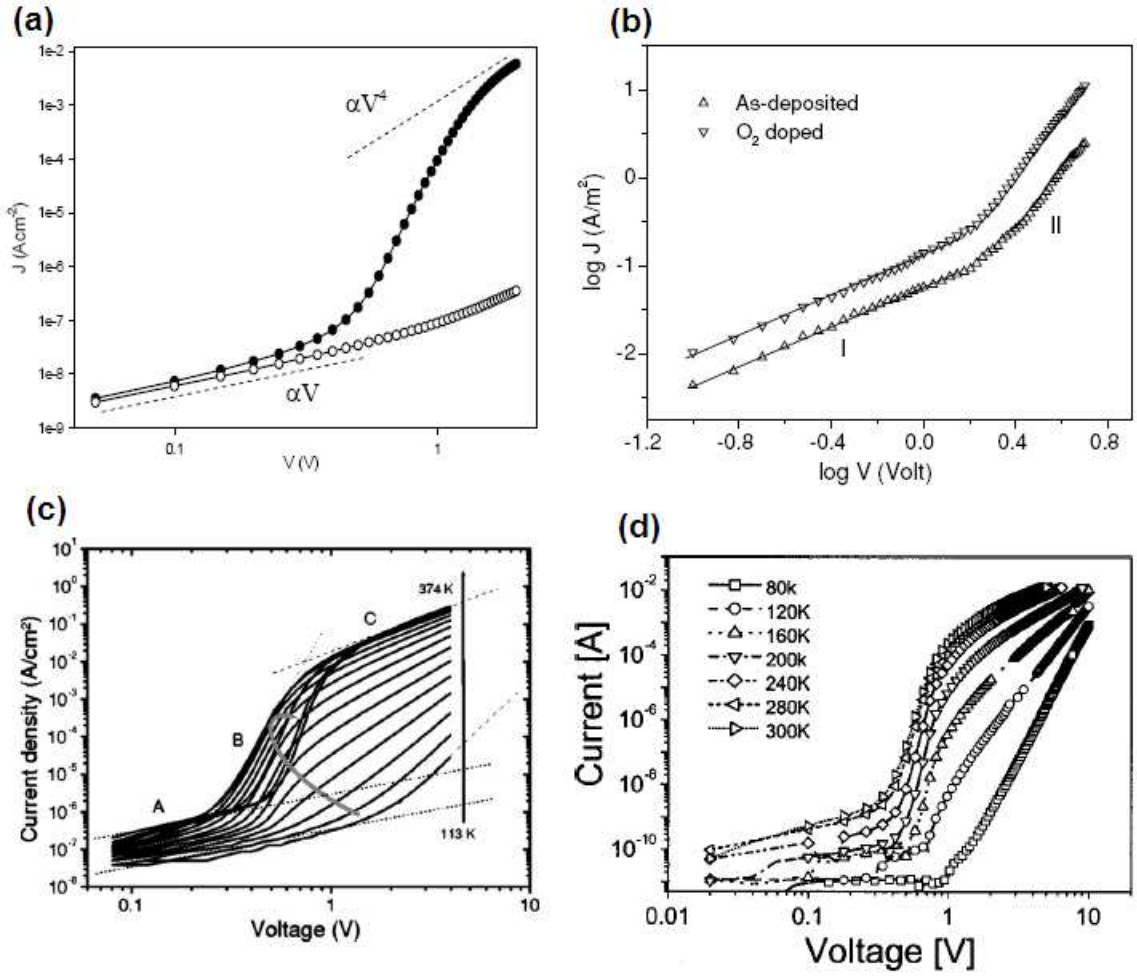

Figure 2.8: Examples of SCL current transport of the current-voltage characteristics in typical polymer Schottky diodes structure in the case of (a) $Al/P3MT/Au$ [24], (b) $Al/AlPcCl/Au$ [29], (c) $Al/P3HT/ITO:PEDOT$ [26], and (d) $Al/P3HT/ITO$ [27]

Figure 2.8 shows the forward current curve versus the applied bias in some of the polymer Schottky diodes reported and studied [24, 26, 27, 29]. In Fig. 2.8a, the structure consists of an electrodeposited film of $P3MT$ or poly(3-methylthiophene) sandwiched between aluminium and gold. In the small applied bias region, the current J follows Ohm's law since it is proportional to V. But with higher bias, the current

J goes into SCL-MG conduction with traps exponentially distributed in energy since it is proportional to V^4 with $l = 3$ [24].

Figure 2.8b shows the polymer $AlPcCl$ or aluminium phthalocyanine chloride is sandwiched between gold and aluminium created using vacuum deposition onto the glass substrate. In the low voltage region (region I), the current J follows Ohm's law and in the high voltage region (region II), the current J follows SCL-MG conduction with exponentially distributed traps with a slope of 3.48 ($J \sim V^{3.48}$) and 3.24 ($J \sim V^{3.24}$) for oxygen doped and as-deposited samples, respectively. The paper also reported the improvement in current by adding oxygen dopant into $AlPcCl$ [29].

In Fig. 2.8c, the $P3HT$ or poly(3-hexylthiophene) is sandwiched between indium tin oxide/polystyrene sulfonate doped polyethylene dioxy-thiophene (ITO/PEDOT) and aluminium electrodes. The carrier for the transport in $P3HT$ is holes. In region A ($V < 0.3$V), the currents follow Ohm's law since not enough holes injected to the polymer, in region B (0.3V < V < 0.7V), the currents are in the SCL-MG conduction with traps exponentially distributed in energy. In region C (V > 0.7V), at high temperature T, the holes have filled all the traps and thus the currents go to the SCL-MG conduction trap-free with slope equals to 2 ($J \sim V^2$). At lower T, the slopes of the current versus voltage curves are still higher than 2 since the hole traps are not fully filled yet. The fraction of free space charge (the space charge in the conduction band) decreases exponentially with lower temperature T [13]. Since J_{TL} $\sim V^{l+1}$ and $l = T_t/T$ (see Eq. 2.9), lower T gives larger value of l and thus steeper slope in the curve. The temperature dependent mobility can also be seen in the figure since at higher temperature, the values of current are also higher due to higher mobility with high T. Similar result with Fig. 2.8c can be seen in Fig. 2.8d with a slight difference of using only ITO as the Ohmic contact [26, 27].

2.5 Applications of SCL Current in Solids

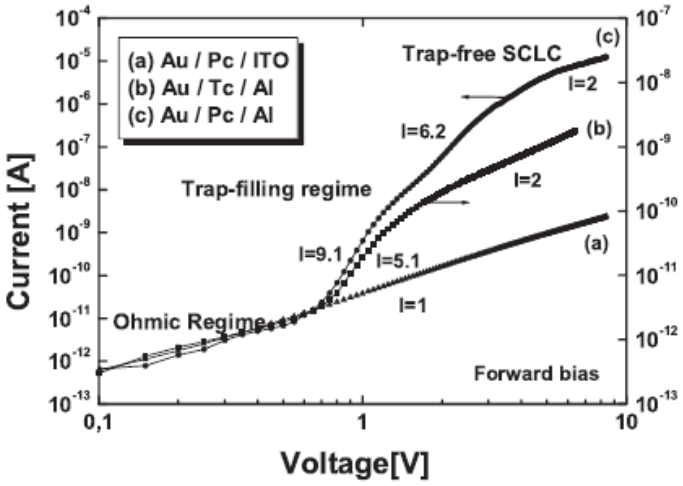

Figure 2.9: Current-voltage characteristics for planar sandwich configuration of (a) $Au/pentacene/ITO$, (b) $Au/tetracene/Al$, and (c) $Au/pentacene/Al$

Figure 2.9 shows another example of organic semiconductor of tetracene ($C_{18}H_{12}$) and pentacene ($C_{22}H_{14}$) sandwiched between aluminium Al as the rectifying contact and gold Au or indium tin oxide ITO as the Ohmic contact. In the case of $Au/pentacene/ITO$ (see Fig. 2.9a), the current shows Ohmic conduction for all voltage range. For $Au/tetracene/Al$ configuration (see Fig. 2.9b) beyond 0.7V, the SCL conduction is reached for SCL-MG regime with traps exponentially distributed in energy with $l = 5.1$, all the traps are filled beyond 2V, and thus the current shows SCL-MG trap-free with slope equals to 2. In the $Au/pentacene/Al$ configuration (see Fig. 2.9c), the transition from Ohmic to SCL conduction also occurs at V around 0.7 V. Above the transition voltage, the current shows two different slopes of $l = 9.1$ and $l = 6.2$ before all the traps are filled at about 4V. The trap- filling region with two different slopes is suggested to be due to two different energy levels of deep traps in the pentacene [31].

More examples of SCL conduction are shown in Fig. 2.10 [33] and Fig. 2.11 [37]. Figure 2.10 shows the current-voltage characteristic in log-log scale for CdS nanowire

measured in air ambient under various laser illumination intensity. The number of free electrons in CdS nanowire are affected by the laser illumination. As the laser intensity increases, the number of free electrons increase. However, the adsorption of oxygen from air to the nanowire depletes or reduces the number of free electrons. Thus, it is harder to reach SCL conduction and the transition voltage to reach SCL shifts to higher applied bias V_D even though the laser intensity is increased[33].

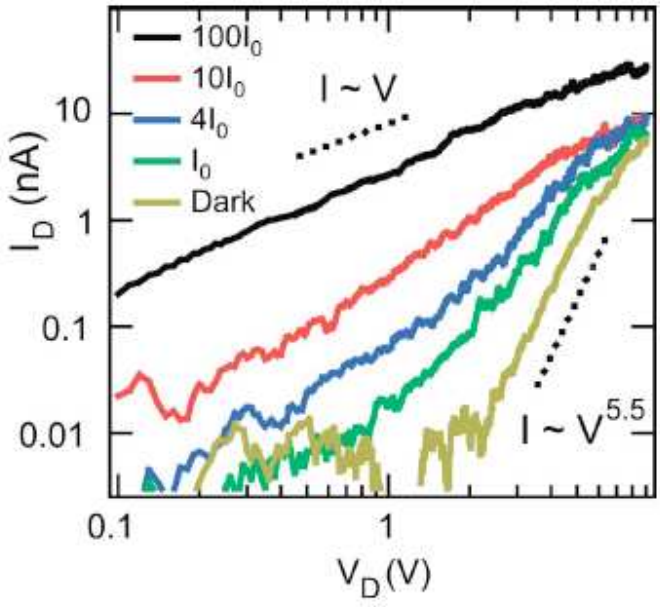

Figure 2.10: Current I_D vs voltage V_D of CdS nanowire in log-log scale measured under different level of laser illuminations

Figure 2.11 shows the forward current characteristic of arrays of $\beta - FeSi_2$ nanocrystals grown in p-type Si substrate. Chromium Cr and gold Au were evaporated to form the Schottky junctions to the nanocrystals. The figure shows one deep energy level of traps in two arrays of $\beta - FeSi_2$ nanocrystals and two deep energy levels of traps in ten arrays of $\beta - FeSi_2$ nanocrystals. The current conduction goes from Ohmic conduction to SCL-MG conduction with deep traps. Other studies on SCL current transport in solids include the occurrence of SCL

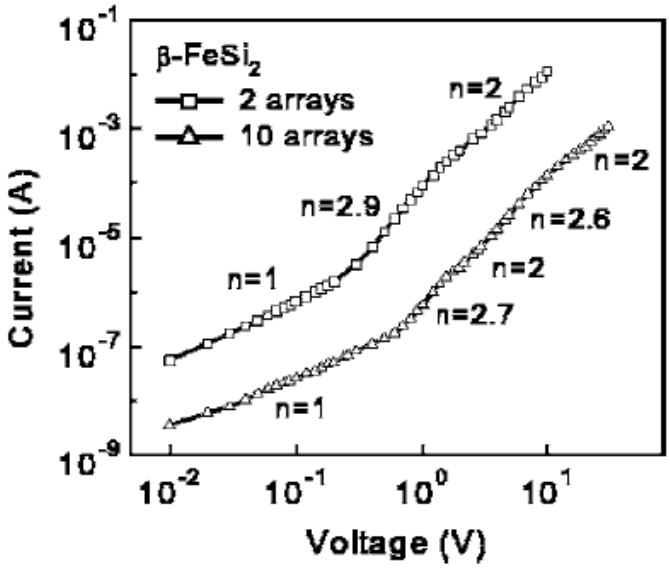

Figure 2.11: The log-log plots of current vs voltage characteristic of two (square symbols with line) or ten (triangle symbols with line) embedded arrays of $\beta - FeSi_2$ nanocrystals

photocurrent in a semiconductor at high light intensities [9] and work on shot noise [18, 19, 20, 21, 22, 23].

CHAPTER 3

TWO-DIMENSIONAL MODEL FOR SPACE CHARGE LIMITED (SCL) CURRENT IN SOLIDS

3.1 Introduction

The theory of high charge current injection (SCL transport) was originally developed in vacuum tubes, known as the Child-Langmuir (CL) law [2, 3]. Since then, the theory of classical 1D CL law has been extended to include multi-dimensional classical models [58, 59, 60], quantum models [61, 62], and short-pulse models [63, 64]. For an extensive review of the multi-dimensional models of CL law, please look at the thesis done by Koh Wee Shing [65]. In comparison with the advancement in the theory of CL law, the developments of the classical 1D MG law had been focused on the influence of trapped charges, temperature dependence, transient behaviour, bipolar and transition from MG law to CL law [66, 10, 11, 16, 17, 44, 67, 68, 69, 70, 71]. Recently, there is renewed interest in the studies and applications of MG law in various materials, such as SCL current fluctuations in organic semiconductors [31], SCL photocurrent in polymers and fullerenes [34], polymer SCL transistor [72], and SCL current in nanowires [33].

In such studies, the length of the solids can be comparable or larger than its cross-section that 1D MG law may not correctly predict the amount of the SCL current in these 2D novel devices. The classical 1D MG law is relatively unexplored in multi-dimensional models. Thus, in this chapter, we will develop a 2D analytical MG law in a solid [73]. The new model will be useful to understand the study of SCL transport in solids where the size of injecting electrode affects SCL current formation.

3.2 Transition from CL to MG law

The study of transition from CL to MG law has been done by Shur [68, 69, 70, 71]. The papers were intended to study the effect of collision on ballistic and near ballistic electron transport in GaAs at low temperature for the application of low power high-speed logic devices. The transition study he has done in his papers will be used to provide the framework for deriving the 2D MG law in this chapter. Three different equations were used to show the transition of CL and MG law by controlling the degree of collision using a collision parameter β. The three equations are the drift current density equation, Poisson equation, and the balance of momentum of electron equation derived from Newton's law of motion:

$$j_n = -en(x)v(x) \tag{3.1}$$

$$\frac{d^2\psi_n(x)}{dx^2} = \frac{e(n(x) - n_o)}{\epsilon_r \epsilon_0}, \tag{3.2}$$

$$m_e{}^* \frac{dv(x)}{dt} = -e\xi(x) - m_e{}^* \frac{v(x)}{\tau_m} \tag{3.3}$$

where j_n is the drift electron current density, $n(x)$ is the electron concentration along the length of the solid dielectric from x=0 to x=L, $\psi_n(x)$ is the potential profile across the solid length, $v(x)$ is the electron drift velocity, n_o is the doping density or the intrinsic or thermal concentration n_i if the solid material is undoped, ϵ_r is relative (dielectric) permittivity and ϵ_0 is vacuum permittivity, $m_e{}^*$ is effective

electron mass, τ_m is the momentum relaxation time, and $\xi(x)$ is the electric field profile along the solid length L. The effect of collision is included in the formulation in the last equation (Eq. 3.3) through the "τ_m" term. Diffusion current is neglected since it is assumed that the applied voltage is much larger than thermal voltage. The effective electron mass and momentum relaxation time are assumed to be constant and independent of energy. This assumption is not accurate at the high field region where the optical phonon scattering process is affected by it. The momentum relaxation time decreases sharply and thus the simplified model overestimates the electron drift velocity. However, we would like to use this simplified model to provide the *qualitative* picture of the electron transport in the ballistic or collision-dominated region because it is important to understand the physics and characteristics of the transition process from ballistic to collision-dominated region.

In the ballistic or CL dominated region, there is no collision. Therefore, τ_m approaches infinity and the second term in right hand side of Eq. 3.3 vanished. Eq. 3.3 can then be solved with $v(x) = \sqrt{2e\psi_n(x)/m_e{}^*}$ is the speed of electrons in vacuum. The derivation of the three equations results in the Child-Langmuir law. While in the collision-dominated regime, the left hand side of Eq. 3.3 vanished since $\frac{dv(x)}{dt} = 0$ (steady state condition). When Eq. 3.3 is then solved, the velocity of electrons becomes the drift velocity, $v(x) = -\mu_n \xi(x)$ with $\mu_n = e\tau_m/m_e{}^*$.

By substituting Eq. 3.1 and 3.3 to 3.2, the equations can also be written in a single closed form equation:

$$\frac{\epsilon_r \epsilon_0 m_e{}^* v(x)}{2e} \frac{d^2 v^2(x)}{dx^2} + \frac{\epsilon_r \epsilon_0 m_e{}^*}{2e\tau_m} \frac{dv^2(x)}{dx} + e n_o v(x) - j = 0, \tag{3.4}$$

which can be written in the normalized form of:

$$\frac{d^2 u(w)}{dw^2} + \frac{\beta}{\sqrt{u(w)}} \frac{du(w)}{dw} + 1 - \frac{1}{\sqrt{u(w)}} = 0. \tag{3.5}$$

Here, $u(w)$ is the dimensionless squared velocity $= (en_0 v(x))^2/j^2$, $w = x/x_0$ is the dimensionless distance, $x_0 = j/(\sqrt{2}en_0\omega_p)$ is the characteristic length, $\omega_p =$

$\sqrt{(e^2 n_0)/(\epsilon_0 \epsilon_r m_e{}^*)}$ is the plasma frequency, $\beta = (\sqrt{2}\omega_p \tau_m)^{-1}$ is the dimensionless collision frequency. The parameter, β, controls the degree of collision in the model with $\beta \ll 1$ showing ballistic transport (CL law) and $\beta \gg 1$ showing collision-dominated transport (MG law). In the space charge limit or high charge current injection, injected electrons $n(x)$ are much higher than the intrinsic or doping density n_o. This equivalently in normalized form can be written as $u(w) \ll 1$ or $1 - \frac{1}{\sqrt{u(w)}} \approx -\frac{1}{\sqrt{u(w)}}$. Therefore, to show the transition at SCL current regime between the 1D CL and MG law, Eq. 3.5 becomes

$$\frac{d^2u(w)}{dw^2} + \frac{\beta}{\sqrt{u(w)}}\frac{du(w)}{dw} - \frac{1}{\sqrt{u(w)}} = 0. \tag{3.6}$$

In the collision-dominated case, the "$\frac{d^2u(w)}{dw^2}$" term in Eq. 3.6 is negligible. Thus, the equation is solved to $u(w) = w/\beta$. By substituting back the values from the normalized parameters, it will recover to MG law (Eq. 2.2). While in the ballistic or no collision case, the "$\frac{\beta}{\sqrt{u(w)}}\frac{du(w)}{dw}$" term in Eq. 3.6 is negligible, and the equation becomes $u(w) = \frac{3}{2}w^{4/3}$, which after back substitution, it will recover to the 1D CL law (Eq. 2.1).

3.3 The Analytical 2D CL law and MG law

As previously mentioned, the above transition model is used to develop the 2D analytical model of SCL transport in solids. Similar to the 2D CL law [58, 74, 59, 60], the enhancement of the 1D MG law for uniform charge injection into a solid is expressed as (in terms of the 1D model)

$$\frac{J_{MG}[2D]}{J_{MG}[1D]} = 1 + F \times G. \tag{3.7}$$

The parameter $F = \frac{\int_0^L (x/L)n(x)dx}{\int_0^L n(x)dx}$ measures the normalized mean position of the injected electrons in a solid of length L, and $n(x)$ is the electron density in a solid,

which is calculated by the 1D MG model (with and without traps). Here, G is a correction parameter, which depends on the geometrical properties of the emission area (between the cathode and the trap-filled solid). The values of G have been derived in the study of 2D CL law for many different shapes of cathode such as: planar, circular, and elliptical shape [58, 74, 59, 60]. For simplicity, the electrons are injected from a planar shape cathode with a cross-sectional area of finite width, W, and infinitely long thickness, d, which corresponds to $G = (4/\pi)/(W/L)$ for $W/L > 1$ [60]. The full derivation of Eq. 3.7 can be found in Appendix A.

3.3.1 2D Trap-free MG law

By using the boundary conditions of $u = 0$ ($v = 0$) and $\frac{du}{dw} = 0$ ($\frac{dv}{dx} = 0$) at w=0 (cathode) for the space charge current injection, the differential equation shown in Eq. 3.6 is solved numerically for $n(x)$ in order to calculate the parameter F which in the normalized form can be shown to be:

$$F = \frac{\int_0^L (x/L)n(x)dx}{\int_0^L n(x)dx},$$

$$\text{since} \quad w{=}x/x_o \quad \text{and} \quad w_L{=}L/x_o,$$

$$F = \frac{\int_0^{w_L x_o} (wx_o/L)n(x)d(wx_o)}{\int_0^{w_L x_o} n(x)d(wx_o)},$$

$$\text{and also} \quad u(w){=}(en_0v(x))^2/(en(x)v(x))^2{=}(n_0/n(x))^2,$$

$$F = \frac{\int_0^{w_L x_o} \frac{wn_0}{L} u(w)^{-1/2}d(wx_o)}{\int_0^{w_L x_o} n_0 u(w)^{-1/2}d(wx_o)},$$

$$F = \frac{\int_0^{w_L} (w/w_L)u(w)^{-1/2}dw}{\int_0^{w_L} u(w)^{-1/2}dw}.$$

The parameter F can be calculated at any given values of β and $w_L = L/x_o$ (< 1). The condition of $w_L < 1$ is imposed to ensure high current injection for which the amount of injected charges is higher than the intrinsic charge. At the anode ($w = w_L$), the relation of the applied voltage V_G with other parameters is

3.3 The Analytical 2D CL law and MG law

$V_G = \frac{2V_{PT}[u_L + 2\beta \int_0^{w_L} u^{1/2} dw]}{w_L^2}$, where $V_{PT} = (en_o L^2)/(2\epsilon_0 \epsilon_r)$ is the punch-through voltage that the space charge has extended through a solid, and u_L is the solution of $u(w)$ at $w = w_L$ which is obtained from solving Eq.(3.6). To see the transition from Ohm's law to MG law it is common to use either V_{PT} or transition voltage $V_{\Omega-MG} = V_{PT}/2$.

Figure 3.1 shows the calculated factor, F, as a function of the normalized collision frequency, β, at different solid length, $w_L = 0.1$ to 10^{-4} (left to right). It is clear that there is a smooth transition from $F = 1/3$ at large β value (trap-free MG law or collision-dominated SCL current) to $F = 1/4$ at small β (CL law or ballistic SCL current). The transition region lies within the range of $\beta = 0.1$ to 100, and the exact value of F will depend on β and w_L. The limit of $F = 1/3$ can also be checked by directly evaluating the integral form of $F = \frac{\int_0^L (x/L) n(x) dx}{\int_0^L n(x) dx}$ where in the MG law limit, the dependence of $n(x)$ is $n(x) \propto x^{-1/2}$ [39].

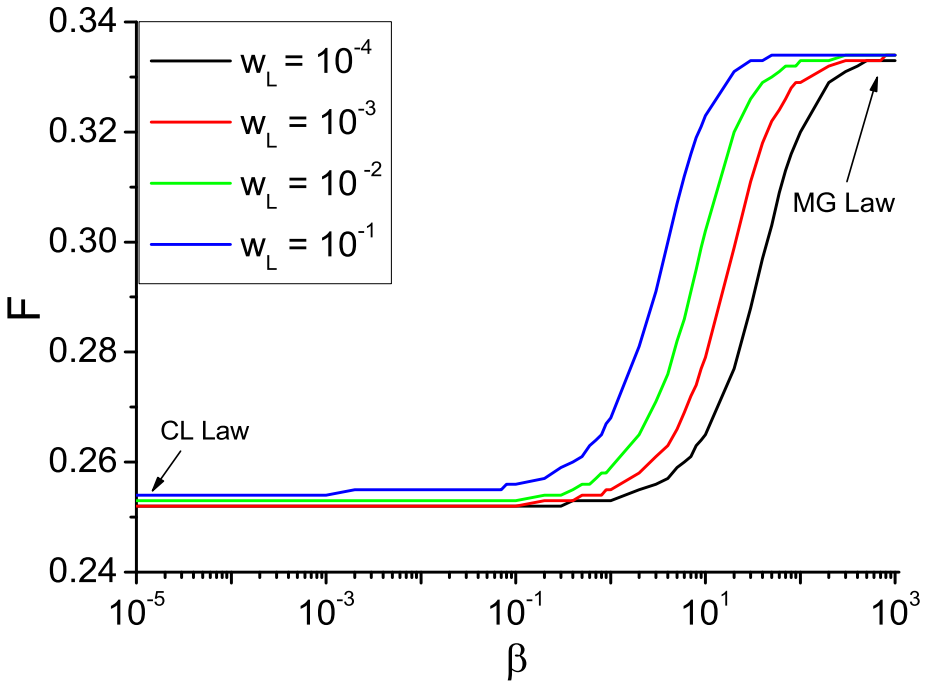

Figure 3.1: Dependence of the normalized mean position, F, of the electron density as a function of collision parameter, β, for various $w_L = 0.1$ to 10^{-4} (left to right) for a trap-free solid

3.3.2 2D Trap-filled MG law

For trap-filled SCL transport in solids, the value of F for shallow traps is equal to the trap-free limit ($F = 1/3$). This is because the traps lowered the SCL current only by a constant fraction of $\left(\frac{\theta}{\theta+1}\right)$ (see Eq. 2.5). As described in section 2.4, the $n(x)$ dependence to x can be found to be $n(x) \propto x^{-l/(l+1)}$ with $l = T_t/T$ (≥ 1) is the ratio of distribution of traps to the free carriers (see Eq. 2.9). For a given l, the factor F can be calculated to be $F = 1/(l+2)$ by evaluating the integral form of $F = \frac{\int_0^L (x/L)n(x)dx}{\int_0^L n(x)dx}$. The enhancement of the 2D MG law for a trap-filled solid will depend on the value of l, which characterizes the energy distribution of traps. The larger the value of l, the smaller the value of F. Thus, in insulators and many organic materials which has been shown to exhibit the trap-filled MG law in solid characteristics, the 2D current enhancement is lower as compared to a trap-free solid. While for $l = 1$, the shallow trap limit of $F = 1/3$ is recovered, which is also identical for a trap-free solid.

3.3.3 Numerical Simulation Using Medici

To verify the analytical 2D trap-free MG law with $F = 1/3$, a 2D device simulator called Medici [75] is used to create a structure of $N^+ - i - N^+$ of silicon (Si) of width W, and length L with heavily doped cathode and anode, in order to have Ohmic contacts. The intrinsic region between them has an intrinsic uniform electron density of about 1.5×10^{10} cm^{-3} and a uniform fixed mobility (μ_n) determined through the relationship of $\mu_n = e\tau_m/m_e{}^*$ at $\beta = 1000$. The beta value of 1000 is used to ensure the transport is at the collision-dominated regime or MG law (see Fig. 3.1). The other parameters used in the simulation are $m_e{}^*/m_e$= 0.31, and $\epsilon_r = 11.8$. The current density vs voltage (J vs V_G) characteristic obtained from Medici is plotted in Fig. 3.2 at a fixed $W/L = 4$ for $L = 100$ μm and $L = 200$ μm, which shows the transition

3.3 The Analytical 2D CL law and MG law

from Ohm's law ($J \sim V_G$) to MG law ($J \sim {V_G}^2$) around the punch-through voltage V_{PT} of about 0.18 V and 0.4 V respectively.

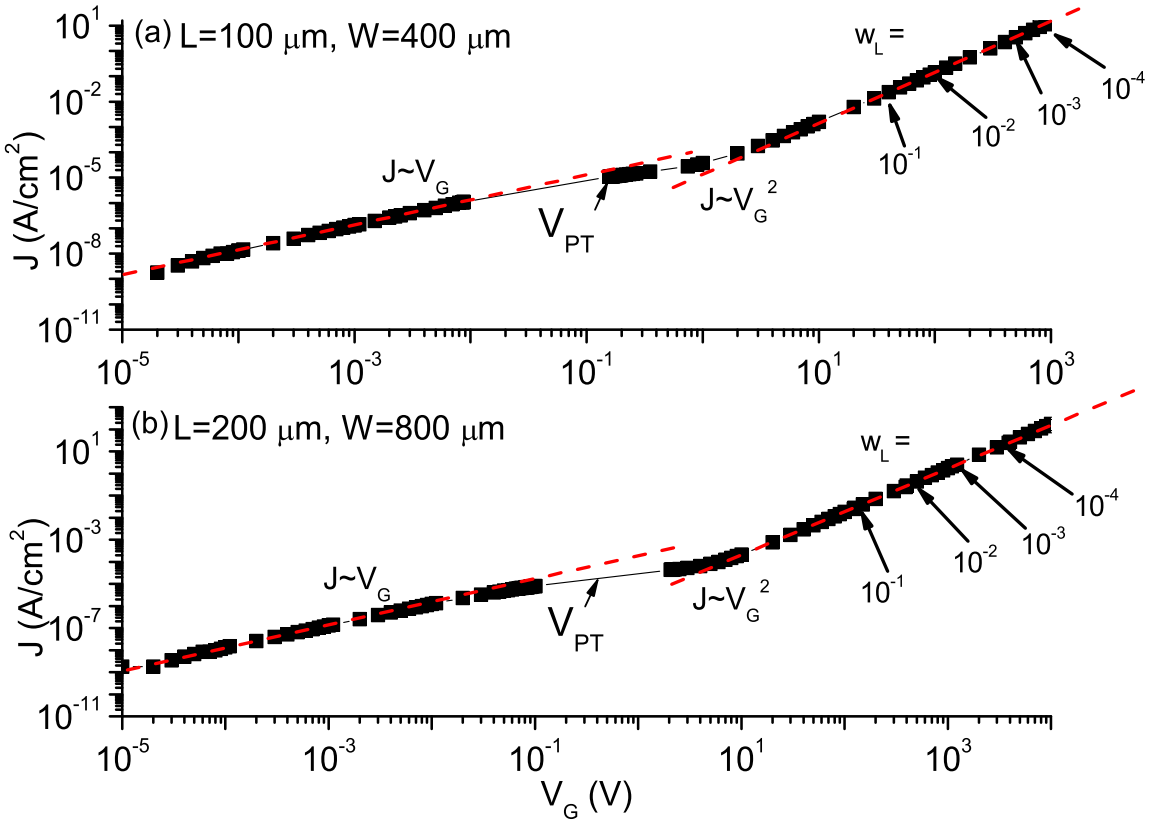

Figure 3.2: SCL current density J obtained from Medici simulator as a function of applied voltage V_G at fixed $W/L = 4$ for (a)$L = 100\ \mu m$ and (b) $L = 200\ \mu m$ (without traps). The red dashed line shows the transition from the Ohmic region ($J \propto V_G$) to the trap-free MG law ($J \propto {V_G}^2$) around the punch-through voltage V_{PT}

For various values of $w_L = 10^{-4}$ to 0.1, the corresponding applied voltage V_G to each w_L as indicated in Fig. 3.2 were found using back substitution. To determine the 2D MG law as function of W/L, Medici is used to obtain the the current density by varying W at fixed $L = 100\ \mu m$ and $L = 200\ \mu m$. The comparison between the simulation results (symbols) and the analytical 2D trap-free MG law of $F = 1/3$ (solid lines) are plotted in Fig. 3.3 as a function of $W/L = 0.5$ to 4. The analytical

results agree very well with the simulation. For comparison, the analytical 2D CL law (ballistic transport) of $F = 1/4$ is also plotted (dashed lines). Note the Medici simulator can not be used to verify the transition region ($1/4 < F < 1/3$) between the MG law and the CL law, as drift-diffusion transport has been assumed in the Medici simulator.

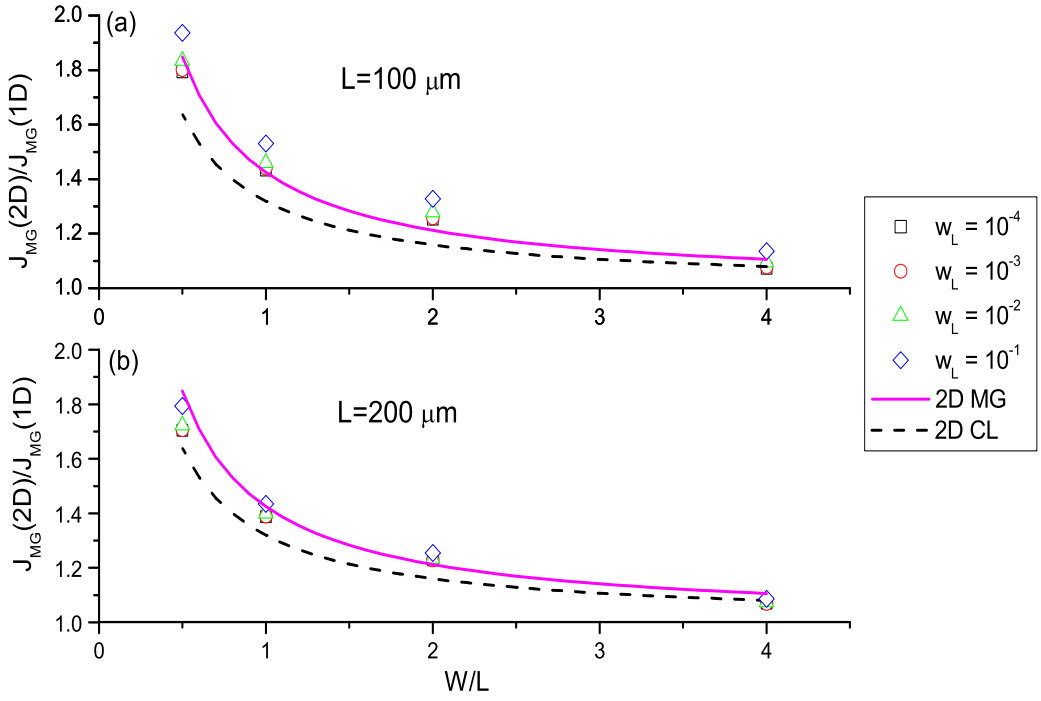

Figure 3.3: The comparison of simulation results (symbols) with the 2D trap-free MG law (solid) and the 2D CL law (dashed) as a function of $W/L = 0.5$ to 4 for $L = 100$ μm and $L = 200$ μm. The corresponding V_G at various $w_L = 10^{-4}$, 10^{-3}, 10^{-2}, and 10^{-1} used for comparison with the analytical 2D scaling are indicated in Fig. 3.2

To verify the enhancement factor of $F = 1/(l + 2)$ for the 2D trap-limited MG law, the same simulator is used at $L = 10$ μm for two different sets of trap distribution: $l = 2$ and $l = 3$, with $N_{t0} = (1 \text{ or } 5) \times 10^{17}$ cm^{-3}. The distribution of traps used in the simulation are created by discretizing the band energy based on the exponential function $N_t(E) = (N_{t0}/k_bT_t)exp[(E - E_C)/k_bT_t]$. Due to the limitation of the simulator, only 50 energy step sizes can be used.

3.3 The Analytical 2D CL law and MG law

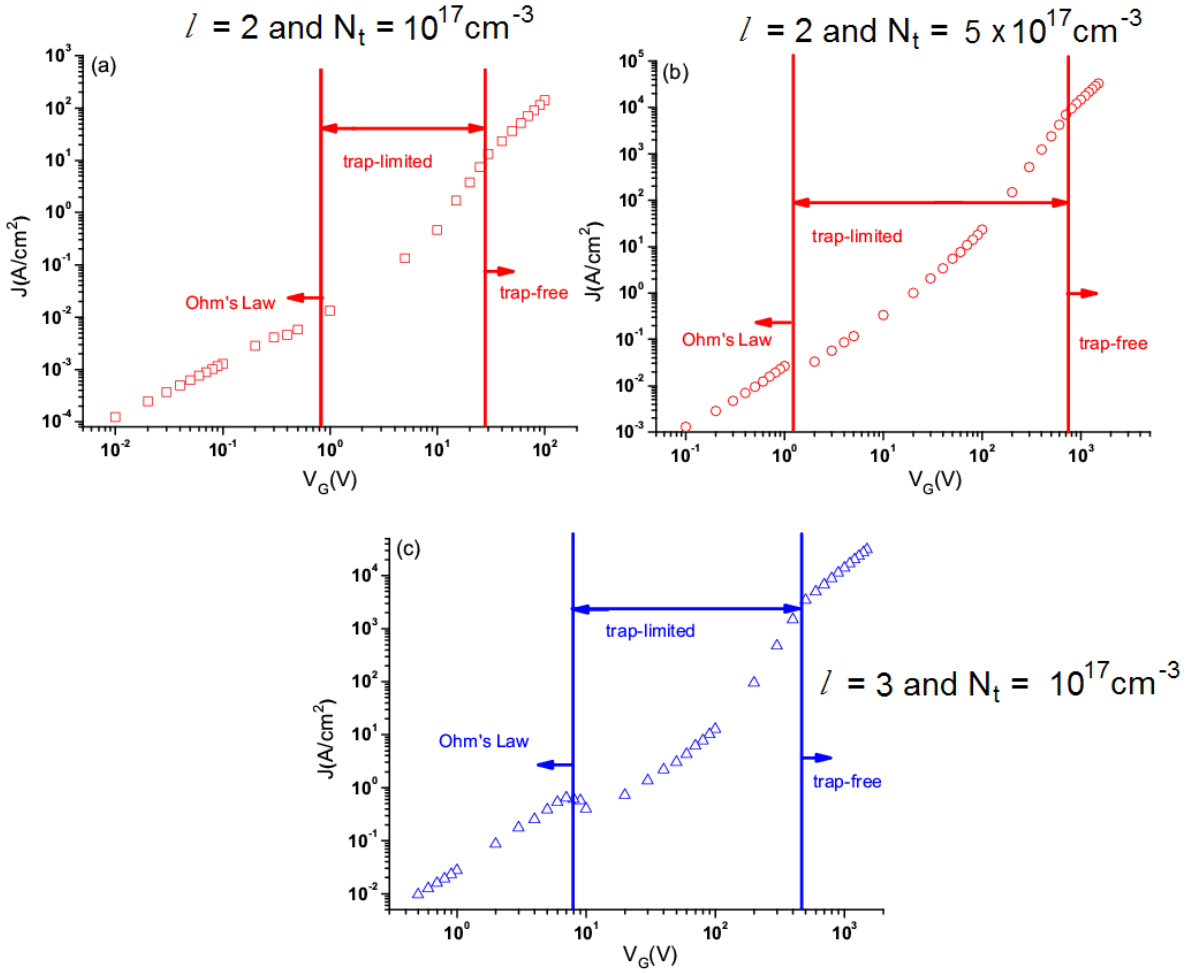

Figure 3.4: SCL current density J obtained from Medici simulator as a function of applied voltage V_G at $W/L = 4$ and $L = 10$ μm for a trap-filled solid of traps exponentially distributed in energy for (a) $l = 2$ and $N_{t0} = 10^{17}$ cm^{-3} (red square); (b) $l = 2$ and $N_{t0} = 5 \times 10^{17}$ cm^{-3} (red circle), and (c) $l = 3$ and $N_{t0} = 10^{17}$ cm^{-3} (blue triangle)

3.3 The Analytical 2D CL law and MG law

In Fig. 3.4, the current densities show transition from Ohm's law to a trap-limited region at $V_{\Omega-trap}$ and from the trap-limited region to MG law trap-free at $V_{trap-MG}$. For the case of $l = 2$ and $N_{t0} = 10^{17}$ cm^{-3}, the trap-limited region is confined between a voltage range of $V_{\Omega-trap} \approx 0.85$ V to $V_{trap-MG} \approx 29$ V, as indicated in the figure (see Fig. 3.4a). Similar transition had also been observed in other cases, but at different voltage ranges. For $l = 2$ and $N_{t0} = 5 \times 10^{17}$ cm^{-3} case, the range is from $V_{\Omega-trap} \approx 1.25$ V to $V_{trap-MG} \approx 750$ V (see Fig. 3.4b). For $l = 3$ and $N_{t0} = 10^{17}$ cm^{-3} case, the value of each voltage will be $V_{\Omega-trap} \approx 8$ V and $V_{trap-MG} \approx 480$ V (see Fig. 3.4c).

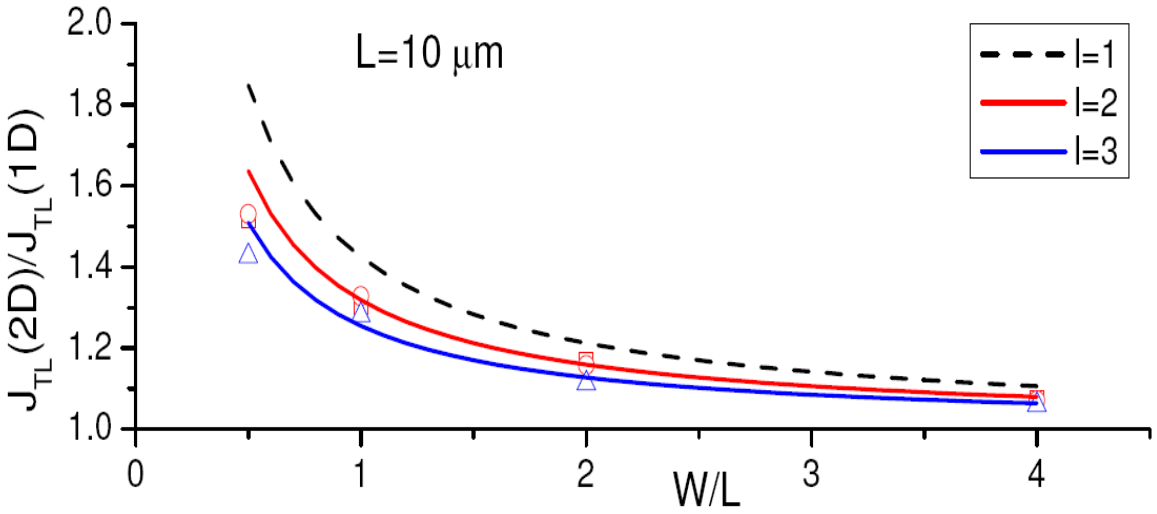

Figure 3.5: The normalized 2D trap-limited current density as a function of $W/L = 0.5$ to 4 at $L = 10$ μm for three simulated cases in their respective trap-limited regions: $l = 2$ with $N_{t0} = 10^{17}$ cm^{-3} at 10 V (red square); $l = 2$ with $N_{t0} = 5 \times 10^{17}$ cm^{-3} at 200 V (red circle), and $l = 3$ with $N_{t0} = 10^{17}$ cm^{-3} at 300 V (blue triangle). The lines are the analytical solutions at $l = 2$ and 3 (solid) and $l = 1$ (dashed)

In comparison with the analytical formula of $F = 1/(l + 2)$, the normalized 2D trap-limited MG law in terms of its 1D limit [see Eq. 2.9] is plotted as a function of $W/L = 0.5$ to 4 in Fig. 3.5. The comparison shows good agreement between the

simulations results (symbols) and the analytical equations (solid lines) at $l = 2$ and 3. Note the simulation results are obtained from a particular voltage in the trap-limited region. These comparison shows that the simple 2D scaling laws derived in this paper remains valid even for a trap-limited solid. The enhancement is directly related to the trap distribution characterized by the value of l, and thus confirms the analytical scaling of $F = 1/(l + 2)$. For completeness, the formula of shallow trap limit at $l = 1$ is also plotted in dashed line.

3.4 Summary

In conclusion, a simple analytical 2D MG law is presented for SCL electron flow in a trap-filled solid [73] (with a simple 2D shape), which is confirmed by a 2D device simulator. The effects of traps are included by assuming traps exponentially distributed in energy states. Smooth transition from the 2D MG law and the 2D CL law is also demonstrated at the trap-free limit. This result may be useful in predicting the amount of maximum SCL current density in novel 2D structures such as: nanotubes, organic semiconductors, and nanowires that have been reported to operate at SCL regime.

CHAPTER 4

CONTACT AND SIZE EFFECT OF 2D SPACE CHARGE LIMITED (SCL) CURRENT IN SOLIDS

4.1 Introduction

The studies of SCL transport in solids have been focused mainly based on one-dimensional consideration and the effect of trap charges. The size effect in which cathode size becomes comparable to the gap spacing has been recently studied [73] (see Chap. 3). By adopting the approach in deriving the cathode size W in the vacuum gap, it can be shown that the solution for the enhancement in a solid dielectric in between the gap and F is derived analytically to be 1/3. However, all of the earlier and published works have not mentioned the contact effect, which will limit the electron injection to the solids. It is important to understand this effect since in real devices, especially in the organic molecules; surface states, impurity, defect states, etc associated with the interface of the contact with a finite barrier will limit the current injection in the devices. In this chapter, the effect of injection by contact in association with SCL transport in solids combined with the size effect is studied [76].

4.2 Theory

The space charge limited current model in the solid dielectric is revised by implementing the contact effect between the cathode and the dielectric. The structure consists of a solid dielectric of length L (x=0 to x=L) with its intrinsic (thermal) concentration of n_i sandwiched between the two electrodes, cathode and anode. The structure has a width of W in the y-direction and is considered infinitely long in the z-direction. The details of the model and its boundary conditions can be found in Appendix A. Our derivation assumes: one carrier transport (electrons) from cathode, a perfect dielectric with no defects in the bulk and no recombination in the bulk. For a non-injecting contact, we assume the contact between cathode and dielectric behaves like a Schottky contact [77]. The current transport mechanism depends not only on the applied voltage V_G but also on how well the electrons can be injected through the contact. For electron transport with a Schottky contact, there will be a finite barrier height of $e\phi_b = e\phi_m - e\chi$ (in eV), where $e\phi_m$ is the work function of the cathode and $e\chi$ is the electron affinity of a dielectric material. The function of the barrier height is to limit or restrict the flow of electron transport to a solid. If the electrons have a higher energy than the barrier, it will be able to move through by thermionic emission.

To solve the model numerically, three basic equations that govern electron concentration, electrostatic potential, and current density are used. Firstly, the electron concentration is related to its electrostatic potential and quasi Fermi potential exponentially by:

$$n(x) = n_i exp\Big[\frac{\psi_n(x) - \phi_n(x)}{k_b T/e}\Big], \tag{4.1}$$

where $n(x)$ is the free electron concentration, n_i is the intrinsic (thermal) electron concentration, $\psi_n(x)$ is the electrostatic potential, $\phi_n(x)$ is the quasi Fermi electron potential, k_b is the Boltzmann's constant, T is the electron temperature, and e is

the electronic charge. The equation is valid only for a *non-degenerate* semiconductor and thus it is appropriate in our model since the dielectric is undoped. Secondly, the electrostatic potential is described by Poisson equation:

$$\frac{d^2\psi_n(x)}{dx^2} = \frac{e\Big(n(x) - n_i\Big)}{\epsilon_r\epsilon_0}, \tag{4.2}$$

where ϵ_r is the relative (dielectric) permittivity and ϵ_0 is the vacuum permittivity. Both equations (Eqs. 4.1 and 4.2) are inter-related and they are to be solved self-consistently. To solve for the current density, the steady state current continuity equation is needed:

$$\frac{dj_n}{dx} = eG(x), \tag{4.3}$$

where $G(x)$ is the net generation rate of electrons in cm^{-3}, $j_n = -en(x)\mu_n\frac{d\psi_n(x)}{dx} + eD_n\frac{dn(x)}{dx} = -en(x)\mu_n\frac{d\phi_n(x)}{dx}$ is the drift-diffusion electron current density , D_n is the electron diffusion coefficient in cm^2/s, μ_n is the electron mobility in $\mathrm{cm}^2/\mathrm{V.s}$.

To represent the property of a non-injecting contact, two parameters are used: the barrier height $e\phi_b$ and surface recombination current $j_n(x = 0) \equiv j_{sn} = ev_{sn}(n_s - n_{eq})$ with $v_{sn} = \frac{A^*T^2}{eN_C}$ is the surface recombination velocity, A^* is the effective Richardson constant, N_C is the effective density of states of electrons in conduction band, n_s (n at x=0) is the actual surface electron concentration and n_{eq} is the equilibrium electron concentration ($\phi_n = 0$). This surface recombination current acts as a current boundary condition at the contact between the cathode and the solid dielectric [78, 79]. Here, j_{sn} also represents surface states available at the contact interface with the dielectric. As it will be elaborated later in this chapter, tunneling through the surface states plays an important role to reach space charge limited current in the presence of a non-injecting contact. Below we give a brief description of the underlying physics that we used to represent the contact properties. More details on these can be found in Chap. 5 of S. M. Sze book [78].

4.2 Theory

The barrier height affects the contact by limiting the availability of the amount of injected electrons by thermionic emission. The difference in work function in the metal-semiconductor interface controls the amount of injected electrons. Meanwhile, due to the discontinuity of the lattice structure at the interface, there will be a lot of generation-recombination centers at that region. These localized energy states are usually known as the surface states. With the surface states effect neglected (no surface states are available), the injected electrons will have infinite surface recombination. The velocity of electrons injected from the cathode is limited to the maximum velocity electrons can achieve, that is, the average thermal velocity $v_{th} = \sqrt{3k_bT/m_e{}^*}$, $m_e{}^*$ is the effective electron mass. In this case, $v_{sn} \approx v_{th}$ and $j_{sn} = 0$ since $n_s = n_{eq}$. If surface states are present at the contact, the injected electrons will have finite recombination. And thus, $j_{sn} \neq 0$ since $n_s \neq n_{eq}$.

The boundary conditions at the cathode (x=0) and anode (x=L) are used to solve the three equations shown above (Eqs. 4.1, 4.2, and 4.3): ψ_n(x=0) = $\psi_0 - \phi_b$, $\psi_0 = \frac{E_g}{2e} + \frac{k_bT}{2e} ln \frac{N_C}{N_V}$ is the built-in potential with E_g is the bandgap of a dielectric, N_V is the effective density of states of holes in the valence band; ψ_n(x=L) = V_G+(ψ_0-$\frac{E_g}{2e}$), with V_G is the applied bias; ϕ_n(x=0) = 0 for infinite surface recombination; ϕ_n(x=0) = ψ_n(x=0) - $\frac{k_bT}{e} ln \frac{n_s}{n_i}$ for finite surface recombination; ϕ_n(x=L) = V_G. At x=0, the potential value comes from the difference between the built-in potential, ψ_0, and the barrier height potential ϕ_b (in V). The electrons in the conduction band energy need to overcome the built-in potential to move into the metal. The details of the physics involved in deriving these boundary conditions can be found in Chapter 1 and 5 of S. M. Sze book [78].

4.3 Results and Discussion

The current density J is solved at each applied bias V_G by implementing SOR (Successive-Over-Relaxation) with iterative method. The values of the matrices $\boldsymbol{\psi_n}$ and $\boldsymbol{\phi_n}$ are guessed initially (and thus, the matrix $\boldsymbol{n}$ using Eq. 4.1). Then, the values of $\boldsymbol{\psi_n}$ are updated and solved iteratively using Poisson equation (Eq. 4.2). Using the updated values of $\boldsymbol{\psi_n}$, the values of $\boldsymbol{\phi_n}$ (and thus, j_n) are solved iteratively using current continuity equation (Eq. 4.3). The process is repeated until the values of $\boldsymbol{\psi_n}$ and $\boldsymbol{\phi_n}$ satisfy both the Poisson and the current continuity equations. The details of the numerical calculation in the matrices form can be found in Appendix B and C. For infinite surface recombination, the boundary conditions for ψ_n and ϕ_n are applied directly since the values are known exactly at x=0 and x=L. There is no tunneling since ϕ_n(x=0) = 0 signifies neutral condition and j_n is constant from x=0 to L. The generation term in Eq. 4.3 is zero [$G(x) = 0$] as stated in the above assumptions (no bulk recombination and 1D carrier). When the surface states effect included, the value of ϕ_n(x=0) is not known directly [ϕ_n(x=0) $\neq$ 0]. The value is found by matching j_{sn} with j_n at x=0. In this case, there will be a tunneling component in the total current density since tunneling occurs through surface states. The calculation of the tunneling current component is included in Eq. 4.3 in the generation term as a local tunneling generation rate ($|G(x)| > 0$).

The tunneling component is calculated using the Wentzel, Kramers, and Brillouin (WKB) method [80]. The integrals over distance and energy in the tunneling coefficient are transformed into a double integral over distance alone. Details of the method and calculation of tunneling current can be found in a paper by Ieong [81]. To show the results of the calculation, a numerical code was created in Matlab to solve for the current density in which the result will be compared with a 2D device

simulator Medici. In our numerical code, the abovementioned three equations are transformed using normalization parameters:

$$n(\bar{x}) = exp\big[ay(\bar{x})\big], \tag{4.4}$$

$$\frac{\delta \bar{\mathrm{J}_n}}{\delta \bar{x}} = \frac{eL}{j_0} G(\bar{x}), \tag{4.5}$$

$$\frac{\delta^2 \psi(\bar{x})}{\delta \bar{x}^2} = n(\bar{x}) - 1, \tag{4.6}$$

where $\bar{j_n} = -n(\bar{x})\frac{\delta\psi(\bar{x})}{\delta\bar{x}} + \frac{1}{a}\frac{\delta n(\bar{x})}{\delta\bar{x}} = -n(\bar{x})\frac{\delta\phi_n(\bar{x})}{\delta\bar{x}}$, $\psi(\bar{x}) = \frac{\psi(x)}{V_0}$, $\phi_n(\bar{x}) = \frac{\phi_n(x)}{V_0}$, $n(\bar{x}) = \frac{n(x)}{n_i}$, $\bar{j_n} = \frac{j_n}{j_0}$, $\bar{x} = \frac{x}{L}$ with $V_0 = \frac{eL^2 n_i}{\epsilon_r \epsilon_0}$ is the crossover (transition) voltage from Ohmic region to SCL-MG region, $j_0 = en_i\mu_n\frac{V_0}{L}$ is the crossover current density, $a = \frac{eV_0}{k_bT}$, $y(\bar{x}) = \psi(\bar{x}) - \phi_n(\bar{x})$. The electrostatic potential and electron quasi Fermi potential are scaled to crossover voltage V_0, the electron concentration is scaled to the intrinsic electron concentration (n_i), and the current density is scaled to crossover current density (j_0). The dimensionality and scaling constants are needed to prevent numerical overflow and or underflow. For infinite surface recombination, since $G(\bar{x}) = 0$, we may substitute Eq. 4.4 and 4.5 to Eq. 4.6 to get a 2^{nd} order ordinary differential equation in terms of a dummy variable $y(\bar{x})$:

$$\frac{\delta^2 y(\bar{x})}{\delta \bar{x}^2} + a.\bar{j_n}.exp\big[-ay(\bar{x})\big]\frac{\delta y(\bar{x})}{\delta \bar{x}} - exp\big[ay(\bar{x})\big] + 1 = 0. \tag{4.7}$$

The boundary conditions for Eq. 4.7 are: $y(\mathrm{x}{=}0) = \psi(\bar{x} = 0)$ since $\phi_n(\bar{x} = 0) = 0$ and $y(\mathrm{x}{=}L) = \frac{k_bT}{2eV_0} ln\frac{N_C}{N_V}$. Equation 4.7 can be solved readily by implementing the method together with the boundary conditions. However, when the surface states are incorporated into the system, $|G(\bar{x})| > 0$ and Eq. 4.4 and 4.5 cannot be substituted directly. Therefore, when $|G(\bar{x})| > 0$, there is no closed form and instead the solution has to be solved numerically.

To compare with our numerical calculation, a 2D device simulator Medici is used to simulate the real device characteristics. In the device simulation, an intrinsic silicon

is used as the dielectric ($\epsilon_r = 11.8$ and $E_g = 1.08$ eV) with $L = 10$ μm. The applied bias V_G is from 0 - 10 kV. The results for current density vs voltage, J (A/cm^2) vs V_G (V), from Medici and the numerical computation are in great agreement as shown below in Fig. 4.1 with constant mobility of $\mu_n = 10$ cm^2/V.s and barrier height of $e\phi_b = 0$ (Ohmic), 0.13, 0.33, 0.53, 0.73, 0.93, 1.08 eV. The range of barrier heights under investigation that we calculated here is until 1.08 eV since the bandgap of Si is 1.08 eV. Here, the width $W = 40$ μm ($W/L = 4$) is used to ensure the result is based on the one-dimensional (1D) model.

Current transport to reach the space charge limited (SCL) condition in a trap-free solid is governed by MG (Mott-Gurney) law (see Eq. 2.2)[1, 39]. The current J is proportional to ${V_G}^2$, the voltage scaling (n) in Fig. 4.1 indicates the proportionality of $J \sim {V_G}^n$. The transition voltage from Ohm's law to MG law, $V_{\Omega-MG} = en_iL^2/\epsilon_r\epsilon_0$ [39]. The transition voltage in Fig. 4.1 is approximately 2.2 mV (not shown in figure).

Without the surface states effect (Fig. 4.1a), the current density consists of drift and diffusion components only. The ability to reach the SCL conduction depends on the barrier height that limits the electron injection. At zero barrier height, drift component dominates thus the J value follows MG law from $V_G > V_{\Omega-MG}$. However, as barrier height is increased, the thermionic emission of electrons dominates the mechanism. The availability of electrons and the diffusion current become prominent. Thus, at larger barrier height, the exponent n goes to 1 (Ohmic transport) at large V_G. At small V_G the exponent drops from 2 to below 1. The value of $n < 1$ should indicate the diffusion dominated transport.

In Fig. 4.1b, even with the barrier height is increased, the exponent value, n, is able to reach $n = 2$ at large V_G signifying SCL condition ($V_G > 1$ kV). At small V_G ($V_G < 40$ V) regardless of the barrier height, the current density values in Fig. 4.1a and b are similar since the tunneling component arises from the tunneling of surface states is not significant. However, as V_G value arises, the J value differs quite distinctly

4.3 Results and Discussion

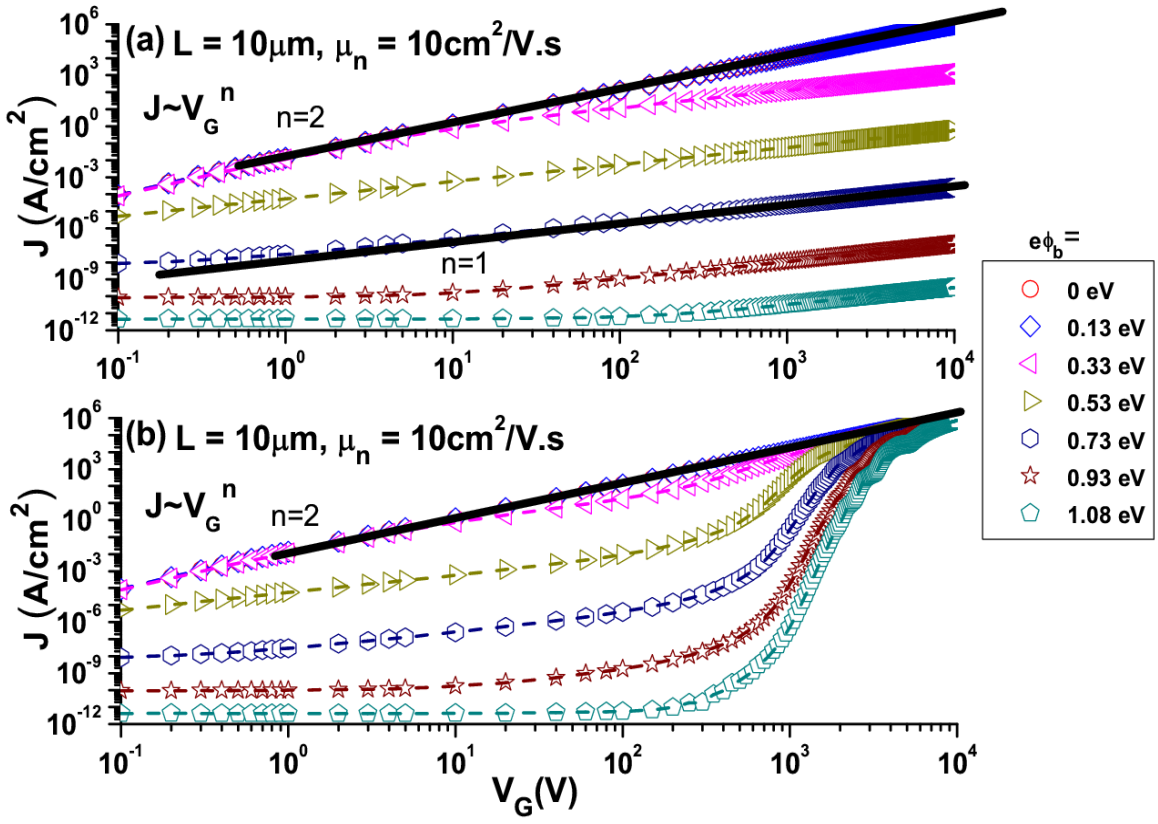

Figure 4.1: J vs V_G for $L = 10$ μm and $\mu_n = 10$ cm^2/V.s, $e\phi_b = 0$, 0.13, 0.33, 0.53, 0.73, 0.93, and 1.08 eV for each symbol from top to bottom with: (a) without surface states effect [ϕ_n(x=0) = 0], and (b) with surface states [ϕ_n(x=0) $\neq$ 0]. Dashed lines represent numerical simulation result and open symbols represent Medici simulation result. Black solid lines represent exponent n from $J \sim V_G{}^n$ with $n = 2$ represents SCL-MG and $n = 1$ represents Ohm's law

in which when the barrier height is increased, the current mechanism goes to Ohmic conduction in Fig. 4.1(a) but it reaches space charge limited (SCL-MG) conduction in Fig. 4.1b. The big difference is caused by electron tunneling through surface states. The surface states are introduced to the system by the surface recombination velocity v_{sn} applied to the contact and hence the surface recombination current j_{sn}. In our model, the electron tunneling through surface states is calculated from the local tunneling generation rate [81].

In Fig. 4.1a, the surface states effect is neglected. There is no tunneling of electrons through surface states so at x=0 the charge is neutral. This condition implied that the quasi Fermi potential for electrons at x=0 is 0 [ϕ_n(x=0) = 0]. The injection of electrons is solely limited to the barrier height $e\phi_b$ between cathode and dielectric through thermionic emission, while in Fig. 4.1b, the effects of surface states are included, $v_{sn} = \frac{A^*T^2}{eN_C}$. Tunneling through surface states exists, quasi Fermi potential for electrons at x=0 is not zero (the value is obtained from matching j_{sn}). Near the interface, the current is not constant. The tunneling current (or j_{tun}) is added as a local generation term into the steady state current continuity equations. The tunneling causes more electrons to be injected at larger voltage so that the space charge limited (SCL) current can be reached. The injection of electrons is limited to the amount of electron tunneling through surface states as well as thermionic emission through the barrier height. The tunneling current dominates at larger V_G in Fig. 4.1b, and thus SCL current is reached.

The potential profiles across a silicon diode along its length $L = 10$ μm, $\mu_n = 10$ cm^2/V.s at $V_G = 10$ kV with $e\phi_b = 0.13$ eV and 1.08 eV (with and without tunneling through the surface states) are shown in Fig. 4.2. In the Ohmic conduction, the potential profile is linearly proportional to the distance x along a solid length [$\psi_n(x) \propto x$] while in the SCL conduction, the potential profile dependence to x is $\psi_n(x) \propto x^{3/2}$ [39]. As can be seen in Fig. 4.2a, at small barrier height $e\phi_b = 0.13$ eV, the

potential profiles are almost identical and roughly proportional to $x^{3/2}$. The result shows that the SCL conduction can still be reached with or without tunneling if the barrier height is still small. However, for a large barrier height, $e\phi_b = 1.08$ eV, the potential profiles are different (see Fig. 4.2b). In the case of no tunneling (black line), the potential profile follows Ohmic conduction [$\psi_n(x) \propto x$] showing it is not able to reach the SCL conduction and when there is tunneling through the surface states (red line), the potential profile is still able to reach SCL conduction [$\psi_n(x) \propto x^{3/2}$].

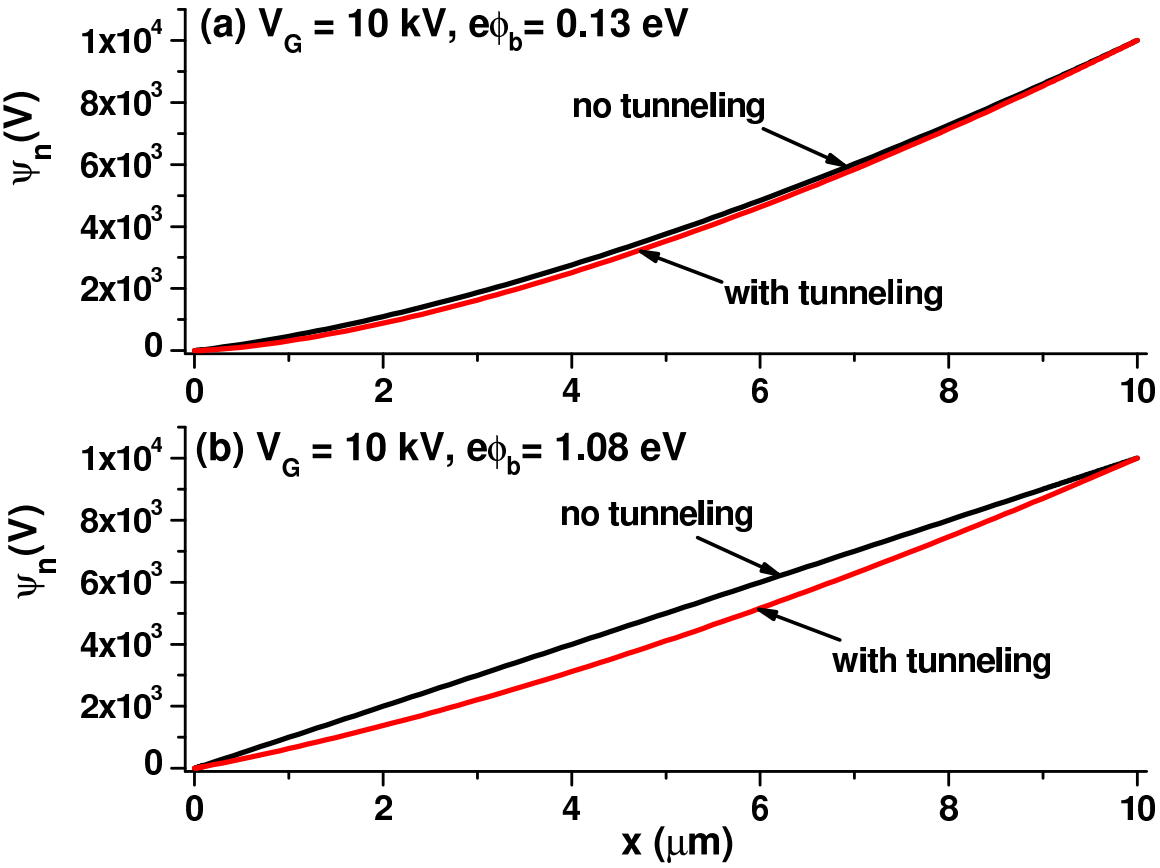

Figure 4.2: $\psi_n(x)$ vs x for $L = 10$ μm, $\mu_n = 10$ cm^2/V.s, $V_G = 10$ kV with: (a) $e\phi_b = 0.13$ eV, and (b) $e\phi_b = 1.08$ eV. The black line shows the potential profile when there is no tunneling through surface states and the red line shows the potential profile when there is tunneling through surface states

4.3 Results and Discussion

The effect of varying intrinsic concentration and mobility are shown in Fig. 4.3a and 4.3b respectively, at $e\phi_b = 0.33$ eV, $N_C = 5{\times}10^{18}$ cm^{-3} with surface states effect included. In Fig. 4.3a, the intrinsic concentration is varied from $10^{10} - 10^{16}$ cm^{-3} at $\mu_n = 10^{-3}$ cm^2/V.s. In Fig. 4.3b, mobility is varied from $10^{-4} - 10$ cm^2/V.s at $n_i = 10^{15}$ cm^{-3}. The range of parametric study in this chapter is well within the various intrinsic parameter values for some well-known organic materials such as: P3HT (Poly3-hexylthiophene), PT (Polythiophenes), AlPcCl (Aluminium phthalocyanine chloride), etc [29, 57, 82, 83, 84, 85, 86, 87]. For example, in P3HT, $\mu_n \approx 10^{-3} - 10^{-4}$ cm^2/V.s, $n_i \approx 6{\times}10^{15}$ cm^{-3}, and $N_C \approx 10^{18} - 10^{19}$ cm^{-3}[82, 83, 84]. As shown in Fig. 4.3a and 4.3b, the results are consistent with data in Fig. 4.1b. With electron tunneling is included through surface states effect, current density is able to reach space charge condition at larger V_G ($n = 2$).

In Fig. 4.3a, at large V_G, the J values converge and follow MG law ($n = 2$). While at small V_G, the J values are different for different n_i values since the transition voltage $V_{\Omega-MG}$ is proportional to n_i. At smaller mobility, the SCL current is reached at lower V_G since tunneling start to dominate at smaller V_G (drift current component is smaller when mobility is smaller). The result suggests that effect of intrinsic concentration n_i is as predicted from the theory of SCL current in solid, and the effect of mobility to the SCL formation comes from the relative value of the drift component to the tunneling. As long as tunneling dominates the current flow, SCL formation will occur. This finding suggests that the result is still applicable in polymer and many organic materials, even though it is well-known that the mobility is field and temperature dependent [25, 28], but the range of mobility in these materials is notably very small (less than 10^{-3} cm^2/V.s).

All of the above Medici results are simulated using cathode width $W = 40$ μm. These results are considered as 1D (the current density is independent of cathode width) since $W \gg L$ ($W = 4L$). In the previous chapter and recent publications

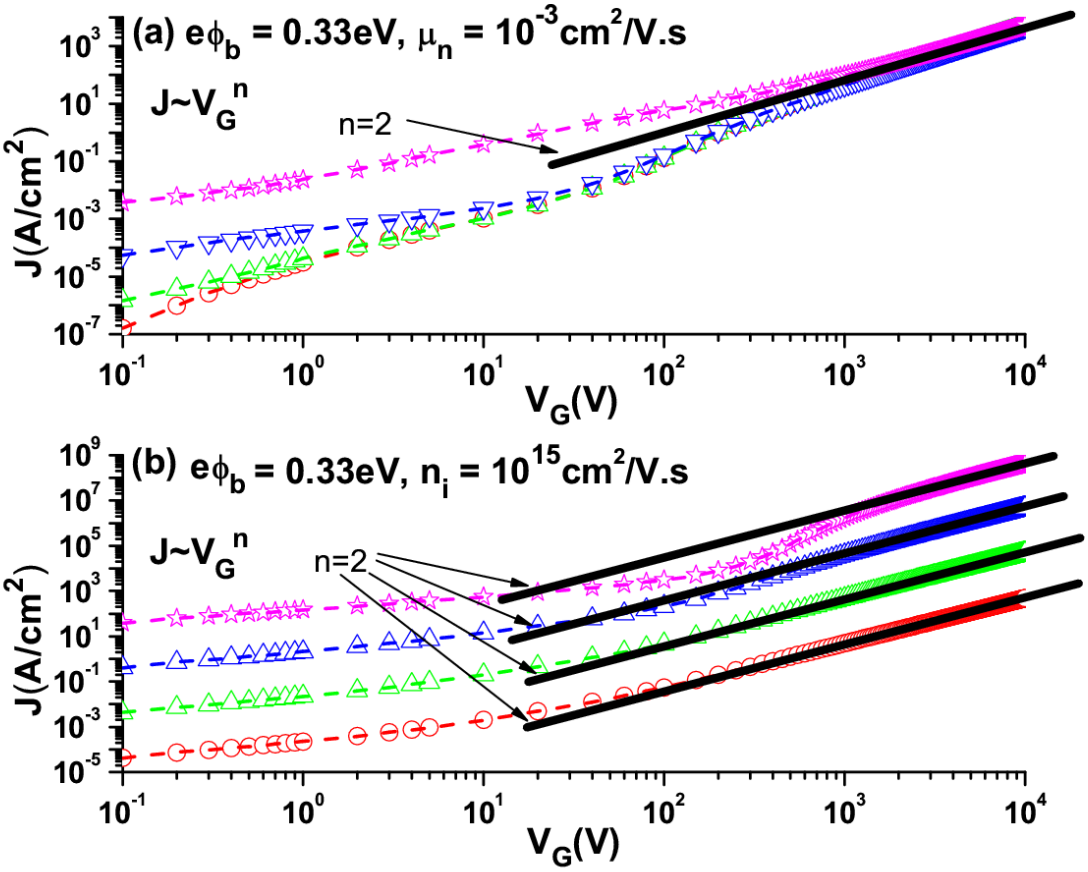

Figure 4.3: (a) J vs V_G for $L = 10$ μm, $e\phi_b = 0.33$ eV, $\mu_n = 10^{-3}$ cm^2/V.s, and $N_C = 5{\times}10^{18}$ cm^{-3}. Each symbol from top to bottom represents n_i from 10^{16}, 10^{14}, 10^{12} to 10^{10} cm^{-3}. (b) J vs V_G for $L = 10$ μm, $e\phi_b = 0.33$ eV, $n_i = 10^{15}$ cm^{-3}, and $N_C = 5{\times}10^{18}$ cm^{-3}. Each symbol from top to bottom represents μ_n from 10^2, 1, 10^{-2} to 10^{-4} cm^2/V.s. Dashed lines represent numerical simulation result and open symbols represent Medici simulation result. Black solid lines represent exponent n from $J \sim {V_G}^n$ with $n = 2$ represents SCL-MG

4.3 Results and Discussion

[58, 59, 60, 73], the theory of enhancement in current has been shown based on simple analytical derivation with $\frac{J_{MG}[2D]}{J_{MG}[1D]} = 1 + G \times F$, with $F = \int_0^L (x/L) n(x) dx / \int_0^L n(x) dx$. The theoretical value of F for a trap-free solid dielectric is 1/3 [73]. The parameter F measures the normalized mean position of the injected electrons in a solid of length L, and $n(x)$ is the electron density in a solid, which is calculated by the 1D MG model. Here, G is a geometrical parameter, which depends on the geometrical properties of the emission area (between the cathode and a trap-free solid). For simplicity, the electrons are injected from a planar shape cathode with a cross-sectional area of finite width, W, and infinitely long thickness, d, which corresponds to $G = (4/\pi)/(W/L)$ for $W/L > 1$ [60]. The values of F are calculated using the above formula for F for J vs V_G that are shown in Fig. 4.1. The results are shown in Fig. 4.4.

The results of F reinforce the findings in Fig. 4.1. In Fig. 4.4a, with the tunneling neglected, $F = 1/3$ only at $e\phi_b = 0$ eV (no barrier height) thus SCL conduction is reached. However, as $e\phi_b$ increases, F values goes up from 1/2 to 1 (at larger V_G). Note that, even at $e\phi_b = 0.33$ eV, the F does not converge to 1/3 (no SCL formation). These two values of $F = 1/2$ and 1 indicate Ohmic conduction with $n(x)$ is constant and $n(x) \approx n_i$ at small $e\phi_b$ thus $F \approx 1/2$. Even though $n(x)$ is also constant but $n(x) \ll n_i$ as $e\phi_b$ getting larger, thus $F \approx 1$ [n(x=L)] dominates both the numerator and denominator in F formula). When surface states incorporated into the calculation (see Fig. 4.4b), F is approximately 1/3 or approaching 1/3 at different barrier heights $e\phi_b$ indicates SCL conduction or on the verge of reaching it. This $F = 1/3$ is similar to the $F = 1/4$ for SCL current in free space [58, 59, 60].

To show the enhancement of the current in SCL region, the J vs V_G characteristics are simulated in Medici by using $W = 20$, 10, and 5 μm, $L = 10$ μm and $\mu_n = 10$ cm^2/V.s. The results are shown in terms of $\frac{J_{MG}[2D]}{J_{MG}[1D]}$ in Fig. 4.5 at $V_G = 10$ kV. The value is calculated using $\frac{J_{MG}[2D]}{J_{MG}[1D]} = 1 + F \times G$ where $J_{MG}[2D]$ is the Medici simulation results using $W = 20$, 10, and 5 μm, with $J_{MG}[1D]$ is the Medici result at $W = 40$

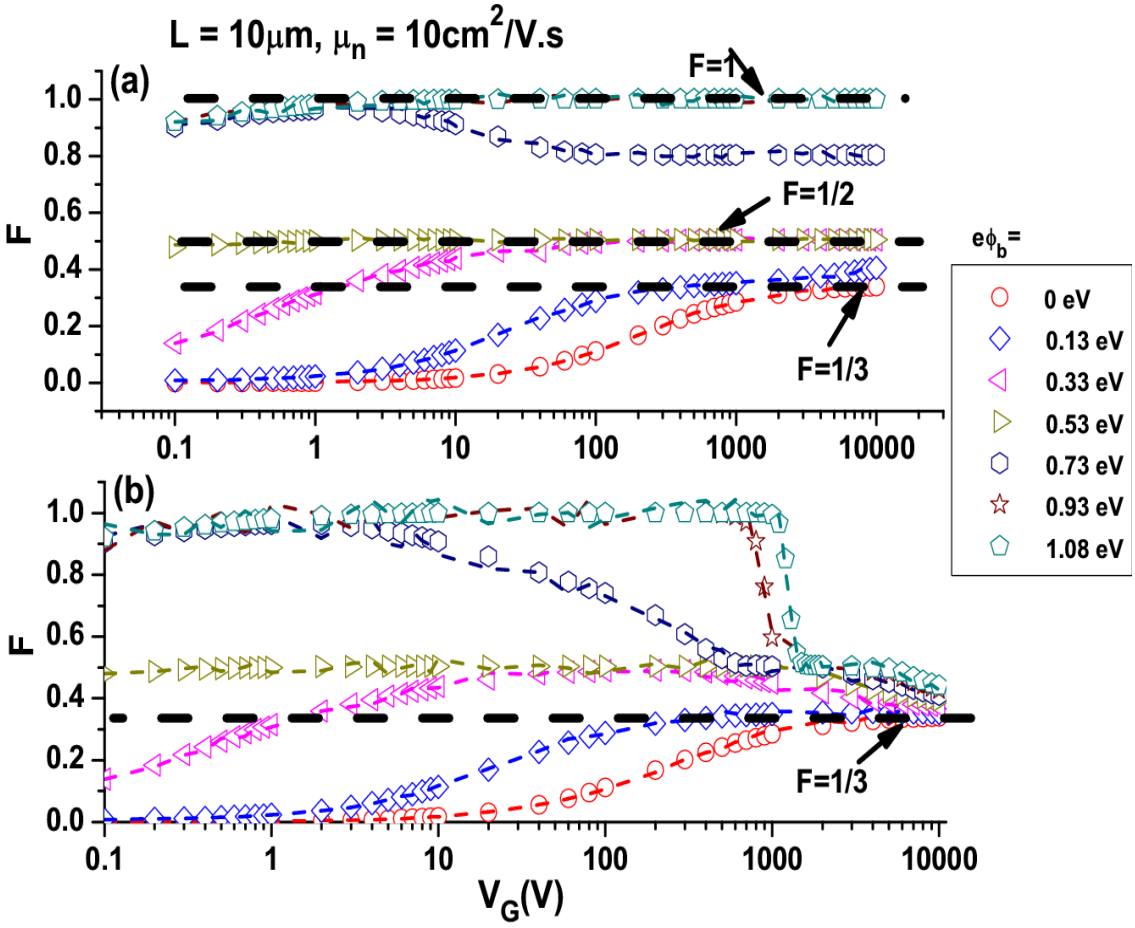

Figure 4.4: F vs V_G for $L = 10$ μm and $\mu_n = 10$ cm^2/V.s, at $e\phi_b$ from 0 eV to 1.08 eV: (a) without surface states, and (b) with surface states. Black dashed lines represent theoretical value for Ohm's law ($F = 1$ and $1/2$) and MG law ($F = 1/3$)

4.3 Results and Discussion

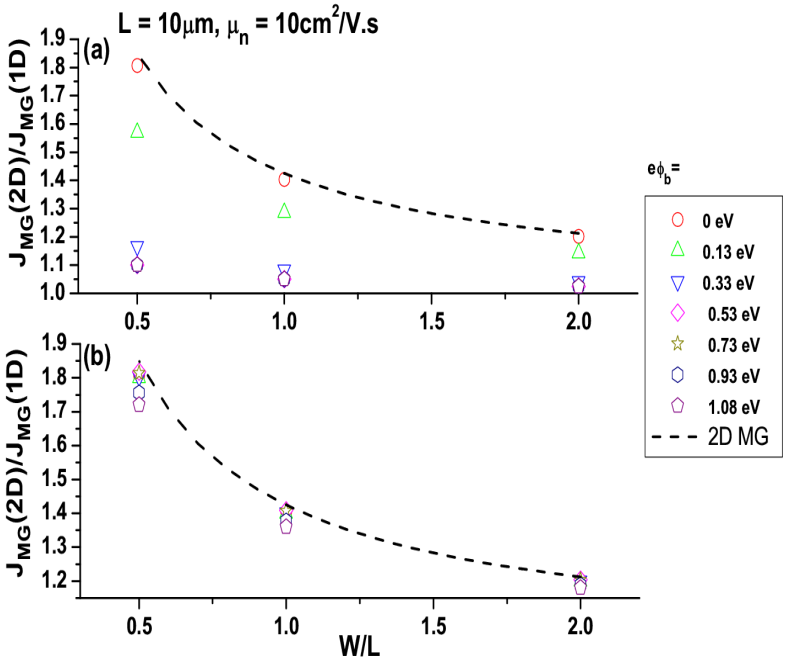

Figure 4.5: $\frac{J_{MG}[2D]}{J_{MG}[1D]}$ vs W/L for $L = 10$ μm and $\mu_n = 10$ cm^2/V.s at $V_G = 10$ kV, $e\phi_b$ from 0 eV to 1.08 eV: (a) without surface states, and (b) with surface states. Black dashed lines represent theoretical value for Ohm's law ($F = 1$ and $1/2$) and MG law ($F = 1/3$)

μm. Without tunneling (Fig. 4.5a), the current enhancement quickly drops to almost 1 for $e\phi_b \geq 0.33$ eV and does not follow the theoretical enhancement for SCL-MG. This result reinforces the findings from Fig. 4.4a in which the SCL conduction is not able to be reached and the current conduction is Ohmic, hence, there is almost no enhancement ($\frac{J_{MG}[2D]}{J_{MG}[1D]} \approx 1$). However, in Fig. 4.5b, with tunneling, at larger $e\phi_b$, it still agrees quite well with the theoretical current enhancement in SCL-MG which means it is able to reach SCL region. The reduction in the enhancement of the current density is because for larger barrier height $e\phi_b$ showing lesser degree of SCL formation.

4.4 Summary

In conclusion, a simple quantitative 2D MG law for SCL electron flow in a trap-free solid (with a simple 2D shape) by incorporating the contact effect. The model has been confirmed by a 2D device simulator Medici. If the energy of electrons is higher than the barrier height, it will be able to move through by the thermionic emission. However, the electrons can also tunnel through the interface by tunneling. Tunneling which is incorporated through surface states plays an important role together with the barrier height in order to reach SCL current region. Tunneling is directly affected by intrinsic material properties such as effective Richardson constant A^* and effective tunneling mass. If tunneling current dominates over drift-diffusion current then SCL region can be reached even for a contact with a finite barrier. This finding is different from the conventional understanding that SCL current or MG law can only be reached with an Ohmic contact. Tunneling through surface states facilitates SCL current formation since it gives rise to more electrons can be injected to the dielectric.

This result may be useful in deciding the amount of maximum SCL current density in novel 2D structures such as: polymer, organic materials, and nanowires that have been reported to be operating at SCL regime [25, 28, 31, 32, 33, 72]. The extension for future study is to include traps in bulk dielectric (such as traps exponentially distributed in energy) and understand the interplay of traps in bulk and interface and also the effect of field and temperature dependent mobility as it is prominent in organic materials and nanowires [88, 89, 90, 91].

CHAPTER 5

SPACE CHARGE LIMITED (SCL) CURRENT IN A GAP OF COMBINED VACUUM AND SOLID

5.1 Introduction

Charge current injection in a solid dielectric can be classified into low and high charge injection. In the low charge injection regime, the amount of injected charge is considerably lower than the intrinsic concentration of the solid and the current-voltage (I-V) characteristic follows Ohm's law. On the other hand, at high charge injection regime, the I-V characteristic is influenced by the self-electric field created, and it will become space charge limited (SCL) current. For a one dimensional (1D) trap-free solid, SCL electron current density is described by the classical MG law (see Eq. 2.2) [1, 39].

There is renewed interest in SCL conduction found in many novel devices, such as: GaN nanorods [92], organic devices [31, 93], polymer transistors [72], nanowires [33], magnetoresistances [94, 95] and nanocrystallites embedded silicon Schottky

junctions [37]. Analytical 2D MG law was also developed recently for Ohmic contact [73] as discussed in Chap. 3 and Schottky contact [96] as discussed in Chap. 4.

On the other hand, for a vacuum (or free space) gap, the equivalent SCL electron current density is known as Child-Langmuir (CL) law (see Eq. 2.1) [2, 3]. The studies of CL law has been an area of active research in the development of non-neutral plasma physics, high current diodes, high power microwave sources, vacuum microelectronics and sheath physics. Recent developments include analytical multi-dimensional models, contact properties, quantum tunneling and ultrafast time scale [58, 59, 60, 61, 97, 98].

While the transition between the MG and CL law can be formulated by controlling the effect of collision in the model [73] (see Chap. 3), there is no model yet to address the SCL electron transport in a system consisting of both solid and free space. In this case, the exponent (n) of the voltage dependence $J \sim {V_G}^n$ will be neither $n = 2$ nor $n = 3/2$ as predicted by MG law and CL law, respectively. A recent experimental result has reported $n = 1.65$ for SCL conduction measured by a set up in using STM with a gap consisted of vacuum and the tested solid dielectric [38]. Thus it is of interest to develop a 1D model to determine the new scaling of n in such a hybrid system with both free space and solid. The value of the exponential dependence of the applied voltage V_G to the current density J (n), will be calculated as a function of mobility, gap length, and the relative length scales of solid and free space. The value of dielectric constant is fixed at $\epsilon_r = 11.7$, unless mentioned otherwise. In the model presented in this chapter, there will be two different cases shown, respectively, showing the SCL electron injection to free space region first before entering the dielectric region, and vice versa.

5.2 Model Formulation for Vacuum and Solid Gap

For the first case, a hybrid system consisting of free space region and dielectric will be shown, which is respectively located in the region of x=0 to x=x_1, and x=x_1 to x=L. The electrons are injected from the grounded cathode at x=0 to the anode at x=L with an applied voltage of V_G. In the free space region (x=0 to x=x_1), the standard derivation of CL law in solving the Poisson equation, drift current density equation and energy balance condition will be used:

$$\frac{d^2\psi_n(x)}{dx^2} = \frac{en(x)}{\epsilon_0}, \tag{5.1}$$

where $\psi_n(x)$ is electrostatic potential and $n(x)$ is electron concentration. And for the drift current density equation:

$$J = -en(x)v(x), \tag{5.2}$$

where J is the electron drift current density and $v(x)$ is the drift velocity in vacuum. The energy balance equation is needed to find the drift velocity $v(x)$ as a function of electrostatic potential $\psi(x)$:

$$\frac{1}{2}m_e v^2(x) = e\psi_n(x), \tag{5.3}$$

where m_e is the electron mass in vacuum. Eq. (5.3) gives the relation between the drift velocity to electrostatic potential, $v(x) = (2e\psi_n(x)/m_e)^{0.5}$. The one-dimensional (1D) CL law can be found by solving the three equations above, which gives:

$$J = \frac{4\epsilon_0}{9}\sqrt{\frac{2e}{m_e}}\frac{{\psi_{x_1}}^{3/2}}{{x_1}^2}. \tag{5.4}$$

Here, ψ_{x_1} is the electrostatic potential at the interface (x=x_1), and it can be later obtained by matching the electric field at the interface given by

$$\xi(x_1) = \sqrt{\frac{-2J}{\epsilon_0}\sqrt{\frac{2m_e}{e}\psi_{x_1}}}. \tag{5.5}$$

5.2 Model Formulation for Vacuum and Solid Gap

In the region of dielectric (x=x_1 to x=L), the Poisson equation and the drift current density equation in the solid dielectric $J = en(x)\mu_n\xi(x)$ are solved, where μ_n is electron mobility in the dielectric. The equations are

$$\frac{d^2\psi_n(x)}{dx^2} = \frac{en(x)}{\epsilon_r\epsilon_0},$$
$$\frac{d\xi(x)}{dx} = \frac{-en(x)}{\epsilon_r\epsilon_0},$$
$$J = -en(x)v(x) \quad \text{and} \quad v(x) = -\mu_n\xi(x),$$

By combining the equations, we have

$$\frac{d\xi(x)}{dx} = \frac{-J}{\mu_n\xi(x)\epsilon_r\epsilon_0},$$
$$\int_{\xi(x_1)}^{\xi(x)} \xi(x)d\xi(x) = \frac{-J}{\mu_n\epsilon_r\epsilon_0}\int_{x_1}^{x} dx,$$
$$\xi^2(x) - \xi^2(x_1) = \frac{-2J}{\mu_n\epsilon_r\epsilon_0}(x - x_1),$$
$$\xi(x) = \sqrt{\frac{-2J}{\mu_n\epsilon_r\epsilon_0}(x - x_1) + \xi^2(x_1)},$$
$$\int_{\psi_{x_1}}^{V_G} d\psi_n(x) = -\int_{x_1}^{x}\left[\sqrt{\frac{-2J}{\mu_n\epsilon_r\epsilon_0}(x - x_1) + \xi^2(x_1)}\right]dx,$$

In doing so, the relationship between $\xi(x_1)$ and ψ_{x_1} are obtained, given by

$$V_G - \psi_{x_1} = -\frac{\mu_n\epsilon_r\epsilon_0}{3J}\left[\left(\frac{-2J}{\mu_n\epsilon_r\epsilon_0}(L - x_1) + \xi^2(x_1)\right)^{3/2} - \xi^3(x_1)\right]. \tag{5.6}$$

Thus for a given L, x_1 and μ_n, Eqs. (5.4) to (5.6) may be solved numerically to obtain the SCL current density J as a function of V_G. In our model, we have fixed $\epsilon_r = 11.7$ and vary μ_n for various values of L, V_G, and x_1.

5.2.1 Results and Discussion for Vacuum and Solid Gap

In Fig. 5.1a - 5.1d, the resulting SCL current density J vs V_G for various values x_1/L (= 10^{-5}, 0.1, 0.5, and 1) are shown at different L (= 10 and 1 μm), and μ_n (= 10 and 10^{-4} cm^2/V.s).

5.2 Model Formulation for Vacuum and Solid Gap

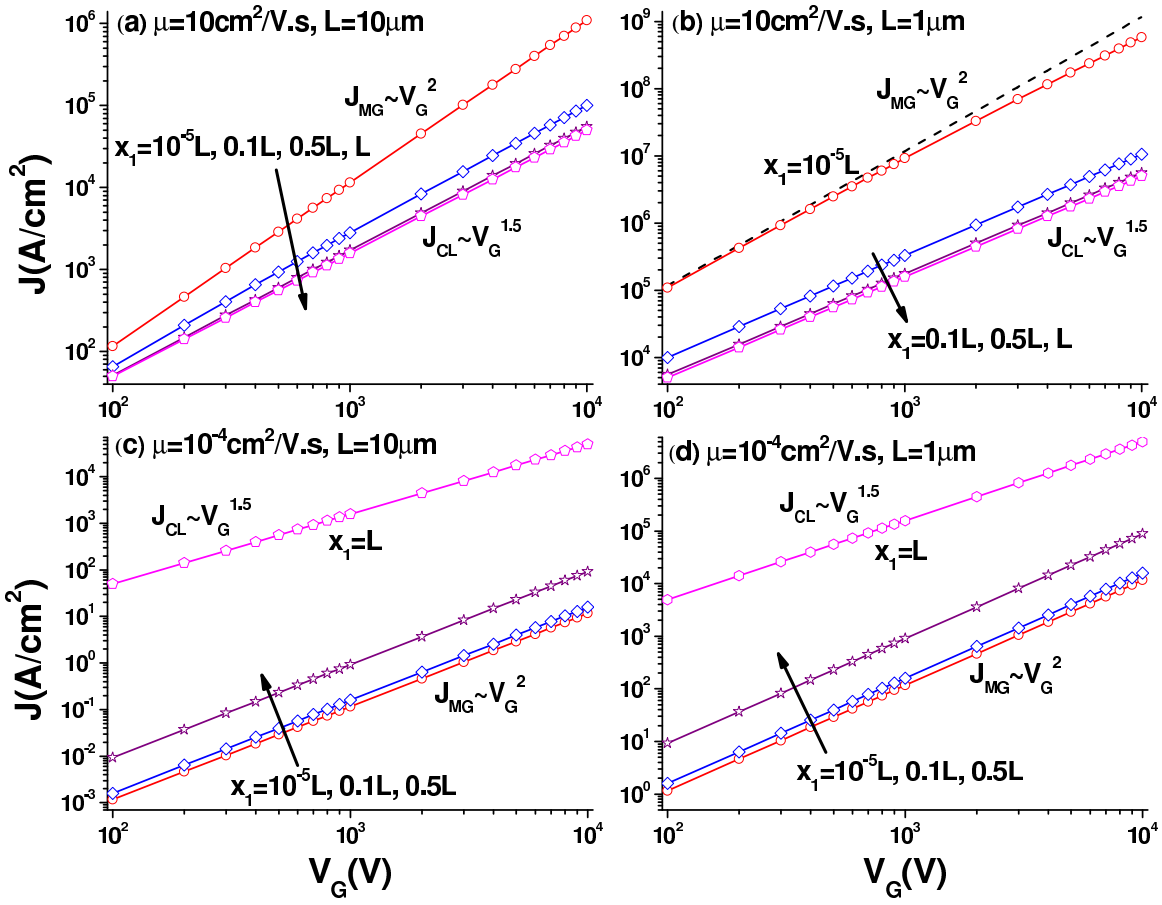

Figure 5.1: J vs V_G plotted in log-log scale in the case of x=0 (cathode) to x=x_1 consists of vacuum and between x=x_1 to x=L (anode) consists of solid dielectric shown at four different x_1=$10^{-5}L$ (near cathode), $0.1L$, $0.5L$, and L (near anode) with, (a) L=10 μm and μ_n=10 cm^2/V.s, (b) L=1 μm and μ_n=10 cm^2/V.s, (c) L=10 μm and μ_n=10^{-4} cm^2/V.s, (d) L=1 μm and μ_n=10^{-4} cm^2/V.s. The arrow indicates the values of x_1 in an increasing order. Black dashed line in (b) near x_1=$10^{-5}L$ shows J_{MG}~$V_G{}^2$. In (a), (c), and (d) the value of J vs V_G at x_1=$10^{-5}L$ coincides with J_{MG}~$V_G{}^2$. While at x_1=L, all the J vs V_G fully recovers to J_{CL}~$V_G{}^{3/2}$

The new scaling between $n = 2$ and 3/2 can be obtained by fitting the numerical results using $J \sim {V_G}^n$ for arbitrary values of x_1. At small $x_1 = 10^{-5}L$, the current density J follows MG law ($J \sim {V_G}^2$) with $n = 2$ as there is nearly no vacuum region in the gap. At $x_1 = L$, it also recovers to the CL law ($J \sim {V_G}^{3/2}$) with $n = 3/2$ as it is a entirely vacuum gap. The magnitude of J is dependent on the mobility used in the model. For high mobility case (μ_n=10 cm^2/V.s), the results show higher MG law as compared to CL law as shown in Fig. 5.1a and 5.1b. On the other hand, CL law is higher than MG law for low mobility case μ_n=10^{-4} cm^2/V.s (see Fig. 5.1c and 5.1d).

In order to clearly show the transition between the MG law and CL law, the n scaling of J vs ${V_G}^n$ is shown in Fig. 5.2 as a function of x_1. The results indicate the fast and slow decreasing rate from $n = 2$ to $n = 3/2$ (as a function of x_1) for high mobility and low mobility case, respectively. These findings show the important effect of mobility in deciding the current density (J) dependence to applied bias (V_G). When the mobility is high (red circle and black square data points), the value of MG law is much higher than the CL law, the transition of $n = 2$ to $n = 3/2$ will occur very fast at small x_1. If the mobility value is low (blue diamond and purple star data points), MG law is much smaller than the CL law, the transition from n=2 to n=3/2 occurs at large x_1. The effect of gap length L is observable although not as strong as the mobility. In the larger gap length ($L = 10$ μm) the decreasing rate of the exponential factor from 2 to 3/2 is slower than the smaller gap length ($L = 1$ μm).

5.3 Model Formulation for Solid and Vacuum Gap

For the second model to be shown below, the location of the free space and dielectric is reversed, such that the electrons will be injected into the dielectric (x=0 to x=x_1) first before entering the free space region (x=x_1 to x=L). In this case, the SCL

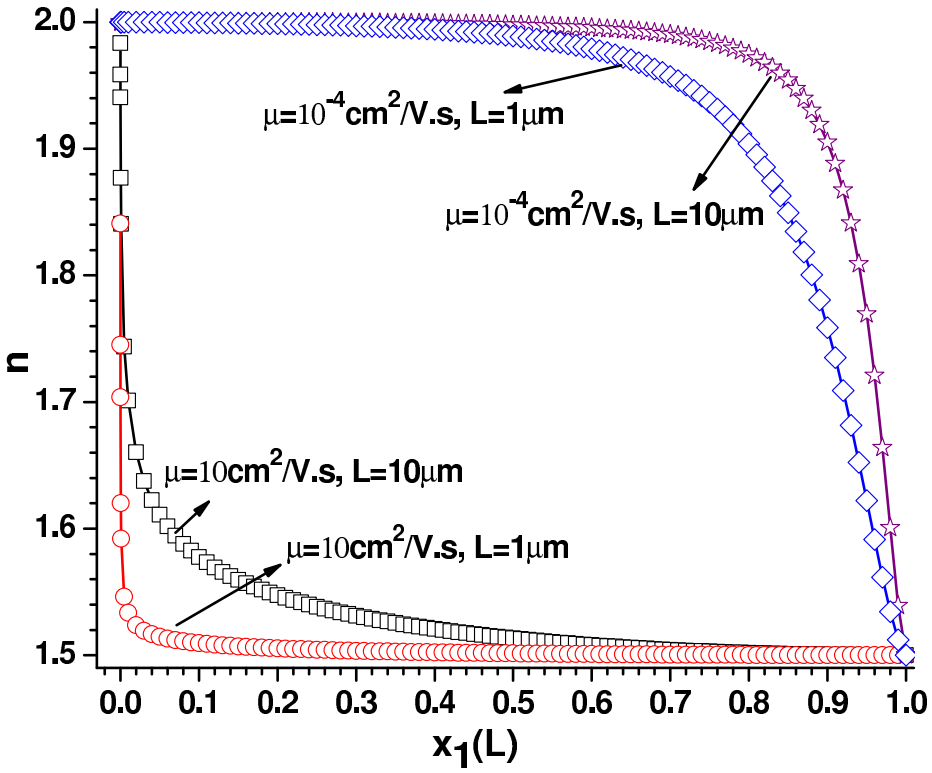

Figure 5.2: The exponential factor n of $J \sim V_G{}^n$ vs x_1 in the case of x=0 (cathode) to x=x_1 consists of vacuum and between x=x_1 to x=L (anode) consists of solid dielectric with, L=10 μm and μ_n=10 cm^2/V.s is represented by black square symbols and line, L=1 μm and μ_n=10 cm^2/V.s is represented by red circle symbols and line, L=10 μm and μ_n=10^{-4} cm^2/V.s is represented by purple star symbols and line, L=1 μm and μ_n=10^{-4} cm^2/V.s is represented by blue diamond symbols and line

current density in dielectric region (according to the MG law) is

$$J = \frac{9}{8}\mu_n \epsilon_0 \epsilon_r \frac{{\psi_{x_1}}^2}{{x_1}^3}. \tag{5.7}$$

The electric field at the interface is

$$\xi(x_1) = \sqrt{\frac{-2J}{\mu_n \epsilon_r \epsilon_0} x_1}. \tag{5.8}$$

In the free space charge region (x=x_1 to x=L), the standard derivation of the CL law is used to obtain the electric field:

$$\frac{d^2\psi_n(x)}{dx^2} = \frac{en(x)}{\epsilon_0},$$

Combining the equations, we have the following derivation

$$J = -en(x)v(x) \quad \text{and} \quad v(x) = \sqrt{2e\psi_{\mathrm{n}}(\mathrm{x})/m_e},$$

$$\frac{d^2\psi_n(x)}{dx} = \frac{-J}{\epsilon_0}\sqrt{2e\psi_n(x)/m_e},$$

$$\int \frac{2d\psi_n(x)}{dx}\frac{d^2\psi_n(x)}{dx^2} = \int \frac{-2J}{\epsilon_0}\sqrt{m_e/2e\psi_n(x)}\frac{d\psi_n(x)}{dx},$$

$$\xi^2(x) - \xi^2(x_1) = \frac{-2J}{\epsilon_0}\sqrt{\frac{2m_e}{e}\Big(\psi_n(x) - \psi_{x_1}\Big)},$$

$$\xi(x) = \frac{-d\psi_n(x)}{dx} = -\left[\frac{-2J}{\epsilon_0}\sqrt{\frac{2m_e}{e}\Big(\psi(x) - \psi_{x_1}\Big)} + \xi^2(x_1)\right]^{1/2}. \tag{5.9}$$

Finally, Eqs (5.7) to (5.9) can be solved numerically with the boundary conditions of $\psi(x) = \psi_{x_1}$ at x=x_1 and $\psi(x) = V_G$ at x=L. In doing so, the SCL current density J as a function of V_G can be obtained numerically for a given L, x_1 and μ_n.

5.3.1 Results and Discussion for Solid and Vacuum Gap

The results of J vs V_G as a function of x_1 are shown in Fig. 5.3a - 5.3d with the same parameters as shown in Fig. 5.1a - 5.1d. In this case, we have $n = 3/2$ (pure CL law) at small $x_1 = 10^{-5}L$ and $n = 2$ (pure MG law) at large $x_1 = L$. If the mobility is

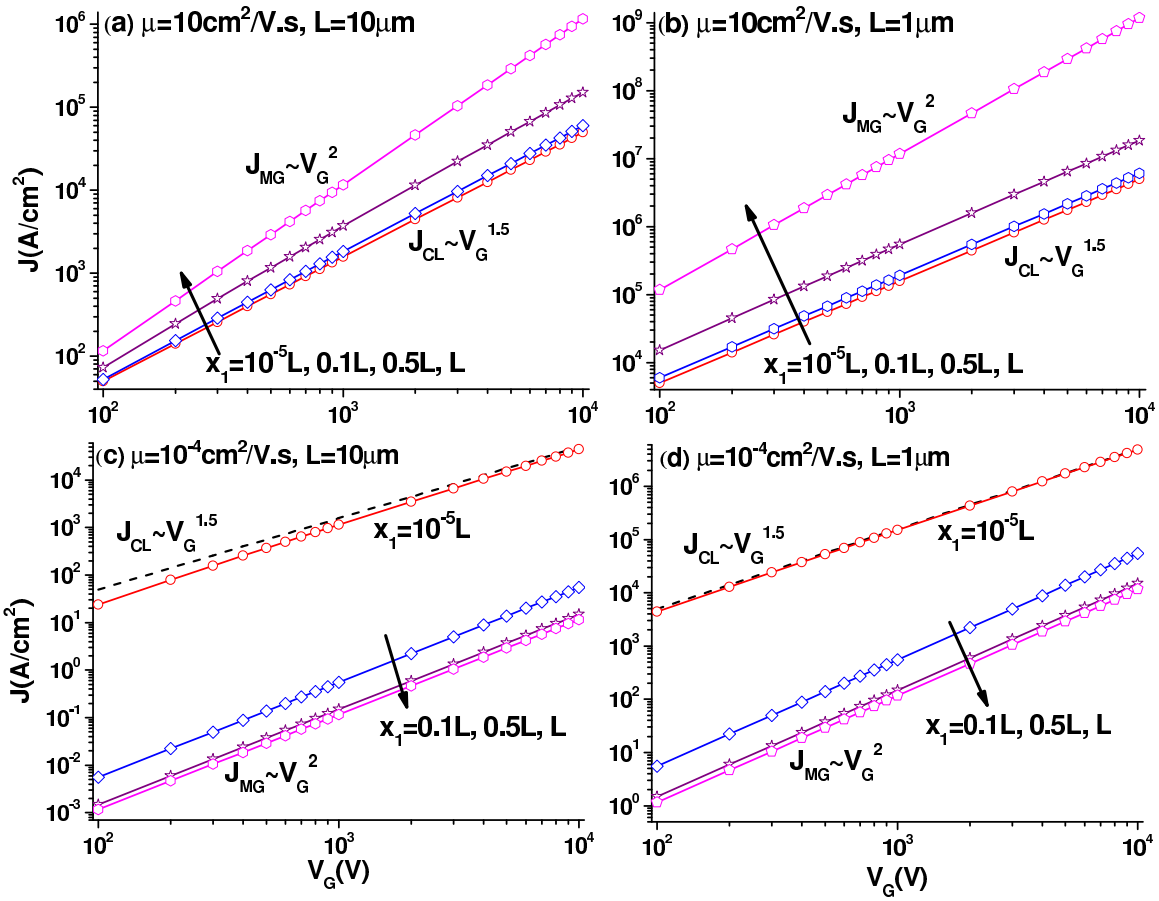

Figure 5.3: J vs V_G plotted in log-log scale in the case of x=0 (cathode) to x=x_1 consists of solid dielectric and between x=x_1 to x=L (anode) consists of vacuum shown at four different x_1=$10^{-5}L$ (near cathode), $0.1L$, $0.5L$, and L(near anode) with, (a) L=10 μm and μ_n=10 cm^2/V.s, (b) L=1 μm and μ_n=10 cm^2/V.s, (c) L=10 μm and μ_n=10^{-4} cm^2/V.s, (d) L=1 μm and μ_n=10^{-4} cm^2/V.s. The arrow indicates the values of x_1 in an increasing order. Black dashed lines in (c) and (d) near x_1=$10^{-5}L$ show J_{MG}~$V_G{}^2$. In (a) and (b) the value of J vs V_G at x_1=$10^{-5}L$ coincides with J_{MG}~$V_G{}^2$. While at x_1=L, all the J vs V_G fully recovers to J_{MG}~$V_G{}^2$

high (μ_n=10 cm^2/V.s), MG law is higher than the CL law as shown in Fig. 5.3b and 5.3d. For low mobility case (μ_n=10^{-4} cm^2/V.s), the results show higher CL law (see Fig. 5.3a and 5.3c.

The exponent n in J vs ${V_G}^n$ dependence is shown as a function of x_1 in Fig. 5.4. In this second case, the transition is from $n = 3/2$ at small $x_1 \approx 0$ (nearly a vacuum gap) to $n = 2$ at large $x_1 = L$ (a dielectric diode). The dependence of n on the range of x_1 will be sensitive to the mobility and L. At low mobility case (μ_n=10^{-4} cm^2/V.s), it behaves almost like a pure solid dielectric diode with $n = 2$ except in the range of very small $x_1 \approx 0$. At high mobility case (μ_n=10 cm^2/V.s), the transition from $n = 3/2$ to 2 is moderate, and the effects of both solid dielectric and the vacuum gap are equivalent. The effect of the gap length L is more significant at high mobility as compared to low mobility.

It is also important to note the results presented in Figs. 5.2 and 5.4 on its dependence of parameters (x_1, μ_n and L) are not symmetrical to each other. The n calculated from each model, solely depends on the matching of the electric field profile at the interface. While $\epsilon_r = 11.7$ with μ_n=10^{-4} – 10 cm^2/V.s have been chosen to present the model, the results presented in the above figure is valid for any fixed value of $\epsilon_r \times \epsilon_0 \times \mu_n$.

In a recent paper [38], an experimental study was performed to understand the physical mechanism of the incorporation of nitrogen in high-κ dielectric hafnium oxide (HfO_2). It was reported that SCL conduction was measured by using scanning tunneling microscopy (STM), which showed a current vs voltage (I-V) of $I \sim V^n$ with $n = 1.65$ in the range of $I = 0.4$ nA at $V = 4$ V to $I = 1.8$ nA at $V = 10$ V (see Fig. 7 in Ref. [38]). The deviation of the reported $n = 1.65$ from $n = 2$ (MG law) is due to a finite vacuum space (0.5 nm) between the STM tip and the dielectric layers consisted of HfO_2 (5.1 nm) and SiO_x (1.6 nm) after the nitrogen annealing. The SCL electron current is injected into the dielectric layers and then collected by the STM

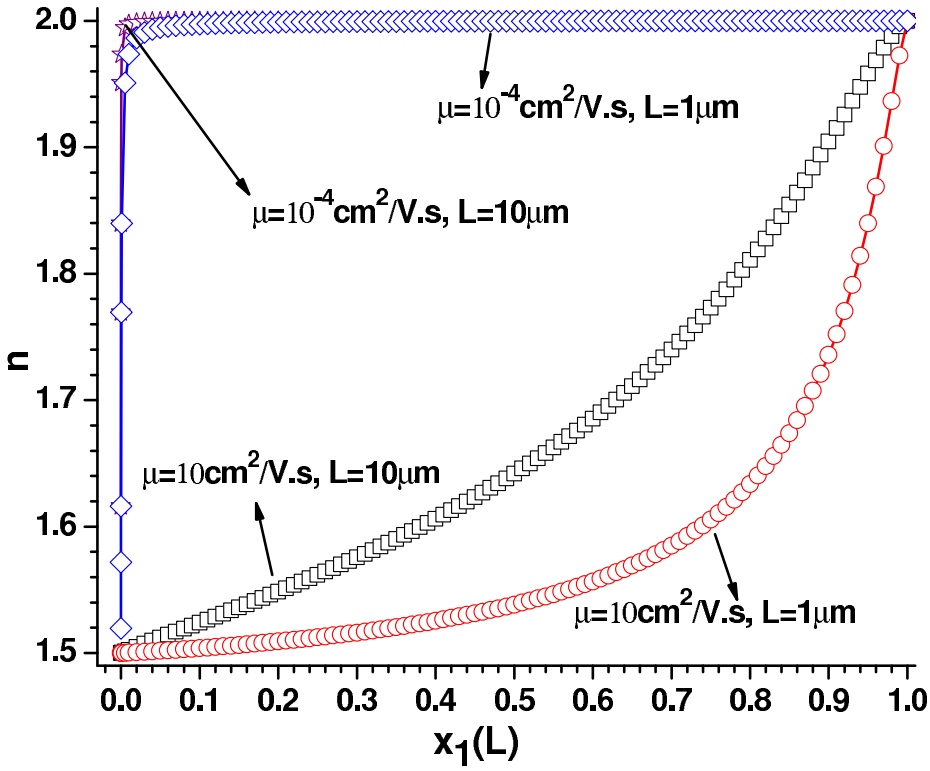

Figure 5.4: The exponential factor n of $J \sim V_G{}^n$ vs x_1 in the case of x=0 (cathode) to x=x_1 consists of solid dielectric and between x=x_1 to x=L (anode) consists vacuum with, L=10 μm and μ_n=10 cm^2/V.s is represented by black square symbols and line, L=1 μm and μ_n=10 cm^2/V.s is represented by red circle symbols and line, L=10 μm and μ_n=10^{-4} cm^2/V.s is represented by purple star symbols and line, L=1 μm and μ_n=10^{-4} cm^2/V.s is represented by blue diamond symbols and line

tip with a circular area of 10 nm in radius. Using the experimental parameters of x_1 = 5.1 + 1.6 = 6.7 nm, and $L = x_1$ + 0.5 nm = 7.2 nm, n = 1.65 can be shown at a value of $\epsilon_r \times \mu_n \approx 3 \times 10^{-4}$ (with μ_n in cm^2/V.s, which corresponds to $\mu_n \approx 10^{-5}$ cm^2/V.s at $\epsilon_r = 25$). The variation of calculated n as a function of $\epsilon_r \times \epsilon_0 \times \mu_n$ is shown in Fig. 5.5.

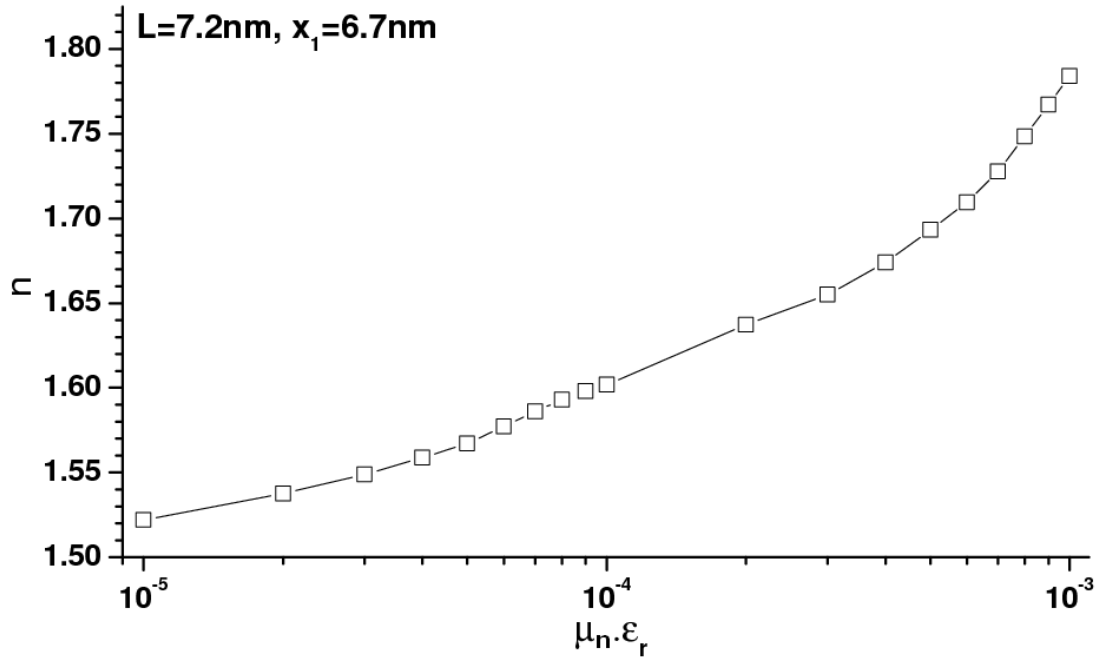

Figure 5.5: n vs $\epsilon_r \times \mu_n$ (in cm^2/V.s) plotted in linear-log scale for the case of the STM tip experiment with L = 7.2 nm and x_1 = 6.7 nm

5.4 Summary

In conclusion, the study of SCL electron current density in a system with a combination of both free space and solid dielectric have been shown. The exponential factor n of J vs $V_G{}^n$ of SCL conduction between $n = 3/2$ (pure free space - CL law)

to $n = 2$ (pure solid - MG law) is determined as a function of $\epsilon_r \times \epsilon_0 \times \mu_n$ and relative length scale of both free space and dielectric. The model has been checked by recovering $n = 3/2$ and 2 at both limits. The differences between the transport of SCL electrons through the vacuum first and then the solid dielectric or vice versa have been studied.

In the case whereby the electrons are injected through vacuum first and then solid, the speed of electron traveling in vacuum (ballistic transport) is much larger than the speed of electron traveling in the solid. When the electrons travel from vacuum to solid, the speed of electrons will be reduced due to the collisions in the solid. At high mobility, the transport is CL dominated since the speed of electron is reduced by a lesser amount since there will be less collisions while at low mobility, the speed of electron is reduced by a greater amount since there will be more collisions in the solid. This can be seen from Fig. 5.2 where at high mobility, $\mu_n = 10$ cm^2/V.s, the exponential factor n drops very fast to $n = 1.5$ ($J \propto J_{CL}$) at small x_1 (CL dominated) while at low mobility, $\mu_n = 10^{-4}$ cm^2/V.s, the dropping rate is much slower. The effect of gap length L is less subtle than the mobility μ_n although it does show the same physical conclusion with smaller L gives faster dropping rate of n to $n = 1.5$ or CL law since with smaller L the electrons will travel at shorter time in the solid (less space charge effects contributed by the solid to the whole system).

The same physical picture can also be derived for the second case whereby the electrons are injected through the solid and then the free space. At low mobility, the transport is MG dominated since the speed of electrons is greatly reduced when traveling in the solid. The exponential factor n rises very fast to $n = 2$ at small x_1 (MG dominated) while at high mobility, the transition to MG law occurs much slower (see Fig. 5.4). In addition, at smaller L, the transition to MG law is slower since the electrons spent lesser time in the solid. The model is also used to explain the reported $n = 1.65$ in a recent experiment [38].

CHAPTER 6

SHOT NOISE REDUCTION IN SPACE CHARGE LIMITED (SCL) ELECTRON INJECTION THROUGH A SCHOTTKY CONTACT FOR A GaN DIODE

6.1 Introduction

Noise inevitably exists in any signal due to the nature of electrons carrying the signal and thus carries information to understand the charge transport of electrons. One type of electrical noise that has been used extensively to study the electron transport is shot noise. Shot noise is the fluctuation in the electrical signal due to the discreteness of electron charges. It was firstly studied by Schottky for the electron thermionic emission in a vacuum tube [99], and the spectral density of the shot noise is $S = 2eI$, where I is the mean value of the transmitted current and e is the electronic charge. The spectral density of shot noise is calculated by taking the Fourier transform of the temporal distribution of the mean current. This is usually known as the uncorrelated (or full) shot noise if the electrons are emitted randomly and independently and thus described by a random Poisson process. The deviation from the uncorrelated shot

noise is normally given by the Fano factor $\gamma = S/2eI$, where $\gamma < 1$ indicates the suppression of shot noise due to the correlations among the electrons such as the Coulomb correlation (classically), and or the effect of quantum partitioning due to Pauli exclusion principle (quantum mechanically) [100, 101]. The study of quantum shot noise is also important to understand the particle-wave duality of electrons in many mesoscopic systems [102].

It was firstly shown by North [103] that shot noise can be suppressed by the Coulomb repulsion of the CL law in a vacuum tube. The early work of shot noise in SCL current in solids is started by Shulman [18] that proves the ohmic nature of contacts of Ga and In to CdS. He found that the noise power spectrum of the photoconductive current measurement represents that of a pure shot noise characteristic. Since then, theoretical works by Sergiescu [20] and van der Ziel [21] shown that shot noise exists in a dielectric diode. Other works of SCL current in relation with shot noise suppression in solids experimentally and theoretically were also reported and studied [19, 22, 23]. More recently, the shot noise reduction at SCL conduction in solids has been found in many different systems such as: tunnelling transport in asymmetric double-barrier junctions where a 1/2 noise-suppression factor has been found [104, 105], diffusive conductors [106, 107, 108, 109] and ballistic conductors [106, 110, 111, 112]. A universal shot noise suppression factor of $\gamma = 1/3$ was found in the SCL conduction in the three-dimensional (3D) system of nondegenerate diffusive conductor by including only the elastic scattering [107, 108], and the model was later revised to include the diffusive current and other types of scattering [109, 113, 114].

On the other hand, in the absence of scattering, the shot noise is pretty much determined by the injecting contact by the potential barrier at the interface. In this case, the correlation comes from the quantum partitioning effect between the incoming charge and the transmitted charge through the potential barrier, and its effect on shot

noise reduction has been shown in many mesoscopic systems [101]. Such effect of the quantum partitioning on shot noise reduction has also been suggested for electron field emission at metal-vacuum interface with a simplified potential profile [115], and it has been extended to include more realistic potential profiles [116, 117], and space charge effect in a quantum model [118].

The theme of this chapter is to calculate the shot noise reduction of SCL charge injection through a metal-semiconductor interface (or Schottky contact) of a diode, including the correlations due to the space charge effect of MG law and quantum partitioning of the electron tunneling through the Schottky barrier. Such a system is relevant to SCL charge injection required in various nanoelectronics or organic based devices, which always have a non-Ohmic contact at the interface.

Thus in this context, several interesting questions arise: (a) Is the correlation due to quantum partitioning important in the high voltage regime where space charge effect is dominant due to the classical Coulomb correlation ? (b) At the same applied electric field, how important is the quantum shot noise for different voltages and diode spacing ? (c) What is the dependence of shot noise on temperature, applied voltage, length of the diode and Schottky barrier height ? (d) How is the presence of traps in varying the shot noise suppression ?

Before showing the exact calculations in answering the above questions (see figures below), some qualitative picture will be presented here. First, at low applied field where the electron transport is based on Ohm's law, there should be no correlations, resulting in zero shot noise suppression ($\gamma = 1$). At high field where the space charge effect becomes important, the classical Coulomb correlation will provide a smoothing effect that suppresses the shot noise. In this regime, the combined effects of Schottky barrier and space charge electrostatic field will serve as a potential barrier for electrons to be injected from metal into the solid through tunneling process, which provides the quantum partitioning correlation that will further suppress the full shot

noise ($\gamma < 1$). The degree of suppression will depend on temperature, applied voltage, length of the diode and Schottky barrier height. With a larger Schottky barrier, the tunneling probability is lower resulting in less shot noise suppression as compared to zero-Schottky barrier case (see Fig. 6.2). At fixed applied field with smaller diode length scale, there will be more shot noise suppression due to the relative significance of electron tunneling at the interface (see Fig. 6.3). At fixed diode length, shot noise suppression increases with higher voltages due to the relative importance of Coulomb correlation due to space charge effect (see Fig. 6.5). The shot noise study in this chapter will also be useful to provide extra information on the carrier dynamics, which is similar to the recent $1/f$ noise measurement of SCL current fluctuations in organic semiconductors [31]. The effect of traps exponentially distributed in energy in a solid on the shot noise will also be studied.

6.2 Model

For simplicity, we will consider for a model with a trap-free solid (or dielectric) of length L (extended from x=0 to x=L) that is sandwiched between two metallic electrodes with an applied voltage V_G at x=L. We assume a one-dimensional (1D) geometry that has only spatial dependence on x, where the contact at x=0 and x=L is, respectively, a Schottky contact with Schottky barrier height of $e\phi_b$ and an Ohmic contact. The model only focuses on the injection of electrons through the Schottky contact, and the hole injection is ignored completely. After tunneling through the contact, the transport of electrons is described by the drift-diffusion equation on the assumption that L is much larger than the inelastic scattering mean free path λ, which is determined by the mobility of the electrons.

Following the Landauer-Büttiker framework, the Fano factor of the shot noise reduction in SCL charge injection through a Schottky barrier may be expressed as

6.2 Model

[115, 116, 117]

$$\gamma = 1 - \frac{\int_{-\infty}^{\infty} C_T^2(E_x) g[-\beta_x E_x] dE_x}{\int_{-\infty}^{\infty} C_T(E_x) h[-\beta_x E_x] dE_x}, \tag{6.1}$$

where $\beta_x = 1/k_b T$, k_b is the Boltzmann's constant, T is the temperature, E_x is the conduction band energy in the solid with respect to the Fermi level E_F, C_T is the transmission coefficient through an energy barrier, $h(z)$ is defined as $h(z) = \ln\big[1+exp(z)\big]$ and $g(z)$ is defined as $g(z) = h(z)$ - $dh(z)/dz$. Note both $g(z)$ and $h(z)$ are strictly positive functions. The transmission coefficient $C_T(E_x)$ is calculated by using the WKB approximation [119]:

$$C_T(E_x) = \exp\Big[-\frac{2}{\hbar} \int_{\mathrm{x_1}}^{\mathrm{x_2}} \sqrt{2\mathrm{m_e}^*(\psi_\mathrm{C}(\mathrm{x})\mathrm{e} - \mathrm{E_x}}\mathrm{dx}\Big]. \tag{6.2}$$

where $\hbar$ is the reduced Plank's constant, $m_e{}^*$ is the effective electron mass, $\psi_C(x)$ is the conduction band potential (to be calculated), e is the electronic charge, x_1 and x_2 are the roots of $\mathrm{e}\psi_C(x) - E_x = 0$.

To obtain the potential profile $\psi_C(x)$, the Poisson equation is solved

$$\frac{\mathrm{d}^2\psi_\mathrm{C}(\mathrm{x})}{\mathrm{dx}^2} = \frac{e(n(x) - n_i)}{\epsilon_r \epsilon_0}, \tag{6.3}$$

where n_i is the intrinsic electron concentration. The electron density $n(x)$ at the conduction band related to the conduction band potential, $\psi_C(x)$, and it is given by:

$$n(x) = N_C \exp\Big[\frac{\psi_\mathrm{C}(\mathrm{x}) - \phi_\mathrm{n}(\mathrm{x})}{\mathrm{k_b T/e}}\Big], \tag{6.4}$$

where N_C is the effective density of states of electrons at the conduction band and $\phi_n(x)$ is the quasi Fermi electron potential. The $\phi_n(x)$ term is solved by using the steady state current continuity equation

$$\frac{\mathrm{dj_n}}{\mathrm{dx}} = eG(x), \tag{6.5}$$

and

$$j_n = -en(x)\mu_n \frac{\mathrm{d}\psi_\mathrm{C}(\mathrm{x})}{\mathrm{dx}} + eD_n \frac{\mathrm{dn(x)}}{\mathrm{dx}} = -en\mu_n \frac{\mathrm{d}\phi_\mathrm{n}(\mathrm{x})}{\mathrm{dx}}. \tag{6.6}$$

6.2 Model

Here, j_n is the drift-diffusion electron current density, D_n is the electron diffusion coefficient and μ_n is the electron mobility, $G(x)$ is the net generation rate of electrons due to the external charge injection at the contact through the process of electron tunneling and thermionic emission (or over barrier injection).

The Schottky contact in the model (at x=0) is characterized by a barrier height of $e\phi_b = e\phi_m$ - $e\chi$ (in eV), and the surface recombination current $j_{sn} = ev_{sn}(n_s - n_{eq})$, where ϕ_m is the work function of electrode, χ is the electron affinity of the solid, v_{sn}= $A^*T^2/(eN_C)$ is the surface recombination velocity, A^* is the effective Richardson constant, n_s is the surface electron density at x= 0, and n_{eq} is the equilibrium electron density at $\phi_n = 0$ [78, 120].

The boundary conditions for solving Eqs. (6.4)-(6.6) numerically are ψ_C(x=0) = -ϕ_b, ψ_C(x=L) = V_G - $E_g/2e$, ϕ_n(x=0) = ψ_C(x=0) + $(E_g/2e)$+ $(k_bT/2e)$ln(N_C/N_V)-(k_bT/e)ln(n_s/n_i), and where $(E_g/2e)$+ $(k_bT/2e)$ln(N_C/N_V) is the built-in potential, ϕ_n(x=L) = V_G. Here, E_g is the bandgap, N_V is the effective density of states of holes in the valence band, V_G is the applied voltage. The details of the numerical calculation can be found in Chap. 4 where the study of MG law with finite Schottky contact has been discussed in great details. To include the effect of electron temperature T, the values of N_C and E_g are calculated as a function of T [78] with $N_C(T) = N_C^{300}\left[\frac{T}{300}\right]^{3/2}$ and $E_g(T) = E_g^{300} + A\left[\frac{300^2}{300+B} - \frac{T^2}{T+B}\right]$ where N_C^{300} is the effective density of states of electrons in the conduction band at T = 300 K, E_g^{300} is the bandgap at T = 300 K, A and B are the parameter constants depending of the solid materials.

The study in this chapter will focus on gallium nitride (GaN) as it has a relative higher breakdown electric field, and it was recently reported to be operated in the SCL current regime [92]. The parameters used in the calculation for GaN are [121] L = 10, 1 , and 0.1 μm, ϵ_r = 9, μ_n = 900 cm^2/(V.s), $e\phi_b$ = 0 to 0.5 eV, and T = 100, 300, and 500K. At this setting, the electron mean free path for the inelastic scattering is about 24 nm for GaN, which is much smaller than the length of the solid $L \geq 100$

nm. Note that the maximum applied electric field used in the simulation is less than the breakdown field of GaN which is about 3.3 MV/cm.

It is important to note that the derivation of Eq. (6.1) is based on the assumption of using a fixed effective mass in the integration of the transverse momentum. In spite of this assumption, the model is however evaluated by comparing the calculated current-voltage (J vs V_G) characteristic with an industry-standard TCAD tool (Medici device simulator) [75] as shown in Fig. 6.1. The comparison shows good agreement, which implies that the calculation of both the transmission coefficient and the Fano factor is reliable on the basis of device simulation.

6.3 Results and Discussion

In Fig. 6.1, the current density J as a function of V_G for GaN is plotted in a log-log plot at $e\phi_b$ = (a) 0.2 eV and (b) 0.5 eV for T= 100, 300, 500 K and $L = 10$ μm At low V_G, the transport obeys Ohm's Law ($J \sim V_G$) since the injected electron density is much lower than the intrinsic electron concentration n_i of GaN. In this regime, electron tunneling is negligible at low V_G, and J will only depend on the amount of available electrons injected at the surface [n(x=0)] described in Eq. (6.4). The transition voltage from Ohm's law to MG law is at about 2 V. Above the transition voltage, the current density will become the SCL conduction following MG law ($J \sim {V_G}^2$). For a given value of $e\phi_b$, SCL conduction can only be reached if the electron tunneling is included self-consistently [96]. Please note the results shown in Fig. 6.1 have been verified (in symbols) by using a 2D device simulator [75], for which the width of the system is simulated at $W = 40$ μm ($>> L$), so that the 1D model is valid.

In Fig. 6.2, the results of the shot noise reduction of Fano factor γ (using Eq. 6.1) are shown at zero barrier $e\phi_b = 0$ eV (solid lines) and $e\phi_b = 0.2$ eV (symbols) as a function of V_G for T= 100, 300, 500 K and $L = 10$ μm. At low V_G (below the

6.3 Results and Discussion

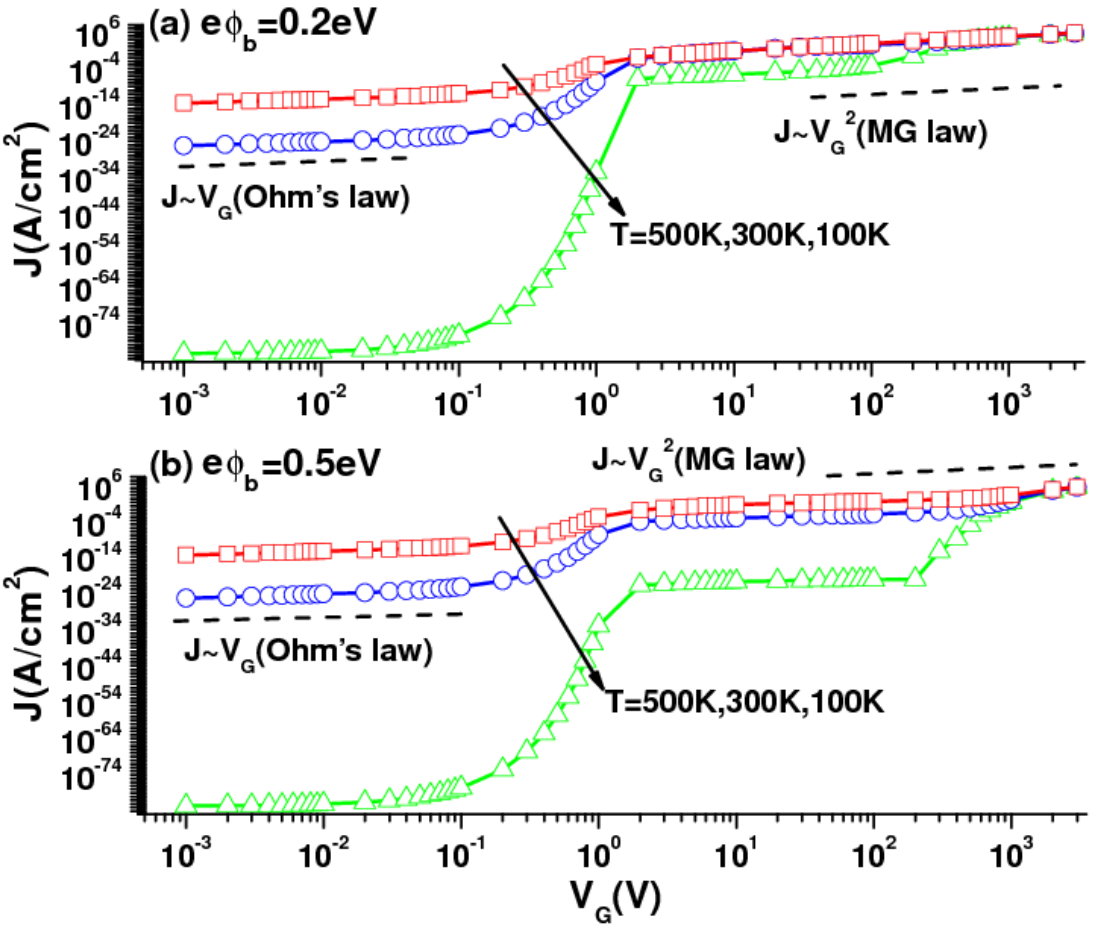

Figure 6.1: The calculated electron current density J as a function of V_G in log-log scale for a GaN diode of L=10 μm and μ_n = 900 cm^2/V.s at (a) $e\phi_b$ = 0.2 eV and (b) $e\phi_b$ = 0.5 eV for different T = 500K, 300K, 100K as indicated by the arrow from top to bottom and are shown in different color lines, respectively, by red (square), blue (circle) and green (triangle)

transition voltage of 2 V) , the γ values are ≈ 1 independent of $e\phi_b$. At this low current regime, the current density follows Ohm's Law and the electron tunneling is negligible. Thus, the Fano factor $\gamma \approx 1$ as there are no correlation effects due to the Coulomb repulsion or quantum partitioning to reduce the shot noise.

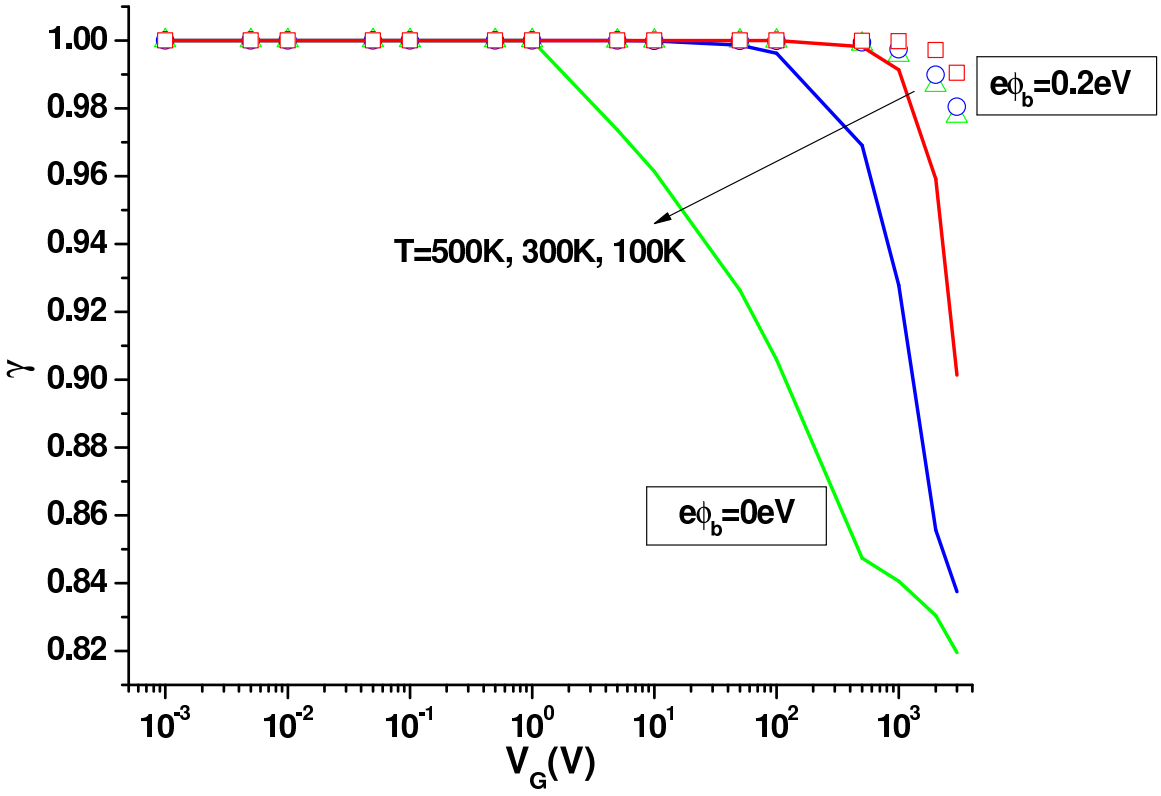

Figure 6.2: The calculated Fano factor γ as a function of V_G for GaN in linear-log scale at $L = 10$ μm and $\mu_n = 900$ cm^2/V.s for $e\phi_b = 0$ eV (in solid lines) and 0.2 eV (in symbols) for different $T = 500$, 300, and 100K as indicated by the arrow from top to bottom. The respective labeling are (T, color line, symbols) = (500 K, red line, square), (300 K, blue line, circle) and (100 K, green line, triangle)

At high voltage regimes, the tunneling probability is lower for $e\phi_b = 0.2$ eV, and thus less shot noise suppression as compared to zero-Schottky barrier case ($e\phi_b = 0$ eV). At this high current regime, the tunneling of electrons through the potential barrier resulting from the Schottky barrier and electrostatic space-charge field will

provide the correlations due to both the Coulomb repulsion and quantum partitioning, which will reduce the Fano factor γ to be less than 1. The Coulomb repulsion has the effect of reducing γ slightly at lower T and the tunneling will further suppress shot noise at large V_G. In terms of temperature, the electron tunneling dominates the current conduction at low temperature, and thus more shot noise suppression at low temperature. For example, at V_G = 3 kV (or 3 MV/cm), and $e\phi_b$ = 0 eV, the γ values are: 0.819, 0.834, and 0.901, respectively at T = 100, 300 and 500 K. At $e\phi_b$ = 0.2 eV, the γ values are: 0.991 to 0.999 in the range of T = 100 to 500 K at the same 3 MV/cm.

It is clear the probability of tunneling does not depend only on the applied field but also on the length of the GaN diode (L). In Fig. 6.3, the dependence of shot noise reduction is shown as a function of barrier height (0 to 0.5 eV) at room temperature T = 300 K and fixed applied electric field of 3 MV/cm with different combination of V_G = (3, 0.3, 0.03) kV and L = (10, 1, 0.1) μm. For smaller L, shot noise suppression is more (smaller γ) as the electron tunneling is more likely. For example, γ is decreased to about 0.71 and 0.93, respectively at $e\phi_b$ = 0 eV and 0.2 eV for the L = 100 nm case as compared to L = 10 μm case.

To see whether shot noise suppression is caused by the tunneling effect or the classical Coulomb repulsion, we show the conduction band energy profile, $E_C(x)$ at the proximity of the contact (x = 0 to 10 nm) in Fig. 6.4. The conduction band profile is shown at the barrier height, $e\phi_b$ = 0.1 eV at room temperature, T = 300K, and the same fixed applied electric field [V_G = (3, 0.3, 0.03) kV and L = (10, 1, 0.1) μm]. As can be seen from Fig. 6.4, As the length L decreases, , the conduction band drops faster. The tunneling probabiliy for the electrons to tunnel through will be larger since the transmission coefficient which is calculated from the WKB method is larger (see Eq. 6.2). The conduction band profile clearly shows that the tunneling is greater at smaller length L. Thus, we believe the larger shot noise suppression at smaller

length L can be attributed to the larger tunneling and therefore the correlation due to quantum tunneling partition should be the dominant effect in comparison with the correlation from classical Coulomb repulsion.

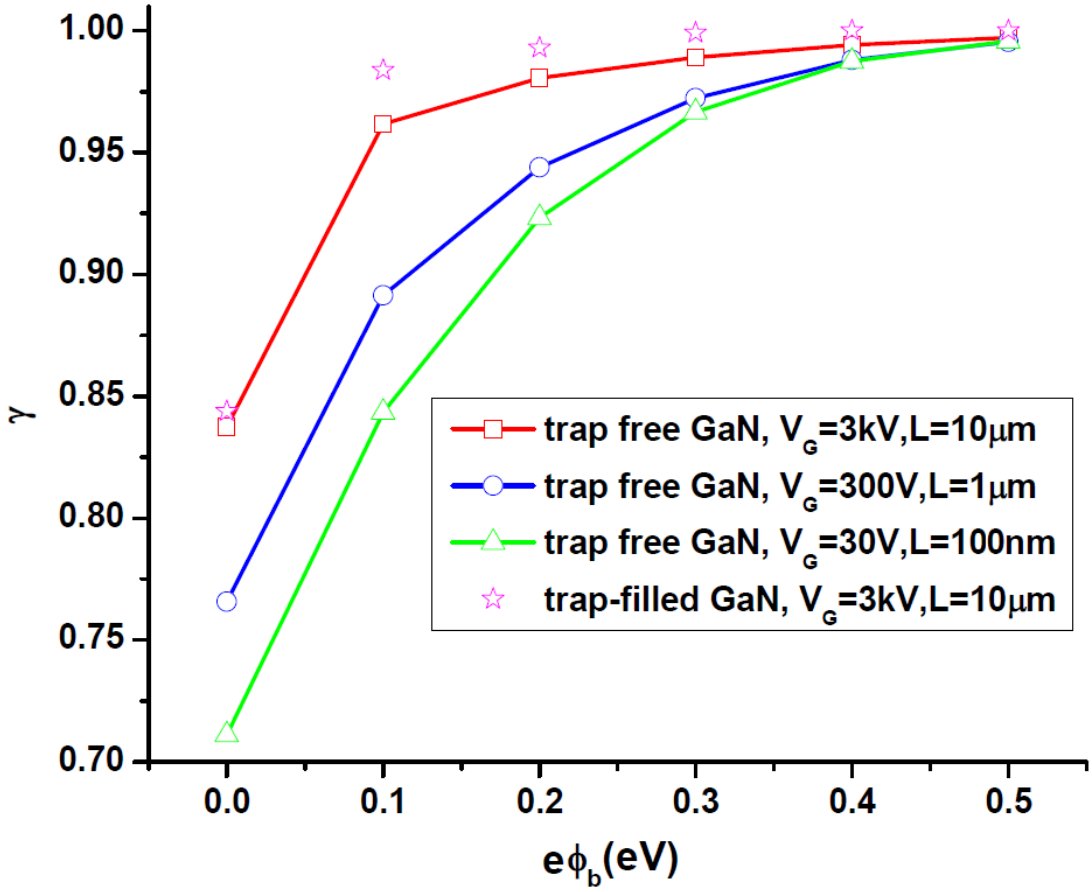

Figure 6.3: The calculated Fano factor γ as a function of $e\phi_b$ = 0.to 0.5 eV for GaN at T = 300 K and fixed average applied field V_G/L = 3 MV/cm for different combinations of V_G = 3, 0.3, 0.03 kV and L = 10, 1, 0.1 μm. The magenta star symbols are the calculations at trap-limited SCL conduction case at L = 10 μm and V_G = 3 kV

In addition, the effect of traps on the shot noise reduction for a trap-filled GaN at the SCL conduction regime is also studied. In doing so, the traps are assumed to be exponentially distributed in energy by the equation: n_t=N_{t0}exp$[(\psi_C-\phi_n)/(l\cdot k_b T/e)]$, where N_{t0} is the trap density, and l=T_t/T with T_t is the characteristic distribution

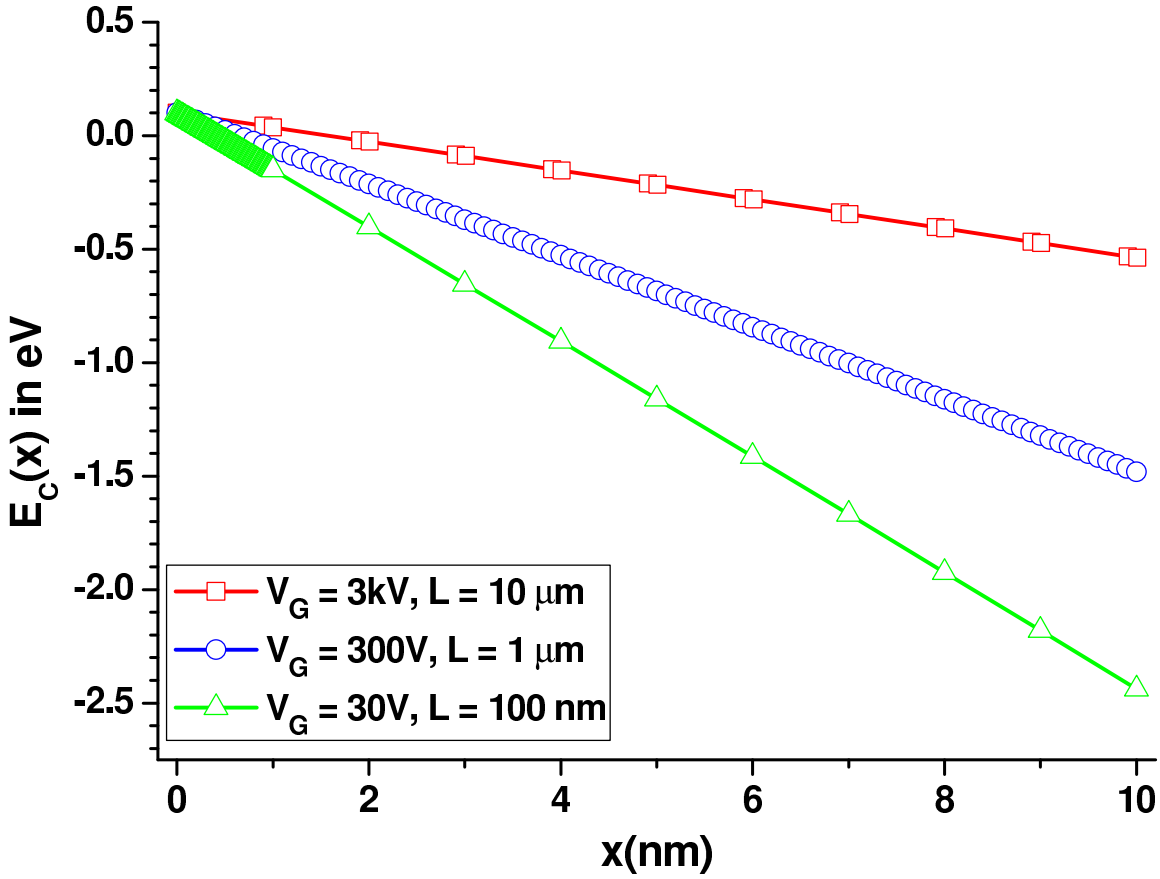

Figure 6.4: The calculated conduction band energy profile, $E_C(x)$ as a function of the distance from the cathode interface of $x = 0$ to 10 nm $x = 0$ to 10 nm for GaN at $T = 300$ K and fixed average applied field $V_G/L = 3$ MV/cm for different combinations of $V_G = 3$, 0.3, 0.03 kV and $L = 10$, 1, 0.1 μm

of the traps. At $l = 1$ ($T_t = T$), the traps are independent of energy and it is equivalent to the trap-free case but with a reduced current density J (by a numerical constant as compared to the trap-free MG law). By using the device simulator [75], the conduction band potential profile $\psi_C(x)$ is extracted from the simulation including the effect of traps and it is used to calculate the Fano factor numerically by using Eq. (6.1). The calculated results using the parameters of ($l = 2$, $N_{t0} = 5 \times 10^{17}$ cm^{-3}, $V_G = 3$ kV and $L = 10$ μm) is plotted (see symbols) in Fig. 6.3 for comparison. The calculations show that shot noise reduction has little effect (within 2 percent) in the trap-limited SCL conduction (symbols) as compared to trap-free case (red solid line). The reason for this is because at high injection or SCL injection regime, the traps are completely or almost fully occupied by electrons therefore the traps have no or little effect to the shot noise suppresion.

For completeness, the dependence of shot noise suppression ($T = 300$ K) is shown in Fig. 6.5 as a function of barrier height (0 to 0.5 eV) at $L =$ (a) 10 μm and (b) 100 nm for various V_G. The results prove that shot noise suppression increases with higher voltages at fixed L, due to the relative importance of Coulomb correlations because of stronger space charge effect at high voltages.

6.4 Summary

In conclusion, shot noise reduction (or Fano factor) of SCL electron injection through a Schottky contact in a GaN diode is calculated, including the correlation effects of Couloumb repulsion and quantum partitioning due to electron tunneling through the self-consistent determined potential barrier near to the Schottky contact. The effects of the shot noise reduction on temperature, Schottky barrier height, applied voltage, length of the diode are investigated. It is found that shot noise suppression cannot be ignored for smaller barrier height (< 0.2 eV) at the interface at high voltage regimes

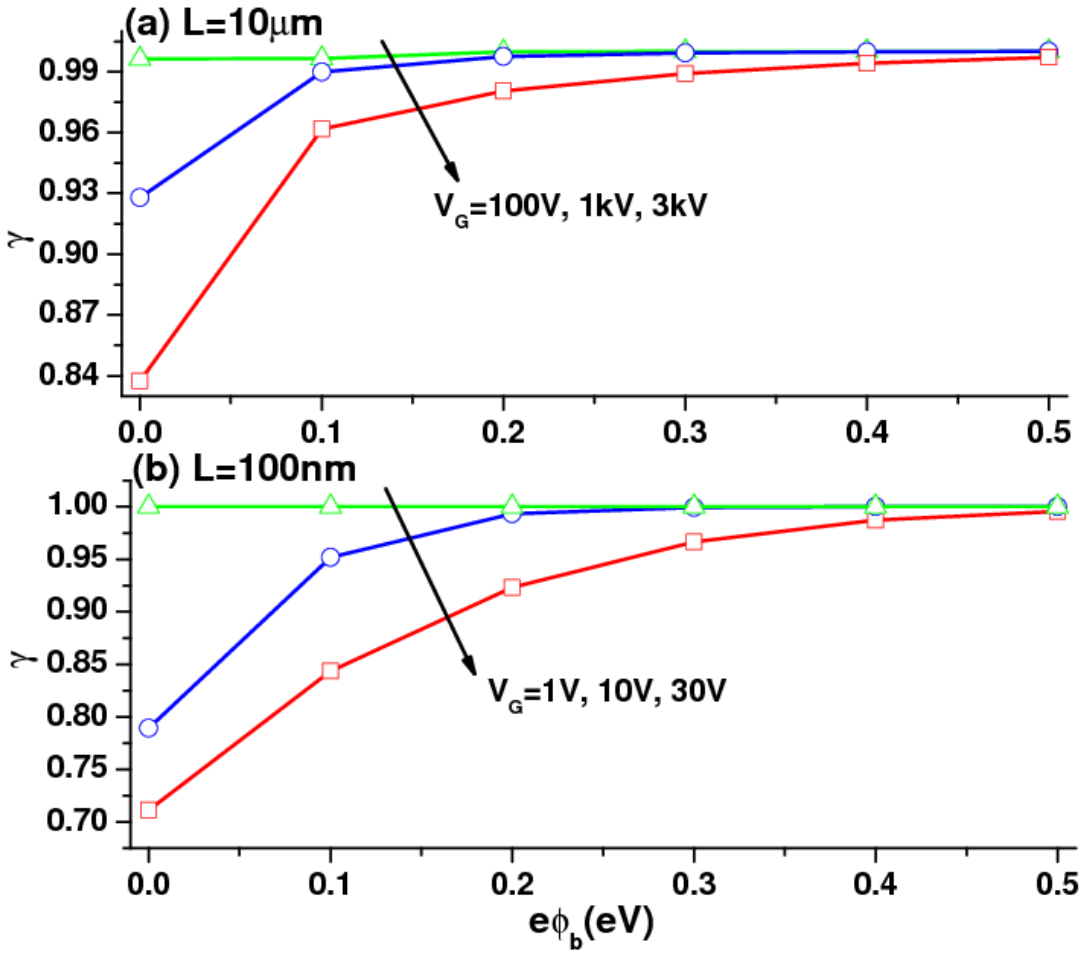

Figure 6.5: The calculated Fano factor γ as a function of $e\phi_b$ for GaN at $T = 300$K and fixed $L =$ (a) 10 μm for $V_G = 100$, 1kV, and 3 kV and (b) 100 nm for $V_G = 1$, 10V, and 30 V

6.4 Summary

especially for smaller diode length scale. At low voltage and low current regime, the electron transport obeys Ohm's law and there is no suppression of shot noise. At high voltage, and high current regime, the electron transport is space charge limited by the MG law and the shot noise suppression increases with large applied voltage, small diode length, low temperature, and small barrier height. The model also indicates that the distributed traps in the solid nearly has no effect to the shot noise reduction as compared to trap-free solid. Finally, the values of mobility have been varied also, and it is found that the findings of the shot noise suppression remain valid as long as the electron transport is at space charge limited conduction (SCL) regime.

CHAPTER 7

CONCLUSION AND FUTURE RECOMMENDATIONS

7.1 Conclusion

This thesis focuses on the development of 1D and 2D dimensional theory of space charge limited (SCL) transport in solids. The original theory of SCL current in solids, known as MG (Mott-Gurney) Law, is based on the assumptions that the SCL current injection in solids neglects the effect of contact formation (Ohmic contact) and it is a 1D model. However, in real device applications, usually the contact formation and the size of the charge injecting electrode are important. It is common to have a contact with a small barrier height $e\phi_b$ and the size of solid dielectric along the other directions maybe comparable to the SCL transport direction (L) and thus a 2D or 3D model is required. The SCL theory developed and shown in this dissertation uses a standardized diode structure with a solid dielectric sandwiched in between cathode, which is grounded, and anode, which is biased, with an applied voltage V_G. Only electron transport (unipolar injection) is considered and thus the contact formation

is either Schottky (when contact formation is under study) or Ohmic (when contact effect is neglected) at the cathode.

In Chap. 3, a smooth transition from SCL current in vacuums to SCL current in solids is demonstrated. The model uses the energy balance momentum equation for electrons with the collision parameter β to control whether it is a SCL current in vacuums (CL law) or SCL current in solids (MG law). At high injection region with no collision, the conduction will become CL law or ballistic SCL current. While at collision-dominated region, it will become MG law or collision-dominated SCL current. The analytical 2D model for SCL current in solids is developed. The enhancement in current due to size effect (the width of the injecting contact W is comparable to the gap length L) can be shown in a simple analytical form in terms of 1D current. The current enhancement depends on the shape of the emitting electrode and the electron concentration profile along a solid length L.

The results are verified with a 2D device simulator Medici in a simple 2D planar shape where the width of the injecting electrode is comparable to the length of a solid. This result may be helpful in predicting the maximum amount of SCL current density in novel 2D structures such as: nanotubes, organic semiconductors, and nanowires that have been reported to be operating at SCL regime.

In Chap. 4, the study of SCL current in solids focuses on the effect of finite barrier height in the contact formation for the electron injection in the solid dielectric and the imperfections in the lattice structure between the electrode and a solid interface. The imperfection creates defects or localized energy states at the interface in the form of surface states. The electrons can be injected to the solid by thermionic emission at finite barrier height and they can also tunnel to the solid through the surface states. The contact effects are included in our model by including the barrier height in the Poisson boundary conditions and the tunneling through the surface states in the steady state current continuity equation. The calculation of the tunneling

current through the surface states are calculated using WKB method. In addition, the proposed 2D MG law has also been verified with a 2D device simulator Medici and confirmed that with the availability of surface states and low barrier height $e\phi_b$, the current conduction can still reach SCL transport due to the tunneling through surface states, for a given barrier height.

In Chap. 5, the theoretical study of SCL electron transport for a hybrid structure of a combined vacuum and solid in between cathode and anode is studied. This setup is investigated due to the resemblance to the STM experiment which has been reported of a possible SCL transport conduction due to both vacuum and solid (and vice versa) inside the gap [38]. The theoretical model is developed by assuming a controlled parameter x_1 to measure the relative length of vacuum and solid. The current density can be found by matching the electric field at the interface. The results show our models recovers at both limits in a pure free space (vacuum) [CL law] and in a pure solid [MG law]. Our model has also discussed the effect of gap spacing, electron mobility and dielectric constant of a solid. In addition, the model has also been used to explain a recent STM experiment [38].

In Chap. 6, the shot noise reduction of SCL current in solid in particular for a GaN diode is studied. Using the developed model in the previous chapter (Chap. 4), the shot noise reduction or Fano factor for SCL electron injection through a Schottky contact in a GaN diode is calculated. The results are calculated and simulated in Medici by varying many parameters, such as: temperature, barrier height, applied voltage, length of the diode structure. At high voltage and high current regime (SCL transport regime), the shot noise suppression increases with large applied voltage, small diode length, low temperature, and small barrier height. The results also show that at SCL trap-limited region, the shot noise reduction is not sensitive to the trap distribution inside the solid. In addition, the variation of electron mobility shows

little effect to the shot noise reduction or Fano factor values as long as the current conduction is still at the SCL transport regime.

7.2 Recommendations for Further Research

Some possible extensions from the topics of this thesis are given as follows :

- Extend the theory to further account the SCL transport in solid in the bipolar case including the hole transport together with electron transport. In the bipolar case, recombination of electrons and holes in the bulk of the dielectric will influence the SCL formation. The study may also cover various types of charge trap distributions, contact effect, and size effect, as studied in this thesis.

- In the area of organic materials and semiconductors, the mobility is known to be dependent on field and temperature. Also, hopping mechanism of charge transport together with the Gaussian density of states is typically found in the organic materials. The study of SCL formation in organic materials may be extended based on these factors and to compare the theory developed for SCL transport in the regular inorganic materials.

- Extend the dependence of other 3D geometrical shape of the cathode upon the availability of 3-D device simulator. Formulation of the scaling for a very small size of $W/L << 1$ is also much desired as the current model is only valid for $W/L \geq 1$.

- The typical SCL transport in solid under study is a diode set-up with a dielectric between the electrodes (cathode and anode). It is of interest to study different structure such as: field effect transistor structure including a third electrode, the gate electrode. The purpose of such a study is to see the possibility of understanding the formation of SCL current in the transistor structure and how

does it relate to the current behavior in the defective environment or "leaky" gate oxide materials leading to the gate oxide breakdown.

AUTHOR'S PUBLICATIONS

Journal Papers

1. W. Chandra and L. K. Ang. and K. L. Pey and C. M. Ng. "Two-dimensional analytical Mott-Gurney law for a trap-filled solid", *Appl. Phys. Lett.*, **90**:153505 (2007).

2. W. Chandra and L. K. Ang. and W. S. Koh. "Two-dimensional model of space charge limited electron injection into a diode with Schottky contact", *J. Phys. D: Appl. Phys.*, **42**:055504 (2009).

3. W. Chandra and L. K. Ang. "Space charge limited current in a gap combined of free space and solid", *Appl. Phys. Lett.*, **96**:183501 (2010).

4. W. Chandra and L. K. Ang. and X. Zhou "Shot noise reduction of space charge limited electron injection through a Schottky contact for a GaN diode", *Phys. Rev. B*, **81**:125321 (2010).

Conference Papers

1. W. Chandra and L. K. Ang. "Two-dimensional collisional Child-Langmuir law", *2007 IEEE Pulsed Power and Plasma Science Conference, Albuquerque, United States, New Mexico, United States* (June 2007).

AUTHOR'S PUBLICATIONS

2. W. Chandra and L. K. Ang. and W. S. Koh. "High current electron injection in a gap with both vacuum and solid", *The 8th International Vacuum Electron Sources Conference, Nanjing, China*, (Oct 2010).

BIBLIOGRAPHY

[1] N. F. Mott and R. W. Gurney. *Electronic Processes in Ionic Crystals*. Oxford, Clarendon Press (1940).

[2] C. D. Child. *Phys. Rev.*, **32**:492 (1911).

[3] I. Langmuir. *Phys. Rev.*, **2**:450 (1913).

[4] P. K. Weimer and A. D. Cope. *RCA Rev.*, **12**:314 (1951).

[5] P. K. Weimer. *IRE Trans. Electron Dev.*, **8**:421 (1961).

[6] P. K. Weimer. *Proc. IRE*, **50**:1462 (1962).

[7] S. V. Vorgue, R. R. Goodrich, and A. D. Cope. *RCA Rev.*, **12**:335 (1951).

[8] A. Rose and M. A. Lampert. *Phys. Rev.*, **113**:1227 (1959).

[9] A. M. Goodman and A. Rose. *J. Appl. Phys.*, **42**:2823 (1971).

[10] A. Rose. *RCA. Rev.*, **12**:362 (1951).

[11] A. Rose. *Phys. Rev.*, **97**:1538 (1955).

[12] R. W. Smith. *Phys. Rev.*, **97**:1525 (1955).

Bibliography

[13] R. W. Smith and A. Rose. *Phys. Rev.*, **97**:1531 (1955).

[14] W. Shockley and R. C. Prim. *Phys. Rev.*, **90**:153 (1953).

[15] G. C. Dacey. *Phys. Rev.*, **90**:759 (1953).

[16] M. A. Lampert. *Phys. Rev.*, **103**:1648 (1956).

[17] P. Mark and W. Helfrich. *J. Appl. Phys.*, **33**:205 (1962).

[18] C. Shulman. *Phys. Rev.*, **98**:384 (1955).

[19] J. R. Fassett and K. M. van Vliet. *Proc. Intern. Conf. Semicon. Phys.*, **6**:886 (1962).

[20] V. Sergiescu. *Brit. J. Appl. Phys.*, **16**:1435 (1965).

[21] A. van der Ziel. *Solid-State Electronics*, **9**:123 (1966).

[22] W. J Anderson and B. Meltzer. *J. Electron. Control.*, **11**:111 (1961).

[23] R. J. J Zijlstra and A. van der Ziel. *Physica*, **29**:78 (1963).

[24] D. M. Taylor and H. L. Gomes. *J. Phys. D:Appl. Phys.*, **28**:2554 (1995).

[25] D. M. Taylor. *Trans. on Dielectrics and Electrical Insulation*, **13**:1063 (2006).

[26] Z. Chiguvare and V. Dyakonov. *Phys. Rev. B*, **70**:235207 (2004).

[27] V. R. Nikitenko, H. Heil, and H. von Seggern. *J. Appl. Phys.*, **94**:2480 (2003).

[28] P. W. M. Blom, M. J. M. de Jong, and M. G. van Munster. *Phys. Rev. B*, **55**:R656 (1997).

[29] M. Samuel, C. S. Menon, and N. V. Unnikrishnan. *Semicond. Sci. Technol.*, **21**:677 (2006).

Bibliography

[30] L. S. Roman and O. Inganäs. *Synthetic Metals*, **125**:419 (2002).

[31] A. Carbone, B. K. Kotowska, and D. Kotowski. *Phys. Rev. Lett.*, **95**:236601 (2005).

[32] J. Reynaert, V. I. Arkhipov, G. Borghs, and P. Heremans. *Appl. Phys. Lett.*, **85**:603 (2004).

[33] Y. Gu and L. J. Lauhon. *Appl. Phys. Lett.*, **89**:143102 (2006).

[34] V. D. Mihailetchi, J. Wildeman, and P. W. M. Blom. *Phys. Rev. Lett.*, **94**:126602 (2005).

[35] H. C. F. Martens, W. F. Pasveer, H. B. Brom, J. N. Huiberts, and P. W. M. Blom. *Phys. Rev. B*, **63**:125328 (2001).

[36] P. S. Davids, I. H. Campbell, and D. L. Smith. *J. Appl. Phys.*, **82**:6319 (1997).

[37] A. Tsormpatzoglou, D. H. Tassis, C. A. Dimitriadis, L. Dózsa, N. G. Galkin, D. L. Goroshko, V. O. Polyarnyi, and E. A. Chusovitin. *J. Appl. Phys.*, **100**:074313 (2006).

[38] Y. C. Ong, D. S. Ang, S. J. O'Shea, K. L. Pey, S. J. Wang, C. H. Tung, and X. Li. *J. Appl. Phys.*, **104**:064119 (2008).

[39] M. A. Lampert and P. Mark. *Current Injection in Solids.* Academic, New York (1970).

[40] R. H. Bube. *J. Appl. Phys.*, **33**:1733 (1962).

[41] E. Harnik. *J. Appl. Phys.*, **36**:3850 (1965).

[42] K. Hinotani and M. Sugigami. *Japan J. Appl. Phys.*, **3**:731 (1965).

[43] J. L. Hartke. *Phys. Rev.*, **125**:1177 (1962).

Bibliography

[44] A. Many and G. Rakavy. *Phys. Rev.*, **126**:1980 (1962).

[45] W. Helfrich and P. Mark. *Z. Phys.*, **166**:370 (1962).

[46] W. Helfrich and P. Mark. *Z. Phys.*, **168**:495 (1962).

[47] W. Helfrich and P. Mark. *Z. Phys.*, **171**:527 (1965).

[48] B. L. Gregory and A. G. Jordan. *Phys. Rev.*, **134**:A1378 (1964).

[49] D. C. Hoestery and G. M. Letson. *J. Phys. Chem. Solids*, **24**:1609 (1963).

[50] S. Z. Weisz, R. C. Jarnagin, M. Silver, M. Simhony, and J. Balberg. *J. Chem. Phys.*, **40**:3365 (1963).

[51] J. Adolph, E. Baldinger, W. Czaja, and I. Gränacher. *Phys. Lett.*, **6**:137 (1963).

[52] W. Helfrich and W. G. Schneider. *J. Phys. Chem.*, **44**:2902 (1966).

[53] I. Gränacher. *Solid-State Commun.*, **3**:331 (1965).

[54] W. Büchner and W. Mehl. *Z. Phys. Chem.*, **69**:376 (1965).

[55] A. Many, S. Z. Weisz, and M. Simhony. *Phys. Rev.*, **126**:1989 (1962).

[56] M. Simhony and J. Gorelik. *J. Phys. Chem. Solids*, **26**:1133 (1965).

[57] A. S. Riad. *Physica B*, **270**:148 (1999).

[58] J. W. Luginsland, Y. Y. Lau, and R. M. Gilgenbach. *Phys. Rev. Lett.*, **77**:4668 (1996).

[59] Y. Y. Lau. *Phys. Rev. Lett.*, **87**:278301 (2001).

[60] W. S. Koh, L. K. Ang, and T. J. T. Kwan. *Phys. Plasmas*, **12**:053107 (2005).

[61] L. K. Ang, T. J. T. Kwan, and Y. Y. Lau. *Phys. Rev. Lett.*, **91**:208303 (2003).

Bibliography

[62] L. K. Ang, W. S. Koh, and T. J. T. Kwan. *Phys. Plasmas*, **13**:056701 (2006).

[63] A. Valfells, D. W. Feldman, M. Virgo, P. G. O'Shea, and Y. Y. Lau. *Phys. Plasmas*, **9**:2377 (2002).

[64] W. S. Koh, L. K. Ang, and T. J. T. Kwan. *Phys. Plasmas*, **13**:063102 (2006).

[65] Koh Wee Shing. *Ph. D. thesis*, pages Nanyang Technological University, Singapore (2007).

[66] W. Shockley and R. C. Prim. *Phys. Rev.*, **90**:753 (1953).

[67] R. H. Parmenter and W. Ruppel. *J. Appl. Phys.*, **30**:1548 (1959).

[68] M. S. Shur. *IEEE Trans. Electron Devices*, **28**:1120 (1981).

[69] M. S. Shur and L. F. Eastman. *Solid-State Electronics*, **24**:11 (1981).

[70] M. S. Shur and L. F. Eastman. *IEEE Trans. Electron Devices*, **26**:1677 (1979).

[71] M. S. Shur and L. F. Eastman. *IEEE Electron Devices Lett.*, **1**:147 (1980).

[72] Y. C. Chao, H. F. Meng, and S. F. Horng. *Appl. Phys. Lett.*, **88**:223510 (2006).

[73] W. Chandra, L. K. Ang, K. L. Pey, and C. M. Ng. *Appl. Phys. Lett.*, **90**:153505 (2007).

[74] J. W. Luginsland. *Bull. Am. Phys. Soc*, **46(8)**:175 (2001).

[75] Synopsis. *Medici User Manual* (2003).

[76] W. Chandra, L. K. Ang, K. L. Pey, and W. S. Koh. *to be submitted* (2008).

[77] W. Schottky. *Naturwissenschaften*, **26**:843 (1938).

[78] S. M. Sze. *Physics of Semiconductor Devices*. Wiley and Sons, New York (1981).

Bibliography

[79] C. R. Crowell and S. M. Sze. *Solid-State Electronics*, **9**:1035 (1966).

[80] M. Razavy. *Quantum Theory of Tunneling*. World Scientific, New Jersey, London, Singapore, Hongkong (2003).

[81] M. Ieong, P. M. Solomon, S. E. Laux, Hon-Sum P. Wong, and D. Chidambarrao. *IEDM Tech. Digest*, page 733 (1998).

[82] V. Kazŭkauskas and M. Pranaitis. *Mol. Cryst. Liq. Cryst.*, **447**:141 (2006).

[83] Yan-Zhong Hao and Cai Chun-Li. *Material Sci. and Eng.*, **23**:166 (2007).

[84] R. Valaski, L. M. Moreira, L. Micaroni, and I. A. Hümmelgen. *J. Appl. Phys.*, **92**:2035 (2002).

[85] T. G. Abdel-Malik and R. M. Abdel-Latif. *Thin Solid Films*, **305**:336 (1997).

[86] Z. Bao, A. Dodabalapur, and A. J. Lovinger. *Appl. Phys. Lett.*, **69**:4108 (1996).

[87] Q. T. Zhang and J. M. Tour. *J. Am. Chem. Soc.*, **119**:5065 (1997).

[88] V. I. Arkhipov, H. von Seggern, and E. V. Emelianova. *Appl. Phys. Lett.*, **83**:5074 (2003).

[89] N. I. Craciun, J. Wildeman, and P. W. M. Blom. *Phys. Rev. Lett.*, **100**:0566601 (2008).

[90] F. Neumann, Y. A. Genenko, C. Melzer, and H. von Seggern. *J. Appl. Phys.*, **100**:084511 (2006).

[91] F. Neumann, Y. A. Genenko, C. Melzer, S. V. Yampolskii, and H. von Seggern. *Phys. Rev. B*, **75**:205322 (2007).

[92] A. Alec Talin, F. Leonard, B. S. Swartzentruber, X. Wang, and S. D. Hersee. *Phys. Rev. Lett.*, **101**:076802 (2008).

Bibliography

[93] N. I. Craciun, J. Wildeman, and P. W. M. Blom. *Phys. Rev. Lett.*, **100**:056601 (2008).

[94] F. L. Bloom, M. Kemerink, W. Wagemans, and B. Koopmans. *Phys. Rev. Lett.*, **103**:066601 (2009).

[95] S. Miyanishi, M. Yagura, N. Teguchi, K. Shirakawa, K. Sakuno, Y. Murakami, K. Kojima, A. Takahashi, and K. Ohta. *Appl. Phys. Lett.*, **91**:192104 (2007).

[96] W. Chandra, L. K. Ang, and W. S. Koh. *J. Phys. D:Appl. Phys.*, **42**:055504 (2009).

[97] Y. Y. Lau, D. Chernin, D. G. Colombant, and P.-T. Ho. *Phys. Rev. Lett.*, **66**:1446 (1991).

[98] L. K. Ang and P. Zhang. *Phys. Rev. Lett.*, **98**:164802 (2007).

[99] W. Schottky. *Ann. Phys.*, **57**:541 (1918).

[100] Rolf Landauer. *Nature*, **392**:658 (1998).

[101] Y. M. Blanter and M. Buttiker. *Phys. Rep*, **336**:1 (2000).

[102] Carlo Beenakker and C. Schonenberger. *Phys. Today*, **56**:37 (2003).

[103] D. O. North. *R. C. A. Rev.*, **4**:441 (1940).

[104] H. Birk, M. J. M. de Jong, and C. Schönenberger. *Phys. Rev. Lett.*, **75**:1610 (1995).

[105] H. C. Liu, Jianmeng Li, G. C. Aers, C. R. Leavens, M. Buchanan, and Z. R. Wasilewski. *Phys. Rev. B*, **51**:5116 (1995).

[106] T. González, J. Mateos, D. Pardo, O. M. Bulashenko, and L. Reggiani. *Semicon. Sci. Technol.*, **13**:714 (1998).

Bibliography

[107] T. González, C. González, J. Mateos, D. Pardo, L. Reggiani, O. M. Bulashenko, and J. M. Rubí. *Phys. Rev. Lett.*, **80**:2901 (1998).

[108] C. W. J. Beenakker. *Phys. Rev. Lett.*, **82**:2761 (1999).

[109] H. Schomerus, E. G. Mischenko, and C. W. J. Beenakker. *Phys. Rev. B*, **60**:5839 (1999).

[110] O. M. Bulashenko, J. M. Rubí, and V. A. Kochelap. *Phys. Rev. B*, **61**:5511 (2000).

[111] O. M. Bulashenko, J. M. Rubí, and V. A. Kochelap. *Phys. Rev. B*, **62**:8184 (2000).

[112] O. M. Bulashenko and J. M. Rubí. *Phys. Rev. B*, **64**:045307 (2001).

[113] K. E. Nagaev. *Phys. Rev. B*, **52**:4740 (1995).

[114] V. I. Kozub and A. M. Rudin. *Phys. Rev. B*, **52**:7853 (1995).

[115] O. M. Bulashenko and J. M. Rubí. *Phys. Rev. B*, **67**:115322 (2003).

[116] K. Rangaswamy, M. Cahay, and K. L. Jensen. *Appl. Phys. Lett.*, **85**:3763 (2004).

[117] K. Rangaswamy, M. Cahay, and K. L. Jensen. *J. Vac. Sci. Technol. B*, **23**:380 (2005).

[118] L. Wu, L. K. Ang, and W. S. Koh. *Phys. Rev. B*, **77**:115351 (2008).

[119] Y. Hishinuma, T. H. Geballe, B. Y. Moyzhes, and T. W. Kenny. *Appl. Phys. Lett.*, **78**:2572 (2001).

[120] C. R. Crowell and S. M. Sze. *Solid-State Electronics*, **9**:1035 (1966).

[121] T. P. Chow, V. Khemka, J. Fedison, N. Ramungul, K. Matocha, Y. Tang, and R. J. Gutmann. *Solid-State Electronics*, **44**:277 (2000).

APPENDIX A

DERIVATION FOR 2D MG LAW FOR A PLANAR WIDTH 2D SHAPE

The derivation of the classical MG law is based on a one-dimensional (1D) model. The current density formula J_{MG} only takes into account the direction along the electron transport inside a dielectric with diode structure from x=0 to x=L. All the other directions of the solid dielectric are considered to be infinitely long hence it does not effect the calculation. For the 2D model discussed in this thesis, the derivation is based on using the Gauss' law to calculate the electric field at the center of the injecting contact, which is analytically in the form of: form of:

$$\frac{J_{MG}[2D]}{J_{MG}[1D]} = 1 + F \times G. \tag{A.1}$$

In our model (see Fig. A.1), we have the dielectric length L between the cathode and anode along the x-direction, the width W is along y-direction and the thickness d is infinitely long along the z-direction. The differential element of electric field profile dξ can be shown to be:

$$\oint \boldsymbol{\xi}.\boldsymbol{dA} = \frac{Q}{\epsilon_0},$$

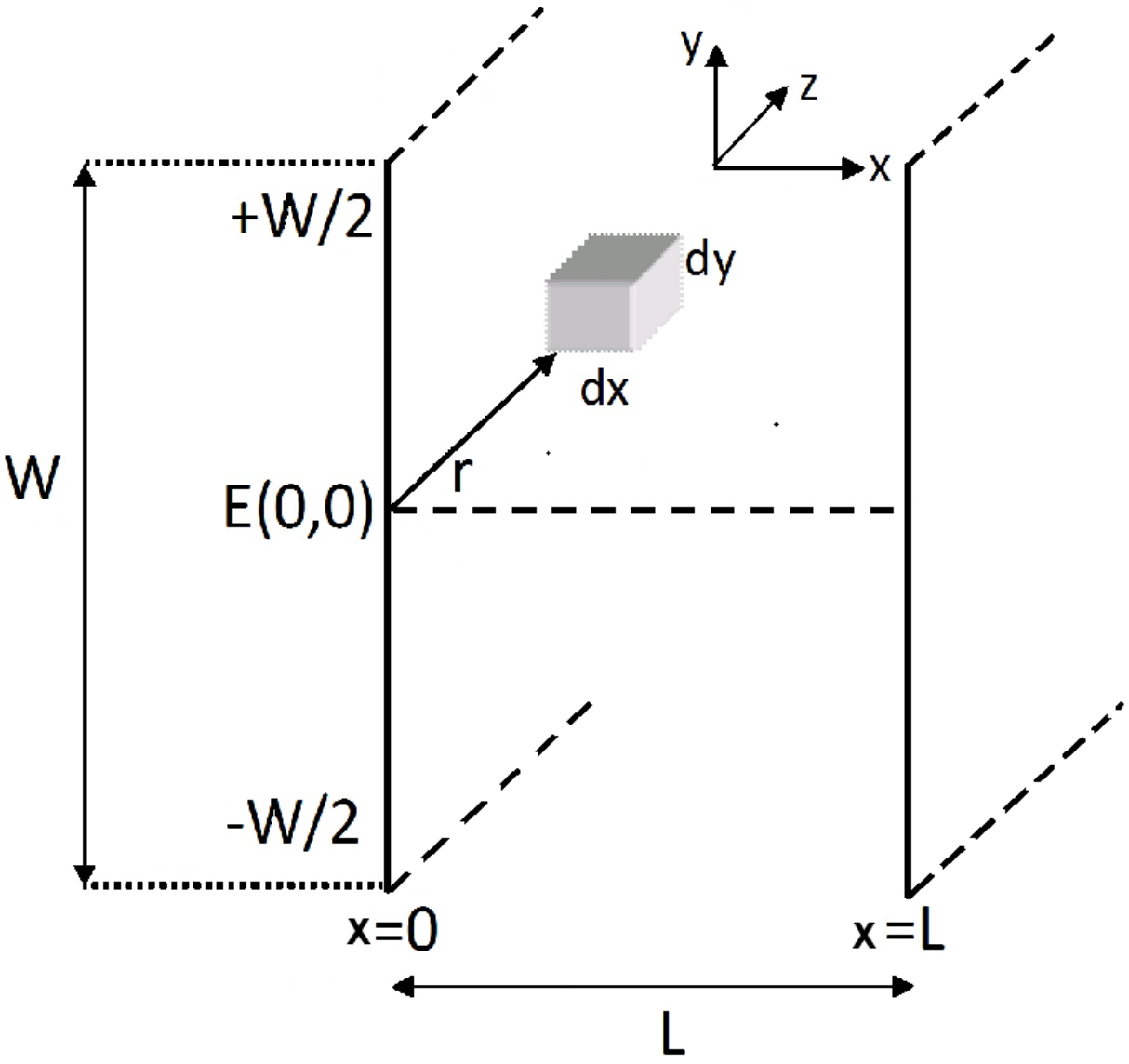

Figure A.1: The geometrical representation of the solid dielectric with length L and width W. The thickness of the solid dielectric d in the z-direction is assumed to be infinitely long

where $\boldsymbol{\xi}$ is the electric field vector and $\boldsymbol{dA}$ is the differential element of the area vector. The differential element of the electric field at the center [(x,y) = (0,0)] can now be written as:

$$d\xi(0,0) = \frac{\rho(x,y)dxdy}{2\pi\epsilon_0\sqrt{x^2+y^2}},$$

where ρ is the charge density and the electric field to be calculated is the electric field along the x-direction, that is:

$$d\xi_x = d\xi\frac{x}{\sqrt{x^2+y^2}},$$

hence, the surface integral form above can be written as:

$$\int d\xi_x = \frac{1}{2\pi\epsilon_0}\int_0^L \rho(x,y)xdx\int_{-W/2}^{+W/2}\frac{dy}{x^2+y^2},$$

The electron density ρ (x,y) $\simeq$ ρ (x) if $W \gg L$ and also the integral in y-direction is symmetrical from -$W/2$ to 0 and from 0 to +$W/2$, so the simplification now shows as:

$$\int d\xi_x = \frac{1}{2\pi\epsilon_0}\int_0^L \rho(x)xdx\int_0^{+W/2}\frac{2dy}{x^2+y^2},$$

$$\int d\xi_x = \frac{1}{\pi\epsilon_0}\int_0^L \rho(x)\tan^{-1}\frac{\mathrm{W}}{2\mathrm{x}}\mathrm{dx},$$

with $\tan^{-1}$(p) = $\pi/2$ - 1/p for p $\gg$ 1, the form can be simplified again to be:

$$\int d\xi_x = \frac{1}{\pi\epsilon_0}\int_0^L \rho(x)\big(\frac{\pi}{2}-\frac{2x}{W}\big)dx,$$

$$\xi_x = \frac{1}{2\epsilon_0}\int_0^L \rho(x)\big(1-\frac{4x}{\pi W}\big)dx.$$

The space charge condition is reached when the total self electric field equals to applied bias V_G/L, thus the 2D and 1D SCL MG current density can be found by comparing the electric field ξ_x at SCL condition, that is, by rewriting the electric field expression as:

$$\xi_x = \frac{J}{2\epsilon_0}\int_0^L \frac{1}{v(x)}\big(1-\frac{4x}{\pi W}\big)dx,$$

since,

$$J = \rho(x)v(x) = constant,$$

and then, the J_{MG} in 2D and 1D can be written as:

$$\frac{J_{MG}[2D]}{2\epsilon_0}\int_0^L \frac{1}{v(x)}\big(1-\frac{4x}{\pi W}\big)dx = V_G/L,$$

$$\frac{J_{MG}[1D]}{2\epsilon_0}\int_0^L \frac{1}{v(x)}dx = V_G/L,$$

The last two expressions can be compared with each other:

$$\frac{J_{MG}[2D]}{J_{MG}[1D]} = \frac{\int_0^L \frac{1}{v(x)}dx}{\int_0^L \frac{1}{v(x)}\big(1-\frac{4x}{\pi W}\big)dx},$$

$$\frac{J_{MG}[2D]}{J_{MG}[1D]} = 1 + F \times G.$$

Here, $F = \frac{\int_0^L (x/L)n(x)dx}{\int_0^L n(x)dx}$ measures the normalized mean position of the injected electrons in a solid of length L and $G = (4/\pi)/(W/L)$ for $W/L > 1$ is the correction factor for the geometrical shape in 2D for planar width. The expressions for G for other 2D shapes and 3D shapes have been derived elsewhere and can be found in [59, 60].

APPENDIX B

SOLVING EQUILIBRIUM 1D POISSON EQUATION IN MATRIX FORM

Since it is not always possible to find the analytical form of a given equation, numerical simulation codes can be formulated to solve many calculations in trying to find the solution of complex mathematical problems. For example in this appendix, the numerical method in solving the 1D Poisson equation in this thesis will be shown below.

The equilibrium Poisson equation in 1D will be solved along the x-direction. It is only solved for one carrier (electrons) only and the potential profile is solved along x=0 to x=L. And also, since it is at equilibrium, the quasi fermi level is always zero. The discretized form of Poisson equation in 1D can be written using central difference method as:

$$\frac{\psi_{j-1} - 2\psi_j + \psi_{j+1}}{(\triangle x)^2} = \frac{en_i}{\epsilon_r \epsilon_0}\Big[exp(\frac{\psi_j}{k_b T/e}) - 1\Big].$$

The value of j = 1, ... , N-1 with N is the total number of equations that depends on the number of discretizations used in the system. To solve the potential ψ_j at each x_j, the boundary conditions at ψ(x=0) and ψ(x=L) are needed, assuming

they are ψ_0 and ψ_L, respectively. In matrix form, the discretized 1D Poisson equation can be written in the form of:

$$\boldsymbol{A\psi} = \boldsymbol{F}.$$

with

$$\mathbf{A} = \frac{1}{(\triangle x)^2}\begin{pmatrix} -2 & 1 & 0 & \dots & 0 \\ 1 & -2 & 1 & \dots & \vdots \\ 0 & \ddots & \ddots & \ddots & 0 \\ 0 & \dots & 0 & 1 & -2 \end{pmatrix}$$

$$\psi = \begin{pmatrix} \psi_1 \\ \psi_2 \\ \vdots \\ \psi_{N-1} \end{pmatrix}$$

$$\mathbf{F} = \begin{pmatrix} \frac{en_i}{\epsilon_r\epsilon_0}\left[exp\left(\frac{\psi_1}{k_bT/e}\right) - 1\right] - \frac{\psi_0}{(\triangle x)^2} \\ \frac{en_i}{\epsilon_r\epsilon_0}\left[exp\left(\frac{\psi_2}{k_bT/e}\right) - 1\right] \\ \vdots \\ \frac{en_i}{\epsilon_r\epsilon_0}\left[exp\left(\frac{\psi_{N-1}}{k_bT/e}\right) - 1\right] - \frac{\psi_L}{(\triangle x)^2} \end{pmatrix}$$

The potential profile ψ_1, ..., ψ_{N-1} can then be found by iteration. The initial values for each ψ_j are guessed first and then the iteration is done until the error of the iteration is below an acceptable value that has been set (usually the error value for the potential matrix $\boldsymbol{\psi}$ is set to be few percent below the thermal voltage V_{th}). Some of the methods that have been used for the iteration purpose are:

1. Jacobi method

$$\boldsymbol{\psi^{(k)}} = \boldsymbol{D^{-1}(L+U)\psi^{(k-1)}} + \boldsymbol{D^{-1}F}.$$

with $\boldsymbol{A}$ = $\boldsymbol{D}$ - $\boldsymbol{L}$ - $\boldsymbol{U}$, $\boldsymbol{D}$ is the diagonal parts of matrix $\boldsymbol{A}$, $\boldsymbol{L}$ is the strictly lower triangular parts of matrix $\boldsymbol{A}$, $\boldsymbol{U}$ is the strictly upper triangular parts of matrix $\boldsymbol{A}$,

and $\boldsymbol{k}$ is the number of iterations.

2. Gauss-Seidel method

$$\boldsymbol{\psi^{(k)} = (D - L)^{-1}(U\psi^{(k-1)} + F)}.$$

3. Successive Over Relaxation (SOR) method

$$\boldsymbol{\psi^{(k)} = (D - \omega L)^{-1}[\omega U + (1 - \omega)D]\psi^{(k-1)} + \omega(D - \omega L)^{-1}F}.$$

with ω is the extrapolation factor ($0 < \omega < 2$). With the value of $\omega = 1$, the SOR method recovers to Gauss-Seidel method. In our code, we use Gauss-Seidel method to compute the simulation data.

APPENDIX C

SOLVING 1D POISSON EQUATION COUPLED WITH CURRENT CONTINUITY EQUATION

In chap. 4, the Poisson equation is solved together with the current continuity equation. The numerical code is solved in matrix form. The difference with the equilibrium Poisson equation solved before in Appendix B is the quasi fermi level $\boldsymbol{\phi_n}$ is not zero along the x-direction since the potential bias V_G is now applied at the anode side of the diode structure. The codes mainly divided into two different categories, with the first case is for the code when there is no tunneling through surface states exist in the solid (the cathode to the solid dielectric has an ohmic contact with infinite surface recombination) and the other case accounts for the tunneling through surface states at the contact between cathode and the solid.

As mentioned in chap. 4, for the no tunneling code, the parameters $\boldsymbol{\psi}$,$\boldsymbol{\phi_n}$,$\boldsymbol{n}$, $\boldsymbol{j_n}$ are normalized to $\bar{\boldsymbol{\psi}} = \boldsymbol{\psi}/V_0$, $\bar{\boldsymbol{\phi_n}} = \boldsymbol{\phi_n}/V_0$, $\bar{\boldsymbol{n}} = \boldsymbol{n}/n_i$, $\bar{\boldsymbol{j_n}} = \boldsymbol{j_n}/j_0$ with V_0 is the crossover (transition) voltage from ohmic to SCL-MG $= \frac{eL^2 n_i}{\epsilon_r \epsilon_0}$, j_0 is the crossover current density $= en_i\mu_n\frac{V_0}{L}$, and n_i is the intrinsic electron concentration. Thus, for the Poisson equation, in normalized form, it can be written as:

$$\frac{d^2\bar{\boldsymbol{\psi}}}{d\bar{x}^2} = \bar{\boldsymbol{n}} - 1.$$

In the matrix form (as shown in Appendix B), the normalized Poisson equation can be written as:

$$\boldsymbol{A}\bar{\boldsymbol{\psi}} = \boldsymbol{F}.$$

with

$$\mathbf{A} = \begin{pmatrix} -2 & 1 & 0 & \dots & 0 \\ 1 & -2 & 1 & \dots & \vdots \\ 0 & \ddots & \ddots & \ddots & 0 \\ 0 & \dots & 0 & 1 & -2 \end{pmatrix}$$

$$\bar{\psi} = \begin{pmatrix} \bar{\psi}_1 \\ \bar{\psi}_2 \\ \vdots \\ \bar{\psi}_{N-1} \end{pmatrix}$$

$$\mathbf{F} = \begin{pmatrix} (\bar{n}_1 - 1)d\bar{x}^2 - \bar{\psi}_0 \\ (\bar{n}_2 - 1)d\bar{x}^2 \\ \vdots \\ (\bar{n}_{N-1} - 1)d\bar{x}^2 - \bar{\psi}_L \end{pmatrix}$$

where $\bar{\psi}_0$ and $\bar{\psi}_L$ are the boundary conditions for the potential value at x=0 and x=L.

The matrix equation above needs to be solved in coupled with the current continuity equation since the value of $\bar{\boldsymbol{\phi}}_{\boldsymbol{n}}$ is not zero with $\bar{\boldsymbol{n}} = \exp\left[\mathrm{a}(\bar{\boldsymbol{\psi}} - \bar{\boldsymbol{\phi}}_{\boldsymbol{n}})\right]$ where $a = \mathrm{e}V_0/k_bT$. Since there is no tunneling through surface states, the recombination rate $\bar{\boldsymbol{G}} = 0$. And then, expression for $\bar{\boldsymbol{j}}_{\boldsymbol{n}}$ will be:

$$\bar{\boldsymbol{j}}_{\boldsymbol{n}} = \frac{1}{a} exp(a\bar{\boldsymbol{\psi}}) \frac{d}{d\bar{x}^2} \left[exp(-a\bar{\boldsymbol{\phi}}_{\boldsymbol{n}}) \right].$$

In matrix form, the expression above can be written as:

$$\boldsymbol{A}\bar{\boldsymbol{S}} = \boldsymbol{F}.$$

with

$$\mathbf{A} = \begin{pmatrix} -C_2 - 2C_1 - C_0 & C_2 + C_1 & 0 & \dots & 0 \\ C_2 + C_1 & -C_3 - 2C_2 - C_1 & C_2 + C_3 & \dots & \vdots \\ 0 & \ddots & \ddots & \ddots & 0 \\ 0 & \dots & 0 & C_{N-2} + C_{N-1} & -C_N - 2C_{N-2} - C_{N-2} \end{pmatrix}$$

$$\bar{\mathbf{S}} = \begin{pmatrix} exp(-a\bar{\phi}_{n1}) \\ exp(-a\bar{\phi}_{n2}) \\ \vdots \\ exp(-a\bar{\phi}_{nN-1}) \end{pmatrix}$$

$$\mathbf{F} = \begin{pmatrix} -S_0(C_1 + C_0) \\ 0 \\ \vdots \\ 0 \\ -S_N(C_N + C_{N-1}) \end{pmatrix}$$

where $\boldsymbol{C}$ = exp(a$\bar{\boldsymbol{\psi}}$) and $\bar{\boldsymbol{S}}$ = exp(-a$\bar{\boldsymbol{\phi}}_{\boldsymbol{n}}$) and it is usually called as the Slotboom variable matrix. The values for S_0 and S_{N-1} are from the quasi fermi level at x=0 ($\bar{\phi}_0$) and x=L ($\bar{\phi}_L$), respectively. The initial values of matrix $\bar{\boldsymbol{\psi}}$ and $\bar{\boldsymbol{\phi}}_{\boldsymbol{n}}$ are guessed and then solved by iteration using any of the three methods of solving matrix equation described in Appendix B, and then the processes are repeated until convergence is achieved.

For the case of tunneling from cathode contact through the surface states, slightly more complicated numerical code is needed to compute the potential and quasi fermi level profile along the x-direction. Firstly, since the local generation rate is not equal

to zero due to the net local tunneling generation rate, the matrix form for the current continuity equation will be different from the no tunneling case. And also, the code needs to implement different differential element (dx) along the x-direction with more refinement near the cathode contact (near x=0) is necessary to correctly calculate the tunneling. A very small dx is needed and usually it is calculated up to about 5 - 10 nm from the contact. For the matrix form of Poisson equation, the modification of the code only involves in incorporating different dx into the matrix expression.

For the matrix form of current continuity equation, the difference in the expression shows up in $\boldsymbol{F}$ matrix. The matrix form of the current continuity equation can be shown to be:

$$\boldsymbol{A}\bar{\boldsymbol{S}} = \boldsymbol{F}.$$

with $\boldsymbol{A}$ and $\bar{\boldsymbol{S}}$ are the same as the no tunneling case while

$$\mathbf{F} = \begin{pmatrix} -S_0(C_1 + C_0)dx_{Tun} - R_1 \\ -R_2 \\ \vdots \\ -R_{x_{Tun}} \\ 0 \\ \vdots \\ 0 \\ -S_N(C_N + C_{N-1})dx_{NoTun} \end{pmatrix}$$

where dx_{Tun} is the dx used to account the tunneling and usually is chosen to be very refined, dx_{NoTun} is the dx used to account for the part along x-direction where tunneling is negligible, and x_{Tun} is the tunneling distance used in the code with the value is usually within 5 - 10 nm. The values of $R_1, \ldots, R_{x_{Tun}}$ are computed from the tunneling components through the surface states. By using the double integration method over the distance [81] and WKB method for the tunneling coefficient, the

form of $\boldsymbol{R}$ can be shown as:

$$\boldsymbol{R} = \frac{-eV_0A^*T}{k_bj_0}\Gamma(\bar{x})ln\Big[\frac{1+exp\big[a(\bar{\psi}_C(\bar{x})-\bar{\phi}_n(\bar{x}))\big]}{1+exp\big[a\bar{\psi}_C(\bar{x})\big]}\Big]\frac{d\bar{\psi}(\bar{x})}{dx_{Tun}},$$

$$\Gamma(\bar{x}) = exp\Big[\frac{-2}{\hbar}\sqrt{2e.m_o.m_{Tun}}\sum_{\bar{x}=0}^{\bar{x}}\sqrt{V_0\big(\bar{\psi}_C(\bar{x})-\bar{\psi}_C(\bar{x'})\big)}Ldx'\Big].$$

where A^* is the effective Richardson constant, $\Gamma(\bar{x})$ is the tunneling coefficient, $\bar{\psi}_C(\bar{x}) = \bar{\psi}(\bar{x})$ - $\left[\frac{\frac{E_G}{2e}+\frac{k_bT}{2e}ln\frac{N_C}{N_V}}{V_0}\right]$ is the normalized conduction band potential, $\hbar$ is the reduced Planck's constant, m_o is the free electron mass, m_{Tun} is the effective electron tunneling mass, $\bar{x}'$ is the small refined value that is chosen to be very close to $\bar{x}$. The solving process is straightforward and similar to the no tunneling case. The potential profile and quasi fermi level profile are guessed initially and iterations are done until convergence is reached.

APPENDIX D

LIST OF SYMBOLS

Table D.1: List of Symbols

Symbol	Definition
J_{CL}	the Space Charge Limited (SCL) current density in a vacuum/free space
ϵ_0	the free space permittivity = 8.85×10^{-14} F/cm
e	the electronic charge = 1.602×10^{-19} C
m_e	the free electron mass = 9.109×10^{-31} kg
V_G	the voltage bias applied between the cathode and anode
L	the gap spacing between the cathode and anode
J_{MG}	the Space Charge Limited (SCL) current density in a solid dielectric
μ_n	the drift electron mobility
ϵ_r	the relative or dielectric permittivity
v	the electron velocity
ψ_n	the electron potential

Continued on Next Page...

Table D.1 – Continued

ξ	the average electric field of electrons
τ_r	the dielectric relaxation time
σ	the electrical conductivity of a material
T_r	the transit time
n_{inj}	the injected electron concentration into a solid material
n_i	the thermal or intrinsic electron concentration of a solid material
Q	the total number of charge per unit area
μ	the drift mobility, the notation is used when talking about drift mobility in general (it can be either electron or hole mobility)
$V_{\Omega-MG}$	the transition voltage from Ohm's law to SCL MG law
k_b	the Boltzmann's constant = 1.38×10^{-23} J/K
T	the electron temperature
E_t	the traps energy level
E_C	the minimum of conduction band energy
E_{F0}	the equilibrium Fermi energy level
E_F	the quasi Fermi energy level
n_f	the free electron concentration
n_t	the filled electron trap concentration
N_C	the effective density of states in the conduction band
N_{t0}	the total concentration of traps
$J_{shallow}$	the Space Charge Limited (SCL) current density in a solid with shallow traps
$V_{\Omega-shallow}$	the transition voltage from Ohmic region to the SCL MG with shallow traps
p_t	the unoccupied electron (occupied hole) trap concentration

Continued on Next Page...

Table D.1 – Continued

V_{TFL}	the trap-filled limit voltage
$V_{\Omega-deep}$	the transition voltage from Ohmic region to the filling of deep traps
$N_t(E)$	the concentration of electron traps per unit energy range
T_t	the characteristic temperature that characterizes the Gaussian distribution in the traps with an exponential distribution in energy
J_{TL}	the Space Charge Limited (SCL) current density in a solid with traps exponentially distributed in energy
$V_{\Omega-TL}$	the transition voltage from Ohmic region to the traps exponentially distributed in energy
V_{TL-MG}	the transition voltage from the traps exponentially distributed in energy to the SCL MG region
J_{UN}	the Space Charge Limited (SCL) current density in a solid with traps with a uniform distribution in energy
j_n	the drift electron current density
$n(x)$	the electron concentration along the length of the solid dielectric from x=0 to x=L
$\psi_n(x)$	the potential profile across the solid length
$v(x)$	the electron drift velocity across the solid length
n_o	the doping density
${m_e}^*$	effective electron mass
τ_m	the momentum relaxation time
$\xi(x)$	the electric field profile along the solid length L
$u(w)$	the dimensionless squared velocity
w	the dimensionless distance
x_0	the characteristic length

Continued on Next Page...

Table D.1 – Continued

ω_p	the plasma frequency
β	the dimensionless collision frequency. It is an important parameter that controls the degree of collision
$J_{MG}[2D]$	the SCL MG current density where the width, W, is comparable to the length, L, in a solid
$J_{MG}[1D]$	the SCL MG current density where the width, W, is much larger than the length, L, in a solid
F	the normalized mean position of the injected electrons in a solid of length L
G	a correction parameter depends on the geometry of the cathode
W	the width of the cathode as the source of electron injection to a solid
d	the thickness of the cathode as the source of electron injection to a solid
V_{PT}	the punch-through voltage that the space charge has extended through a solid
$e\phi_b$	the Schottky barrier height at the interface between the cathode and a solid
$e\phi_m$	the work function of the cathode
$e\chi$	the electron affinity of a dielectric material
ψ_n	the electrostatic potential
ϕ_n	the quasi Fermi electron potential
$G(x)$	the net generation rate of electrons in a solid across the length L
j_n	the total electron current density (drift-diffusion electron current density)
D_n	the electron diffusion coefficient

Continued on Next Page...

Table D.1 – Continued

j_{sn}	the surface recombination current density
v_{sn}	the surface recombination velocity
A^*	the effective Richardson constant
n_s	the actual surface electron concentration
n_{eq}	the equilibrium electron concentration
v_{th}	the average thermal velocity
ψ_0	the built-in potential
E_g	the bandgap of a dielectric
V_0	the crossover (transition) voltage from Ohmic to SCL-MG region, it is equal to $V_{\Omega-MG}$
j_0	the crossover current density
x_1	the parameter to control the relative length of vacuum and solid in a combined gap
ψ_{x_1}	the electrostatic potential at the interface (x=x_1)
ξ_{x_1}	the electric field at the interface (x=x_1)
S	the power spectral density of the shot noise
γ	the Fano factor of shot noise reduction
C_T	the tunneling or transmission coefficient through an energy barrier
$\psi_C(x)$	the conduction band potential
N_C^{300}	the effective density of states of electrons in the conduction band at $T = 300$ K
E_g^{300}	the bandgap at $T = 300$ K